STUDIES ON METAL EXCHANGE AND INHIBITION IN ANTHRAX LETHAL FACTOR

by

Calvin J. Young

A thesis submitted in partial fulfillment
of the requirements for the degree of
Master of Science (M.Sc.) in Chemical Sciences

The Faculty of Graduate Studies
Laurentian University
Sudbury, Ontario, Canada

THESIS DEFENCE COMMITTEE/COMITÉ DE SOUTENANCE DE THÈSE
Laurentian Université/Université Laurentienne
Faculty of Graduate Studies/Faculté des études supérieures

Title of Thesis Titre de la thèse	STUDIES ON METAL EXCHANGE AND INHIBITION IN ANTHRAX LETHAL FACTOR
Name of Candidate Nom du candidat	Young, Calvin
Degree Diplôme	Master of Science
Department/Program Département/Programme	Chemical Sciences
Date of Defence Date de la soutenance	June 15, 2016

APPROVED/APPROUVÉ

Thesis Examiners/Examinateurs de thèse:

Dr. Stefan Siemann
(Supervisor/Directeur(trice) de thèse)

Dr. Gustavo Arteca
(Committee member/Membre du comité)

Dr. Hélène Joly
(Committee member/Membre du comité)

Dr. Steven Rafferty
(External Examiner/Examinateur externe)

Approved for the Faculty of Graduate Studies
Approuvé pour la Faculté des études supérieures
Dr. Shelley Watson
Madame Shelley Watson
Acting Dean, Faculty of Graduate Studies
Doyenne intérimaire, Faculté des études supérieures

ACCESSIBILITY CLAUSE AND PERMISSION TO USE

I, **Calvin Young**, hereby grant to Laurentian University and/or its agents the non-exclusive license to archive and make accessible my thesis, dissertation, or project report in whole or in part in all forms of media, now or for the duration of my copyright ownership. I retain all other ownership rights to the copyright of the thesis, dissertation or project report. I also reserve the right to use in future works (such as articles or books) all or part of this thesis, dissertation, or project report. I further agree that permission for copying of this thesis in any manner, in whole or in part, for scholarly purposes may be granted by the professor or professors who supervised my thesis work or, in their absence, by the Head of the Department in which my thesis work was done. It is understood that any copying or publication or use of this thesis or parts thereof for financial gain shall not be allowed without my written permission. It is also understood that this copy is being made available in this form by the authority of the copyright owner solely for the purpose of private study and research and may not be copied or reproduced except as permitted by the copyright laws without written authority from the copyright owner.

Abstract

Anthrax lethal factor (LF) is a zinc-dependent endopeptidase, and a component of the anthrax toxin secreted by *Bacillus anthracis*. LF demonstrates two interesting contradictory features: a propensity to readily exchange the active site metal ion with extraneous metal ions in solution, while having at the same time a very high affinity (femto- to picomolar) for metals in its active site. The hypothesis of this thesis was that metal exchange in LF occurs via an associative mechanism involving the formation of a di-metal species through the occupation of an inhibitory metal-binding site (by the incoming metal) located adjacent to the active site. We demonstrate here that the spontaneous demetallation of LF is slow, especially for the release of zinc ($t_{1/2}$ ~3 h). In contrast, metal exchange (with $^{70}Zn^{2+}$, Co^{2+} and Cu^{2+}) was found to occur with $t_{1/2}$ values between 5 s and 180 s, hence supporting an associative mechanism of exchange. In addition, the mode of inhibition exerted by Zn^{2+} on zinc-containing LF (ZnLF) was observed to be non-competitive with an inhibition (pseudo)constant of ~30 μM, a feature in agreement with turnover studies using stopped-flow UV-Vis spectroscopy. Finally, present studies using Tb^{3+} suggest that the lanthanide ion competes with other metal ions (Zn^{2+}, Cu^{2+}) for binding to the inhibitory metal site in LF, hence decreasing the rate of metal exchange. This observation provides further support for the intimate link between a putative inhibitory binding site and metal exchange. The results of this study provide insight into how cellular metal pools may remain dynamic *in vivo*, and have implications not only for LF, but for many other zinc-dependent enzymes where metal substitution is used for spectroscopic studies.

Acknowledgements

It is my pleasure to acknowledge the individuals who were instrumental in the completion of this thesis. First and foremost I am grateful to my supervisor, Dr. S. Siemann, for his counsel and support. His guidance throughout this research has been immensely valuable. I sincerely thank my supervisory committee members, Dr. H. Joly and Dr. G. Arteca, for their insightful discussions and valued input that have helped shape this project. I extend my hearty thanks to all of my labmates for their in-lab assistance with instrumentation and experimental protocol. Last but not least, I would like to thank my family and friends for their love and support.

Table of Contents

List of Tables

List of Figures

List of Abbreviations

AMPA	α-Amino-3-hydroxy-5-methyl-4-isoxazolepropionic acid
APS	Ammonium persulfate
ATP	Adenosine triphosphate
ATR	Anthrax toxin receptors
BoNT A	Botulinum neurotoxin serotype A
CA	Carbonic anhydrase
cAMP	Cyclic adenosine monophosphate
CFSE	Crystal field stabilization energy
CHNOPS	Carbon, hydrogen, oxygen, nitrogen, phosphorus, and sulfur
CMG2	Capillary morphogenesis gene-2
cps	Counts per second
DNA	Deoxyribonucleic acid
DMSO	Dimethyl sulfoxide
DPA	Dipicolinic acid
DPP III	Dipeptidyl peptidase III
EDTA	Ethylenediaminetetraacetic acid
EF	Edema factor
EPR	Electron paramagnetic resonance spectroscopy
FcεRI	High-affinity IgE receptor
FRET	Förster resonance energy transfer
g	Relative centrifugal force
Gdn-HCl	Guanidine hydrochloride
Hepes	4-(2-Hydroxyethyl)-1-piperazineethanesulfonic acid
IC_{50}	Half maximal inhibitory concentration
ICP-MS	Inductively-coupled plasma mass spectrometry
InrS	Nickel-responsive efflux derepressor
k_{cat}	Turnover number
K_d	Dissociation constant
K_I	Inhibition constant
K_M	Michaelis constant
k_{off}	Dissociation rate constant
k_{on}	Association rate constant
LF	Lethal factor
LpxC	Uridine diphosphate-(3-*O*-(R-3-hydroxymyristoyl))-*N*-acetylglucosamine deacetylase
MAPKK	Mitogen-activated protein kinase kinase
MT	Metallothionein
MWCO	Molecular weight cut-off
N	Number of exchanged metal ions
Nlrp1	Nod-like receptor protein 1
PA	Protective antigen
PAR	4-(2-Pyridylazo)resorcinol
PDB ID	Protein data bank identification code
PEG-8000	Polyethylene glycol 8000
ppb	Parts per billion

ppm	Parts per million
RA	Relative activity
Rpe	Ribulose-5-phosphate 3-epimerase
rRNA	Ribosomal ribonucleic acid
S.D.	Standard deviation
SDS-PAGE	Sodium dodecyl sulfate polyacrylamide gel electrophoresis
*S-p*NA	Anthrax lethal factor protease substrate II
$t_{1/2}$	Half-time of exchange
TEM8	Tumor endothelial marker 8
TEMED	Tetramethylethylenediamine
TFIIIA	Transcription factor IIIA
Tris	Tris(hydroxymethyl)aminomethane
Trx2	Zn-thioredoxin 2
ttr	Tracer-to-tracee ratio
UV-Vis	Ultraviolet–visible
V	Velocity
V_{max}	Maximum velocity
v/v	Volume/volume
w/v	Weight/volume
ZiaR	Zinc-responsive efflux derepressor

1. Introduction

1.1 The chemistry of life

Biochemistry is the study of chemical processes that occur in living organisms. There are six key elements that form the constituent of the vast majority of the molecules required for these processes. They are: carbon, hydrogen, oxygen, nitrogen, phosphorus, and sulfur (CHNOPS). These six elements account for 99% of the mass of all life forms (see Table 1.1) (1). However, many biological processes rely on proteins and enzymes containing other elements for their unique properties. Photosynthesis, dioxygen transport, gene expression, metabolism, and cellular respiration are all examples of processes that require metals (2). Although these metals may represent a very small mass of living organisms, it is estimated that up to 30% of all proteins bind or require metal in some way, demonstrating their crucial role (3).

Table 1.1: Average elemental composition of the human body (adult, 79 kg) (4,5).

Element	**Symbol**	**Mass (g)**
Oxygen	O	45500
Carbon	C	12600
Hydrogen	H	7000
Nitrogen	N	2100
Calcium	Ca	1050
Phosphorus	P	700
Sulfur	S	175
Potassium	K	140
Chlorine	Cl	105
Sodium	Na	105
Magnesium	Mg	35
Iron	Fe	4.2
Zinc	Zn	2.3
Copper	Cu	0.11
Manganese	Mn	0.02

Metal-protein bonds are formed through coordination with specific amino acids. Amino acids that can act as ligands include cysteine, methionine, histidine, glutamate,

aspartate, tyrosine, serine, threonine, asparagine, and glutamine (6). Some examples include the Cu-Cys bonds in blue copper proteins, the Zn-His bonds in carbonic anhydrase, and the Fe-Tyr bond in transferrin (2). The binding affinity of these amino acids for metals varies depending on the metal presented and the pH of the system (2).

In biological systems, transition metals typically play a structural, catalytic, or regulatory role. Metals are also involved in electron transfer and in the transport of dioxygen. It is the individual properties of each metal that makes them suitable for these roles.

Metals can also play a structural role where they may help at maintaining complex folding patterns required for the structural integrity of proteins (5). For a metal to be useful in a structural role, it must be redox inert and have a relatively high affinity for the binding site. Ions such as Ca^{2+}, Zn^{2+}, and Mg^{2+} act often in this way due to their redox inertness and their biological availability (2). Zinc is ideal in this role as complexes formed with this metal are generally more stable than those formed with other transition metals (except for copper), a consequence of the Irving-Williams series (7). One class of proteins that uses metals to maintain structure are zinc fingers, a class of transcription factors characterized by their zinc-requirement for stabilizing protein folds (8). Transcription factors are proteins that recognize and bind DNA to regulate (by enhancing or inhibiting) the rate of transcription. Generally, this class of proteins uses a combination of cysteine and histidine residues to coordinate a zinc ion. In the absence of the metal, these motifs lose partially their native contacts and become non-functional (2). A prime example of a zinc finger protein is transcription factor IIIA (TFIIIA). This protein is found in all organisms, and is required for the transcription of 5S rRNA genes (9). TFIIIA functions by binding the internal control region of 5S rRNA

genes, and recruiting the transcription complex. The binding of TFIIIA to DNA is made possible by nine consecutive Cys_2–His_2 type zinc finger motifs, as shown in Figure 1.1. There is also evidence to suggest that TFIIIA binds to the 5S rRNA product to protect it from degradation (9). These associations are only possible using the zinc finger motifs; without zinc being present, they lose their functionality, hence the importance of zinc in a structural role.

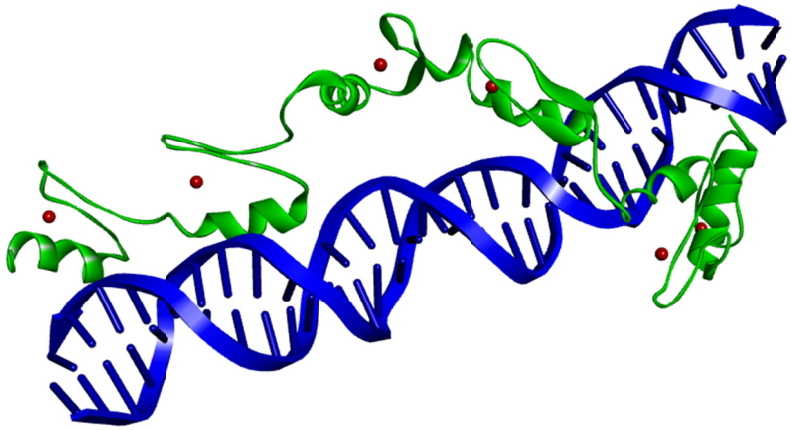

Figure 1.1: Structure of transcription factor IIIA bound to DNA (PDB ID: 1TF3) (10). TFIIIA is shown in green, DNA in blue, and zinc ions are depicted in red.

Transition metals are commonly involved in the active sites of enzymes, where they facilitate their function. One property that allows some metals to be more desirable in enzyme catalysis than others is a low crystal field stabilization energy (CFSE). CFSE is defined as the difference between the energy of an electron configuration of a transition metal in a ligand field and in an isotropic field. A high CFSE will typically lead to a preference for specific coordination environments. If a metal has no CFSE, it does not have a preference for a particular coordination environment. Therefore, there is no CFSE barrier or penalty to overcome when adding or removing ligands, steps typically required in enzymatic reactions. Having little to no stabilization energy allows the coordination

environment to remain flexible, a feature which results in high ligand-exchange rates, and hence rapid reactions (2). This is why zinc is found in the active site of so many enzymes. Due to its d^{10} configuration, it has no CFSE and can remain dynamic.

Many catalytic reactions involving metals are hydrolytic in nature due to the Lewis acidity of metal ions (4). A well-studied example of a metal being used to promote a hydrolytic reaction is nickel in urease. This enzyme catalyzes the hydrolysis of urea to form carbon dioxide and ammonia according to the following reaction:

$$(NH_2)_2CO + H_2O \rightarrow CO_2 + 2NH_3$$

The active site of urease contains two nickel ions (separated by a distance of 3.6 Å) which are bridged by a carbamylated lysine residue (11). Although the mechanism of this reaction is still debated, one nickel ion is likely used to deprotonate a water molecule to form a hydroxide ligand which is employed as a base in the reaction. Substitution of the active site metal with either Mn^{2+} or Co^{2+} has been shown to retain the enzyme in a functional state, although the activity is greatly reduced (12). The ability of proteins to remain functional after metal substitution has been demonstrated for many metal-dependent enzymes (13).

A third role that metals play in biological systems is as signaling ions, e.g. the use of zinc in synaptic signaling in some neurons. Similar to a neurotransmitter, zinc is released following presynaptic stimulation of hippocampal mossy fibers (14). The zinc released travels across the synaptic cleft, and is picked up by cells in the area via Ca^{2+}-permeable α-amino-3-hydroxy-5-methyl-4-isoxazolepropionic acid (AMPA)/kainate (Ca-A/K) channels. This rapid influx of zinc generates reactive oxygen species in the postsynaptic neuron, which can lead to cell death (14). Zinc is also thought to act as a secondary messenger, which serves the role of relaying an extracellular signal to cause an intracellular event. For

example, crosslinking of the high-affinity immunoglobulin E receptor (FcεRI) in mast cells, which is an extracellular stimulus, has been shown to increase intracellular zinc concentrations in a phenomenon termed a "zinc wave" (15). This zinc wave can then relay this signal by inducing cellular changes, including the inhibition of tyrosine phosphatases (15) and FcεRI-mediated cytokine production as part of the delayed-type allergic response (16).

Some transition metals have the capacity to promote one-electron oxidation-reduction processes under physiological conditions, and can therefore be used for electron transport in metalloproteins. The most biologically relevant and attainable redox couples for electron transfer are the Cu^{2+}/Cu^{+} and Fe^{3+}/Fe^{2+} pairs (17). An example of metal-containing electron transport proteins are the blue copper proteins in bacteria and plants. The designation "blue" derives from absorption properties of these proteins resulting from ligand-to-metal charge-transfer transitions (18). Plastocyanin, one of the first blue copper proteins discovered and characterized, is involved in the photosynthetic process, responsible for carrying electrons from cytochrome f to photosystem I (19). The Cu^{2+} ion in plastocyanin is reduced by cytochrome f in the thylakoid membrane. Plastocyanin then dissociates from cytochrome f and diffuses until it binds to photosystem I. Upon delivery of the electron to photosystem I, plastocyanin's metal ion is reoxidized to Cu^{2+} (2,20).

A final role of metals in biology is as oxygen transporters. The most well-known example of a metal used for dioxygen transport is iron in hemoglobin. Hemoglobin is an iron-containing protein found in red blood cells of vertebrates (21). The function of this protein is to transport dioxygen from the lungs to the tissues where it is used in respiration. Hemoglobin is an $\alpha_2\beta_2$ heterotetramer, with each subunit containing a heme group with an

iron center capable of binding a dioxygen molecule (Fig. 1.2). In the oxygen-bound state, the metal ion is coordinated by the N-donors of the porphyrin ring, by an axial histidine residue and the dioxygen molecule (22). Iron is not the only metal utilized for oxygen transport, as copper is used in hemocyanin, which plays the same role in the respiration of various arthropods and mollusks (23).

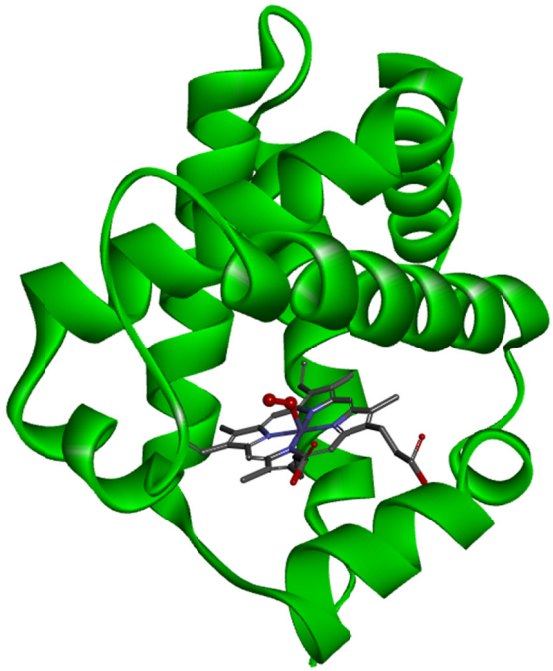

Figure 1.2: Structure of the α subunit of human oxyhemoglobin (PDB ID: 2DN1) (24). The protein is shown in green with the iron-containing central heme group. Dioxygen is shown as two red spheres binding the iron centre of the heme group.

In summary, although a large majority of biological mass derives from the CHNOPS elements, there is a profound dependence on metals for their unique properties in biological systems. The unique properties of individual metals, including their redox activity, ability to form stable complexes, and their bioavailability determine their role in biological systems (4).

1.2 Zinc in biology

One metal that is of particular interest in this thesis is zinc. Zinc is an essential nutrient that is required by all forms of life. It has been estimated that zinc binds approximately 10% of all proteins in the human proteome, is required for function in 2000 transcription factors, and is used in the active site of approximately 300 enzymes (25). These zinc enzymes have a wide range of biological functions, with members falling into each of the six classes of enzymes (see Table 1.2) (26). The average human body contains between 2 and 3 g of zinc, making it the second most abundant transition metal (after iron) (20).

Table 1.2: Examples of zinc enzymes for each enzyme class.

Enzyme class	**Zinc enzyme**	**Function**
1. Oxidoreductase	Alcohol dehydrogenase	Alcohol metabolism (27)
2. Transferase	RNA polymerase	RNA synthesis (28)
3. Hydrolase	Carboxypeptidase A	Pancreatic exopeptidase (29)
4. Lyase	Lactoylglutathione lyase	Isomerization of hemithioacetal adducts (30)
5. Isomerase	Mannose phosphate isomerase	Mannose 6-phosphate and fructose 6-phosphate interconversion (31)
6. Ligase	Pyruvate carboxylase	Pyruvate metabolism (32)

Zinc behaves as a borderline Lewis acid under biological conditions (33). This property allows it to fulfill a large variety of roles. It is capable of binding a huge range of biological ligands, including hard, soft, and borderline Lewis bases. Zinc is also appealing for biological systems as it has a flexible coordination geometry because of the already-mentioned lack of CFSE (due to its filled d-shell [d^{10}]). Typically, enzymes provide zinc with a tetrahedral coordination geometry in the natural (resting) state. As a substrate or ligand binds, the coordination state changes, often resulting in a coordination number of five.

Because zinc has no preference for a particular coordination geometry, the process of substrate binding (and product release) is typically rapid and efficient (1,4). Zinc is redox inert under biological conditions, which also makes it more suitable in a structural role or in the active sites of many enzymes.

Zinc levels must be tightly regulated in cells. Excess zinc results in toxicity while insufficient zinc levels result in deficiency, both of which have severe effects. In humans, excess zinc results in lethargy, nausea and vomiting, diarrhea, altered immune system function, and symptoms of copper deficiency, among others (25). The copper deficiency symptoms are a result of competitive absorption between zinc and copper in enterocytes. As cellular zinc levels increase, metal storage proteins (metallothioneins) are upregulated to handle the excess. Although this will reduce the toxic levels of zinc, it will also decrease the amount of copper physiologically available (25). Symptoms of moderate zinc deficiency include growth retardation, male hypogonadism in adolescents, skin lesions and decreased wound healing, poor appetite, mental lethargy, infertility, and cell-mediated immune disorders (34). For zinc levels to stay in a "healthy" range, a dietary intake of 11 mg/day for men and 8 mg/day for women is recommended (35).

1.3 Properties of zinc enzymes

There are several properties and characteristics that have been observed for many different zinc enzymes. These properties are a high zinc affinity at their metal-binding site, and a chemically labile active site metal. In addition, many zinc enzymes are inhibited by excess zinc, likely due to binding of a second zinc ion to an inhibitory site (36). These will

be discussed in detail as linking these independently studied properties is an objective of this thesis.

1.3.1 Metal binding affinities

As mentioned previously, living organisms must exert a high degree of control over cellular zinc levels. It is clear that zinc is required by a large number of crucial metalloproteins, yet excess zinc is cytotoxic. Although the concentration of free zinc will vary for individual organisms and cell type, it is generally in the mid-to-low picomolar range, and must be tightly regulated (37). Therefore, it is a requirement of cytosolic zinc-dependent enzymes to have a high (pico-to-femtomolar) affinity for zinc. If a protein is zinc-dependent, and it did not possess such high affinities, the protein would lose its functionality in the cytosol. An example of a zinc-dependent enzyme with an experimentally-determined zinc affinity is carbonic anhydrase. This enzyme is found in humans and is responsible for the reaction of carbon dioxide and water to form carbonic acid as follows:

$$CO_2 + H_2O \rightleftarrows H_2CO_3$$

This reaction is important for acid-base buffering in the blood of mammals. Zinc is required in the active site of this enzyme to bind and polarize the water molecule, allowing for the reaction to proceed efficiently (38). The dissociation (pseudo)constant for zinc was experimentally determined to be between 5 and 10 pM (39), which is not only a value typical for many zinc proteins, but is also in line with the requirement of cytosolic zinc enzymes to have a high affinity for the metal ion (Table 1.3).

Table 1.3: Dissociation constants of various eukaryotic zinc proteins (40).

Zinc enzyme	Dissociation constant [a]	Reference
Carboxypeptidase A, bovine	32 pM	(41)
Sonic hedgehog, human	<100 pM	(42)
Glyoxalase I, human erythrocytes	25 pM	(43)
Dipeptidyl peptidase III, rat liver	500 fM	(44)
Carbonic anhydrase II, human	4 pM	(45)

[a] The dissociation (pseudo)constant is defined as $K_d = ([Zn^{2+}][E]/[E\text{-}Zn])$.

1.3.2 Metal exchange in zinc enzymes

A second property that is common to many zinc-dependent enzymes is a chemically labile active site, in that metal exchange can occur relatively rapidly. In biological systems, the active sites of metalloenzymes can be quite dynamic. The metal bound to an active site is likely to undergo exchange with metals from solution under biological conditions. Interestingly, many metalloproteins are known to be capable of using different metals in their active site. As such, a zinc protein could remain functional with other metals bound (e.g. Cu^{2+} or Co^{2+}) (13). This is beneficial to the cell as the bioavailability of some metals may fluctuate, hence allowing for other metals to be used in times of scarcity of the native metal. Ribulose-5-phosphate 3-epimerase (Rpe) of *Escherichia coli*, an enzyme used to interconvert D-ribulose 5-phosphate and D-xylulose 5-phosphate as part of the pentose phosphate pathway, is an example of an enzyme that uses metal substitution in times of cellular stress to remain functional. Under normal conditions, Rpe uses Fe^{2+} in its active site to coordinate its substrate and to stabilize the intermediate oxyanion (46). The ferrous ion is solvent-exposed, and therefore susceptible to oxidation. During times of oxidative stress (experimentally induced by H_2O_2), Fe^{2+} is oxidized, which results in the loss of iron from the active site (47). It has been shown that Mn^{2+} reactivates Rpe by replacing the iron centre, which allows for the pentose phosphate pathway to remain operative during times of H_2O_2-induced oxidative

stress (47). This substitution is possible because of two key factors in the H_2O_2 stress response: an increased manganese import and an increased iron sequestration (47,48). The decreased availability of iron and the increase in the cellular concentration of manganese allows the latter metal to reactivate Rpe (47). Similar metal exchanges and substitutions have been observed for many different metalloenzymes, including ribonucleotide reductase and histone deacetylase 8 (17,49,50). However, the mechanism and rates at which these exchanges occur are not often described in the literature.

In general, there are two mechanisms by which metal exchange can occur: via a dissociative (D- or S_N1-type) or an associative (A- or S_N2-type) pathway (51). In a dissociative mechanism, the protein-bound metal must dissociate in the first step, generating an apoprotein. This dissociation event is the rate-determining step in a D-type mechanism. In the following step, the metal-free protein binds a metal from solution to complete the exchange process (see Fig. 1.3 A).

In an associative exchange, the first step is the formation of a bond between the incoming metal and the metal-protein complex, temporarily forming a two-metal species, or ternary complex. The originally-bound metal then dissociates from the protein, completing the exchange process (see Fig. 1.3 B). The rate of this exchange process is determined by the first step (i.e., the association of a second metal to form the two-metal species).

A $\quad 1.\ \text{E-M}_1 \rightleftarrows \text{E} + \text{M}_1$ (D-type, S_N1)

$\quad 2.\ \text{E} + \text{M}_2 \rightleftarrows \mathbf{\text{E-M}_2}$

B $\quad 1.\ \text{E-M}_1 + \text{M}_2 \rightleftarrows \text{E-M}_1\text{M}_2$ (A-type, S_N2)

$\quad 2.\ \text{E-M}_1\text{M}_2 \rightleftarrows \mathbf{\text{E-M}_2} + \text{M}_1$

Figure 1.3: Scheme representing D-type and A-type exchange mechanisms. E represents the enzyme, M_1 the original active site metal, and M_2 the substituting metal.

It is possible to predict which of these mechanisms is operative during an exchange process if the dissociation constants (K_d, see Table 1.3 for definition) are known. If a dissociative mechanism is assumed, an upper limit for the dissociation rate constant (k_{off}) can be estimated using equation 1:

$$k_{off} = K_d k_{on} \qquad \text{(eq. 1)}$$

where k_{on} is the association rate constant. For instance, if a K_d value of 10^{-13} M is assumed (a value typical of some zinc enzymes (40)), and k_{on} is set to 10^9 M^{-1} s^{-1}, a value approximating the diffusion limit (52), the upper limit of k_{off} can be estimated as $k_{off} \sim 10^{-4}$ s^{-1}. Since the release of the metal ion from a mononuclear holoenzyme is a unimolecular step, a lower limit of the corresponding half-life, i.e., the time required for half of the protein-bound metal to be released ($t_{1/2}$), can be estimated using equation 2:

$$t_{1/2} = \frac{\ln 2}{k_{off}} \qquad \text{(eq. 2)}$$

In the case of k_{off} being 10^{-4} s^{-1}, it would take approximately 2 h for half of the metal to be released from the protein if a purely dissociative mechanism is assumed ($t_{1/2} \sim 7000$ s). Hence, if metal exchange were to proceed via a D-type mechanism, the time required for

exchanging half of the native metal with the desired extraneous metal would be greater or equal to 7000 s. Interestingly, based on cases where the kinetics of metal exchange have been studied and the dissociation constants are known to be in the femtomolar or low picomolar range, it becomes apparent that the exchange process occurs too quickly to be accounted for by a dissociative mechanism (53).

The kinetics of metal exchange are quite well-studied for metallothioneins. These proteins are located in the cytoplasm, where they function as metal buffers involved in the transport and storage of crucial metals, including zinc and copper (54). They also play a role in the detoxification of metals including cadmium, arsenic, and mercury. Metallothioneins are quite efficient at binding metals for a protein of small size (14 kDa), with a total of seven metal binding sites. The dissociation constant for rabbit zinc metallothionein (MT1) is quite low at $K_d = 5\times10^{-13}$ M (40,54,55), yet metal exchange occurs rapidly. One study showed that Zn-loaded metallothionein can donate zinc to apoCA in a time similar to that required for the reconstitution of apoCA with free Zn^{2+} (as $ZnCl_2$) in solution. This metal transfer process has a rate 10^3 times higher than that observed for the zinc transfer between Zn-loaded metallothionein and ethylenediaminetetraacetic acid (EDTA), which has a half-time ($t_{1/2}$) of exchange of > 20 h (56). EDTA is an S_N1-type chelator often used to determine dissociation rate constants in metalloproteins (1,57). These results give strong evidence to suggest that metal removal from metallothionein cannot proceed using a dissociative mechanism, and that there must be an alternative mechanism of exchange in order to explain the high metal exchange rates. The ability of metallothionein to have such high kinetic lability despite such low dissociation constants is attributed to the oxidation/reduction properties of the zinc-sulfur clusters that house the metal (Fig. 1.4) (55). The high affinity state occurs under standard

reducing conditions that allow for the formation of cysteine-Zn bonds in the metal binding sites. Under oxidizing conditions, disulfide bonds form, decreasing the ligand/zinc ratio (to < 4). This drastically lowers the affinity of metallothionein for zinc, thus making the metal kinetically labile (55).

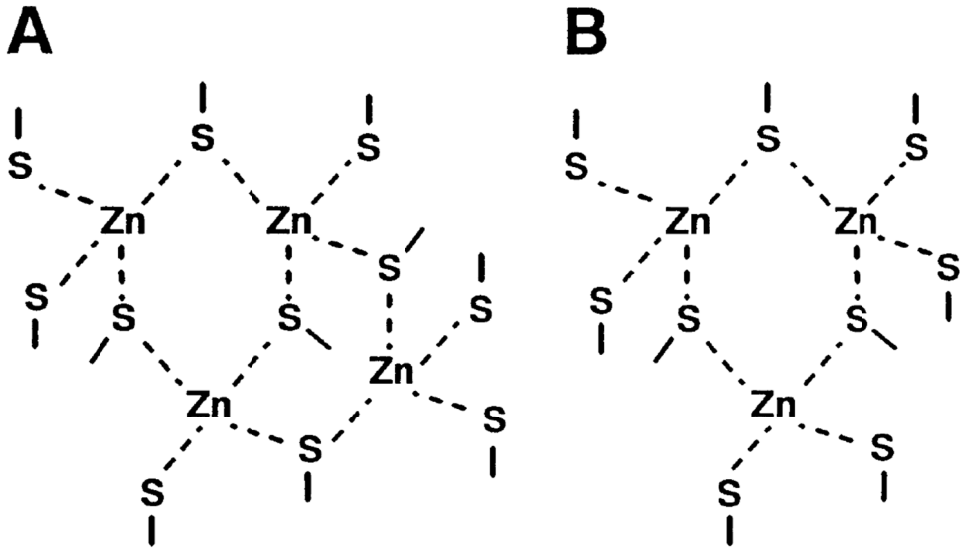

Figure 1.4: Zinc-sulfur clusters in mammalian metallothionein. The four-zinc cluster from the α-domain (A) and the three-zinc cluster from the β-domain (B) are shown under standard (reducing) conditions. Figure taken from (55).

However, cysteine residues are not present in several metal-binding proteins that are still capable of rapid metal exchange. Thus, in proteins in which cysteine residues are absent, there must be additional factors that underlie the apparent *paradox* of high metal affinity and rapid metal exchange. One example is thermolysin, a zinc-dependent metallopeptidase from *Bacillus thermoproteolyticus*. The zinc ion is coordinated by two histidine residues and one glutamate residue in the active site of this protein (6). The dissociation constant has been experimentally determined to be $K_d = 2\times10^{-13}$ M (58), a value similar to that determined for metallothionein discussed above. Hence, if metal exchange were to occur via a dissociative mechanism, a $t_{1/2}$ value of > 3500 s should result. However, a research group studying

cobalt-substitution in thermolysin noted that "…the ready mutual exchange of cobalt for enzyme-bound zinc and of zinc for enzyme-bound cobalt implies a rapid equilibrium between enzyme-bound and free metal" (59). Based on this knowledge, it is probable that metal exchange in thermolysin proceeds via an associative mechanism, implying the formation of a di-metal species, and hence the hypothesis that a second metal binding site must be present. Interestingly, a two-zinc state, in which a second "inhibitory" zinc ion binds in the vicinity of the active site metal has been observed crystallographically for several zinc-dependent enzymes (60-62).

1.3.3 Inhibition of Zinc-dependent enzymes

As mentioned earlier, another feature of zinc enzymes is that many of them are inhibited by excess zinc, most likely through the binding of the metal to a second site in the protein, or as a second (inhibitory) zinc ion at the active site. An example where this has been clearly demonstrated is carboxypeptidase A (CPA), the best studied zinc protease. This enzyme is a pancreatic exopeptidase which breaks down proteins in the digestive process. It preferentially cleaves hydrophobic amino acids from the C-terminal position in proteins (63). The crystal structure (Fig. 1.5) of the zinc-inhibited form of CPA shows two zinc ions, one in the active site and one directly adjacent to it (i.e., akin to an "inhibitory site") (62,64). The ligands of the inhibitory Zn^{2+} are a glutamate residue, a water that bridges to the Zn^{2+} ion at the active site, a chloride ion and a water molecule (64).

The active site zinc ion is coordinated by two histidine residues, a glutamate residue, and a water molecule, which serves as the nucleophile in the peptide bond cleavage reaction (62,64). The second zinc ion binds and inhibits the enzyme by preventing substrate binding

to the active site (competitive inhibition) (65). Interestingly, the active site zinc ion can be exchanged or substituted with other metals, including Ni^{2+}, Co^{2+}, Fe^{2+}, Mn^{2+}, Cr^{3+}, with activities ranging from 350% (Co^{2+}) to 25% (Cr^{3+}) when compared to the activity of the zinc form (29).

Figure 1.5: Crystal structure of bovine carboxypeptidase A in the zinc-inhibited form (PDB ID: 1CPX) (64). The protein is shown in green, with both active site and inhibitory zinc ions shown as black spheres (along with their coordinating residues). In the structure shown, the occupation of the inhibitory zinc site was estimated to be 0.5.

A second example of a zinc-dependent enzyme inhibited by excess zinc is uridine diphosphate-(3-*O*-(R-3-hydroxymyristoyl))-*N*-acetylglucosamine deacetylase (LpxC), a protein found in virtually all Gram-negative bacteria crucial for lipid A (endotoxin) biosynthesis (61). Similar to CPA, LpxC is inhibited by excess zinc, where the inhibitory binding site is located directly adjacent to the active site zinc ion (see Fig. 1.6). The active site zinc ion is coordinated by two histidine residues and an aspartate residue, with its fourth ligand being a water molecule. In the zinc-inhibited form, this water molecule forms a

bridge between the active and inhibitory site zinc ions, the latter of which is also protein-bound by a histidine residue and a glutamate residue. The fourth ligand in the inhibitory zinc site is a solvent molecule (61).

Interestingly, LpxC is also capable of active site metal substitution. The active site Zn^{2+} ion can be exchanged with Fe^{2+} depending on the cellular conditions. The Fe^{2+}-containing protein has an enzymatic activity 6-8-fold greater than that of the zinc form (66). Zinc has a much lower dissociation constant of 60 pM, compared to 100 nM for iron (66). However, iron is more readily abundant *in vivo*, resulting in a mixture of Fe^{2+} and Zn^{2+} in the active site of LpxC when expressed in *Escherichia coli* in various growth media (66).

Figure 1.6: Crystal structure of zinc-inhibited LpxC from *Aquifex aeolicus* (PDB ID: 1P42) (61). Active site and inhibitory zinc ions are shown as black spheres with a bridging water ligand in red.

The enzyme CphA from *Aeromonas hydrophila* is another zinc-dependent hydrolase. It is a metallo-β-lactamase that has a high specificity for penems and carbapenems, and is therefore involved in protecting this organism from these β-lactam antibiotics (67). The β-

lactamases function by cleaving the β-lactam ring in β-lactam antibiotics, which results in a loss of antibiotic activity (68). There are three subclasses of metallo-β-lactamases: B1, B2, and B3. Subclasses B1 and B3 have the highest level of activity with two zinc ions present in their active site (69). However, subclass B2 enzymes (to which CphA belongs), are only functional with one zinc ion bound. The binding of a second zinc ion results in inhibition, and hence an inactive enzyme. This makes this enzyme quite unique when compared to other metallo-β-lactamases. In the active form of CphA, the single zinc ion is coordinated in the high affinity site by an aspartate residue, a cysteine residue, and a histidine residue (70,71). The inhibitory zinc ion is coordinated to two histidine residues, along with a sulfate ion and a water molecule (Fig. 1.7) (69). This inhibitory site has a dissociation constant of 46 μM at pH 6.5 (69,71).

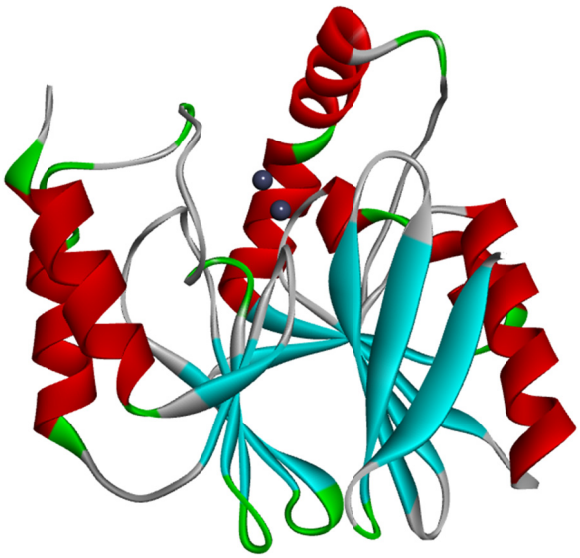

Figure 1.7: Crystal structure of zinc-inhibited CphA from *Aeromonas hydrophila* (PDB ID: 3F9O) (69). Active site and inhibitory zinc ions are shown as grey spheres.

Another example of a zinc-dependent enzyme that is inhibited by excess zinc is thermolysin. Thermolysin is a zinc-dependent endopeptidase from *Bacillus thermo-proteolyticus*. It targets hydrophobic amino acid residues and cleaves peptide bonds to allow

for uptake of protein fragments by the cell (72). It has been crystallized in its zinc-inhibited form (Fig. 1.8).

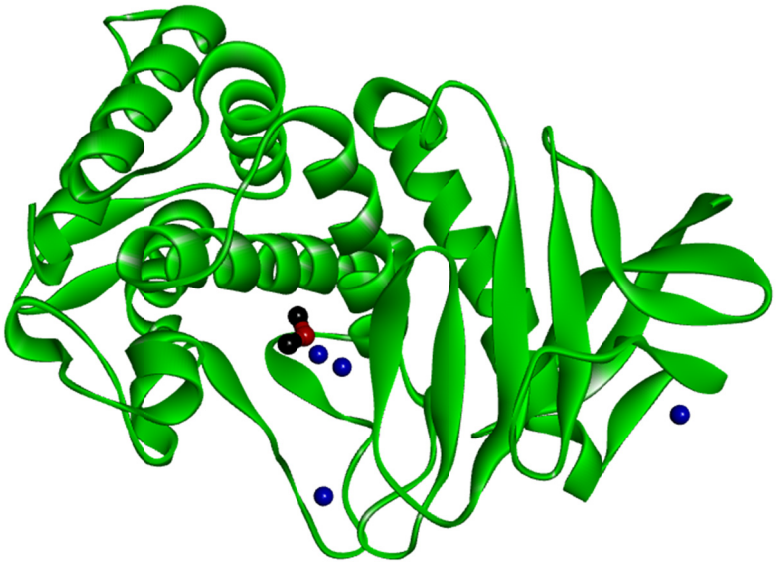

Figure 1.8: Crystal structure of zinc-inhibited thermolysin (PDB ID: 1LND) (60). Active site and inhibitory zinc ions are shown as black spheres with a bridging water ligand (red). Structural calcium ions are shown in blue.

The second zinc ion inhibits the enzyme by steric exclusion of the substrate in the active site (competitive inhibition) (59). The inhibitory zinc ion is bound by a histidine residue and a tyrosine residue, and has a significantly lower affinity for the protein than the active site zinc ion (60).

A final example of a zinc-dependent enzyme which possesses all three of the aforementioned properties (high zinc affinity, kinetically labile active site, and inhibition by excess zinc) is anthrax lethal factor (LF), which will be discussed in detail in the following section and is the focus of this thesis.

1.4 Lethal factor

LF is zinc-dependent endopeptidase, and one of the three components of the anthrax toxin (73), a major virulence factor of anthrax, the potentially lethal disease resulting from infection with *Bacillus anthracis* (74). Edema factor (EF) and protective antigen (PA) are the other two components of this toxin.

1.4.1 Translocation and molecular targets of LF

PA binds to anthrax toxin receptors (ATRs), which are expressed on the surface of host cells (75). The two ATRs currently identified are tumor endothelial marker 8 (TEM8, ATR1) and capillary morphogenesis gene-2 (CMG2, ATR2) (76). Once PA is associated with ATRs, a 20 kDa fragment is cleaved by furin-like cell-surface membrane proteases, and released into the extracellular fluid. This cleavage allows for PA oligomerization, forming a heptamer or octamer pre-pore (76). The pre-pore is capable of binding up to three (heptamer) or four (octamer) molecules of LF or EF, which is then endocytosed and trafficked to endosomes. As the endosome becomes more acidic, the decreased pH allows for structural changes in PA which result in the insertion of the PA oligomer into the membrane, thus forming a pore. This event is followed by the translocation of bound LF and EF into the cytosol (Fig. 1.9). Here, EF converts cellular adenosine triphosphate (ATP) into cyclic adenosine monophosphate (cAMP). This significantly increases cellular levels of cAMP (while rapidly depleting cellular ATP levels), which disrupts water homeostasis in cells (76). As a result, organisms subject to cutaneous exposure to the anthrax toxin present with edema (74). Once inside the cytosol, LF targets and cleaves mitogen-activated protein

kinase kinases (MAPKK), resulting in the disruption of cellular signaling pathways, followed by apoptosis (77).

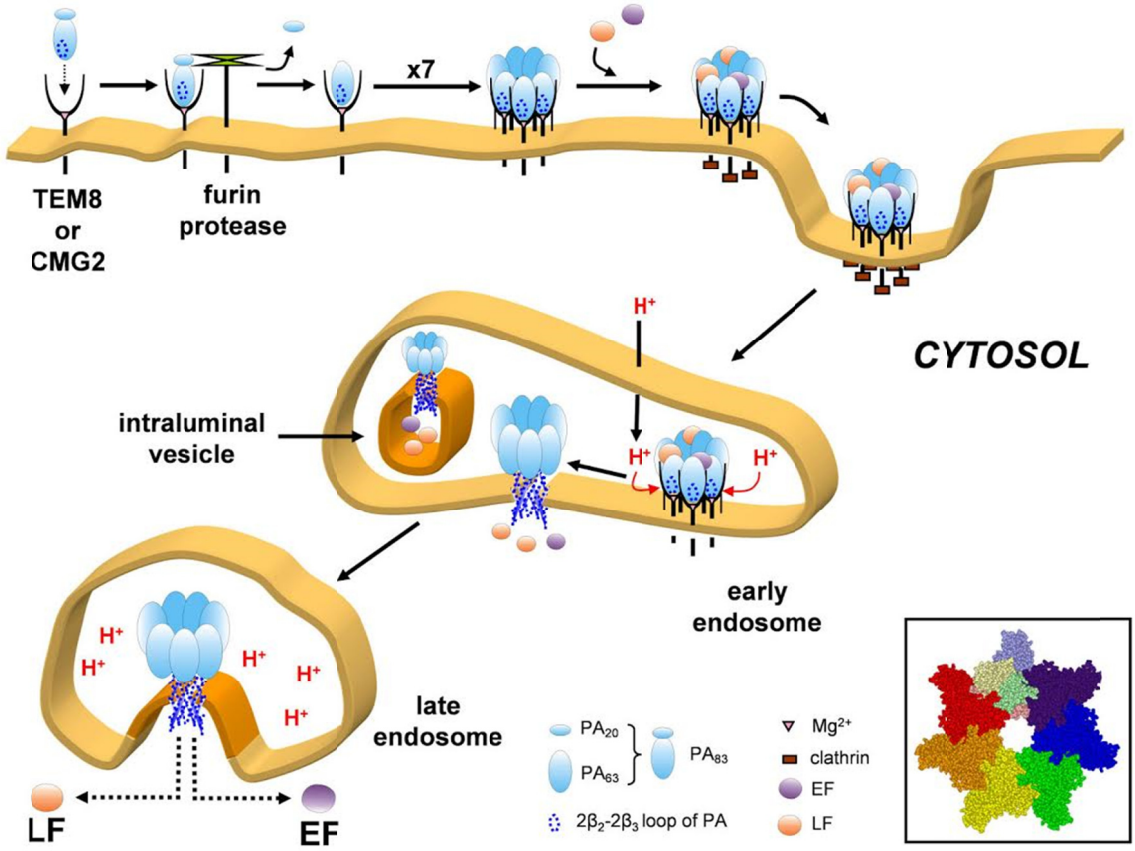

Figure 1.9: Process of LF and EF entry into the cell. Figure (unpublished) courtesy of Dr. Stefan Siemann.

Inflammasomes have been identified as a second target of LF (78). The inflammasome is a multiprotein complex which forms in response to various danger signals in the cell (79). These danger signals include pore-forming toxins, intracellular bacteria, fungi, and β-amyloid (78). LF targets and activates the sensor component of the inflammasome (nod-like receptor protein 1, Nlrp1), which initiates caspase-1 recruitment, activation, and eventually pyroptosis (78). This is the mode by which LF can cause such rapid cell death (1 – 3 h) in macrophages and dendritic cells (78).

1.4.2 Structure of LF

The crystal structure of LF is shown in Figure 1.10. LF contains four domains. While domain I recognizes and binds PA, domains II, III, and IV form the substrate binding pocket. The catalytic site with the zinc ion is housed in domain IV (80). The zinc ion is coordinated in the active site by two histidine residues (His686, His690), a glutamate residue (Glu735), and a water molecule in a fashion similar to that observed for thermolysin (60,80). During catalysis, a glutamate residue (Glu687), which is a part of the HExxH thermolysin-like consensus motif, acts as a general base, activating the zinc-bound water molecule and allowing hydrolytic cleavage of its target (81).

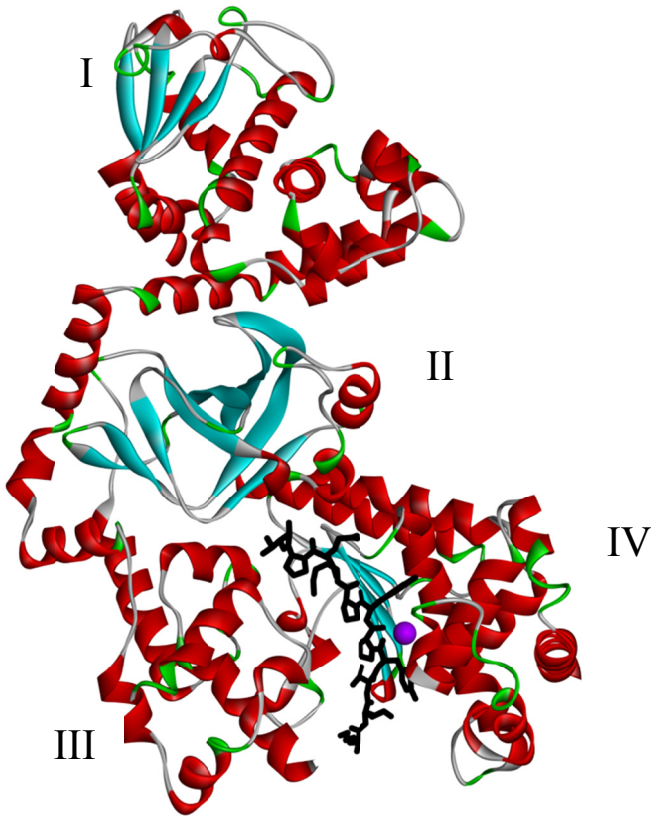

Figure 1.10: Crystal structure of LF complexed with the LF20 peptide substrate (PDB ID: 1PWW) (82). The LF20 substrate is shown in black in its binding pocket. The Zn^{2+} ion is depicted in purple. The individual domains of LF are indicated by Roman numerals.

There is interest in studying LF due to the disease and high mortality it causes in humans and animals, and the threat of anthrax as a weapon of bioterrorism (74). Several physico-chemical properties of this protein have been elucidated through previous research. For instance, the metal binding affinities for zinc, cobalt, and copper are known (see Table 1.4).

Table 1.4: Dissociation constants of various LF species.

LF species	Dissociation Constant (K_d) [a]	Reference
ZnLF	1.2 pM	(83)
CoLF	75 pM	(84)
CuLF	340 fM	(85)

[a] K_d values were determined in Hepes buffer (50 mM, pH 7.4).

The K_d values are in the pico-to-femtomolar range, with copper being the most tightly bound, followed by zinc and cobalt. This order of binding affinities is expected, and can be explained by the Irving-Williams series (7,85). As previously discussed, the magnitude of these dissociation constants is typical of zinc-dependent enzymes.

Metal exchange has been utilized to prepare metal-substituted LF, although the kinetics underlying this process have not been extensively studied (85). Finally, inhibition by multiple metals including Zn^{2+}, Cu^{2+}, Mg^{2+}, Ca^{2+}, and Tb^{3+} has also been observed in LF (83,85).

1.4.3 Metal exchange in LF

The active site of LF is capable of metal substitution resulting in a functional enzyme. Two methods to generate metal-substituted LF have been described: (i) by adding metal to apoLF (which had been generated by removing the active site metal with chelators), and (ii) by a *direct exchange* process, where the substituting metal is provided extraneously to the

zinc form of LF. These processes have been used to generate multiple metal-substituted variants of LF. As Fig 1.11 shows, the level of enzymatic activity in metal-substituted LF is dependent on the nature of the metal introduced into the active site. LF substituted with Co^{2+} (~220%), Ni^{2+} (~220%), or Cu^{2+} (~450%) has an activity that is significantly higher than that of native ZnLF (85). The kinetics of metal exchange have not been extensively studied in LF, although the active site metal has been observed experimentally to exchange relatively rapidly (e.g., CoLF can be prepared by incubation of ZnLF with excess extraneous Co^{2+} in solution in as little as 10-15 min) (84).

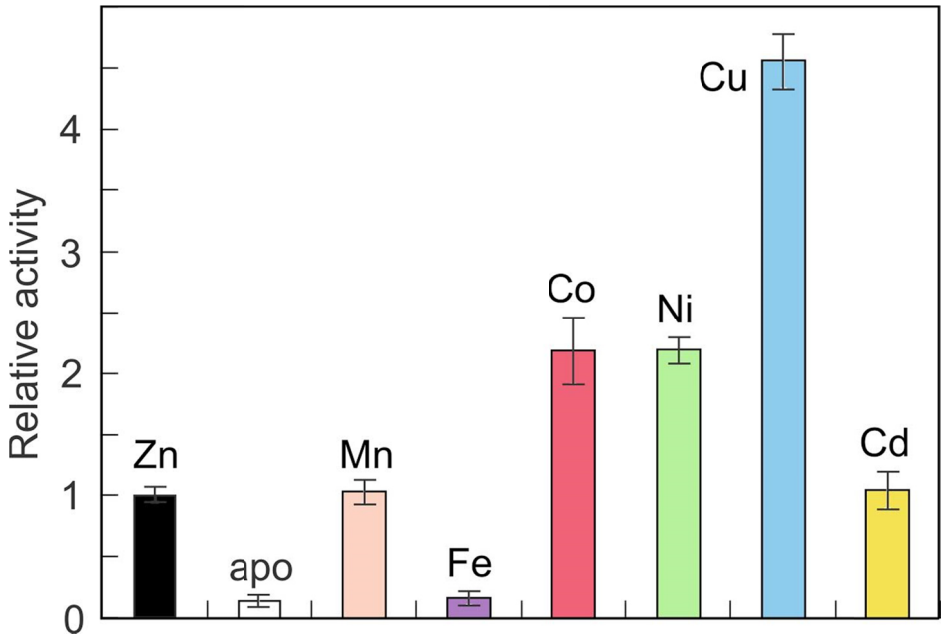

Figure 1.11: Reactivation of apoLF with transition metal ions. Activities are expressed relative to that of native ZnLF. Figure adapted from (85).

1.4.4 Inhibition of LF with metals

Many zinc-dependent enzymes are inhibited by an excess of zinc and other metals (36). LF is no exception to this. The inhibition of LF by excess zinc has been investigated previously, with a half maximal inhibitory concentration (IC_{50} value) of approximately 12 μM (85). LF is also known to be inhibited by Cu^{2+} in the same micromolar range, with an

IC_{50} value of ~15 μM (85). Although there is no direct evidence to suggest that the inhibitory site is directly adjacent to the active site, a crystal structure of the closely related protease thermolysin in its zinc-inhibited form (as previously discussed, see Fig. 1.8) is available, showing that the inhibitory site is located directly adjacent to the active site. Both LF and thermolysin belong to the gluzincin clan, a family of zinc-dependent enzymes characterized by an HExxH...E zinc binding motif, where the zinc is bound to two histidine residues, a glutamate residue (downstream of the HExxH motif), and a water molecule (86). Whether the inhibitory metal binds LF in a site similar to that observed for thermolysin remains to be established experimentally.

Inhibition of LF by alkaline earth metals (Ca^{2+}, Mg^{2+}) has been observed in the low millimolar range (83). However, little is known about how these metals exert their inhibitory effect on LF since there is no information on the location and number of inhibitory Ca^{2+}/Mg^{2+}-binding sites. Nonetheless, studies using Tb^{3+}, a luminescent probe for Ca^{2+}-binding sites (see section 1.5), have revealed that LF is not only inhibited by the trivalent metal ion (IC_{50} ~23 μM), but also competes directly with Ca^{2+} for the aforementioned low-affinity binding site for alkaline earth metals (83). Whether the binding site for inhibitory Zn^{2+}, Cu^{2+}, Ca^{2+}, Mg^{2+}, and Tb^{3+} in LF are one and the same remains to be established.

1.5 Terbium in metalloprotein studies

Terbium is a lanthanide ion often used to explore the properties of metalloproteins. Although terbium is not essential to biological systems, it is useful for its spectroscopic properties as a replacement for Ca^{2+} in calcium-binding proteins (87). The Tb^{3+} ion can mimic Ca^{2+} mimic due to its similar ionic radius, its preference for hard oxygen donor

ligands, and its adaptable coordination geometry (ranging from 6- to 12-coordinate), with 8 and 9 ligands being the most common (87). Typically, substitution of Ca^{2+} by Tb^{3+} in calcium-dependent proteins has little impact on the activity/function of these proteins, with thermolysin and parvalbumin serving as prototypical examples (88). However, there are differences in how Tb^{3+} and Ca^{2+} interact with proteins. For instance, Tb^{3+} has slower ligand exchange rates (compared to Ca^{2+}), and a higher affinity for calcium sites (87,89). These differences can be exploited when investigating Ca^{2+} sites, as it allows for studies to be performed at low concentrations of Tb^{3+}. In addition, the lower chemical lability of Tb^{3+} ensures it remains protein-bound under experimental conditions.

Terbium is most often used in luminescence studies as it is a strong emitter. In particular, tyrosine-sensitized Tb^{3+} luminescence spectroscopy is a technique employed to characterize the interaction of Tb^{3+} with Ca^{2+}-binding proteins. The spectral overlap of tyrosine emission and Tb^{3+} absorption/excitation spectra gives rise to Förster resonance energy transfer (FRET). In this case, excitation of tyrosine residues (~275 nm) can lead to energy transfer to nearby Tb^{3+} ions, which will then emit at ~545 nm (90). Thus, when Tb^{3+} is protein-bound, it will have a dramatically stronger emission intensity than free Tb^{3+} in solution (i.e., in the absence of tyrosine residues) (91).

The energy transfer can be used in various ways to study protein-metal interactions. For example, thermolysin binds both calcium (and therefore terbium), and zinc in its native state. The zinc ion in Tb^{3+}-loaded thermolysin can be replaced by Co^{2+}, a metal ion that quenches Tb^{3+} luminescence (92). By quantifying the degree of this quenching process in thermolysin, the distance between a (Tb^{3+}-housing) calcium binding site and the active site was estimated to be 13.7 Å (93), a value identical to the distance determined using

crystallographic analysis of native thermolysin (94). Hence, Tb^{3+} is a metal useful for the spectroscopic characterization of calcium-binding sites in proteins and may be useful to elucidate the location of the inhibitory site in LF.

2. Hypothesis and Objectives

The hypothesis of this research is that metal exchange in LF (and similar zinc enzymes) occurs via an associative mechanism, and that the second metal binding site required for an associative exchange is the same as the inhibitory metal binding site in LF. In other words, we propose that the metal exchange process occurs by forming a transient di-metal species through the occupation of the inhibitory metal binding site, followed by the release of the initially bound active site metal.

To obtain evidence in support of this hypothesis, LF will be used as a model zinc enzyme. The objectives of this research are to first experimentally determine the dissociation rate constants for Zn^{2+}, Co^{2+}, and Cu^{2+}-containing LF by competition assays with EDTA; according to our hypothesis, one would expect the dissociation process to be slow. Secondly, the metal exchange rates for ZnLF in the presence of Co^{2+} and Cu^{2+} will be determined using activity assays. The property of LF that will be exploited in order to gain insight into the rates of metal exchange is that the level of enzymatic activity is dependent on the type of metal in the active site. Therefore, the exchange process can be monitored by following the activity of the enzyme over time. Furthermore, the rate of naturally abundant zinc (^{64}Zn [48.9%], ^{66}Zn [27.8%], ^{67}Zn [4.1%], ^{68}Zn [18.6%], ^{70}Zn [0.6%]) to ^{70}Zn exchange will be monitored by ICP-MS. Investigations into the inhibition of LF by metals will also be conducted to identify if Co^{2+} has an inhibitory effect on LF, and the mode of inhibition that both Zn^{2+} and Cu^{2+} exert on LF will be determined. Finally, the location of the inhibitory Tb^{3+}-binding site will be determined by competition with other inhibitory metals (Cu^{2+}, Zn^{2+}) using tyrosine-sensitized terbium luminescence spectroscopy. The effect of Tb^{3+} on metal exchange rates will be assessed using both activity assays and ICP-MS.

Determining the mechanism of metal exchange in metalloenzymes is important since metal exchange is a simple method for the preparation of metal-substituted proteins. Zinc, due to its d^{10} configuration, is not amenable to multiple spectroscopic techniques employed to study metalloproteins, such as UV-Vis spectroscopy or electron paramagnetic resonance spectroscopy (EPR). Hence, the metal-binding sites of many zinc-dependent proteins are often studied after substitution with metals that can be observed using these techniques (e.g., Cu^{2+}, Co^{2+}); understanding the mechanism behind metal exchange in these proteins may be of use in optimizing these procedures.

3. Materials and Methods

3.1 Chemicals

Table 3.1: List of chemical reagents and suppliers.

Supplier	Reagent
Amersham Biosciences (Little Chalfont, UK)	Q-Sepharose Fast Flow
BioShop Canada Inc. (Burlington, ON)	Ammonium acetate LB Agar Miller D-Xylose Glycerol Polyethylene glycol 8000 (PEG-8000) Tetracyclin hydrochloride Tryptone Sodium perchlorate Tris(hydroxymethyl)aminomethane (Tris) 4-(2-Hydroxyethyl)-1-piperazineethanesulfonic acid (Hepes) Yeast Extract
Biomatik Corporation (Cambridge, ON)	Anthrax lethal factor protease substrate II (*S-p*NA)
Fisher Scientific Canada (Whitby, ON)	Acetic acid Acrylamide Bis-acrylamide Dimethyl sulfoxide (DMSO) Glycine Guanidine hydrochloride (Gdn-HCl) Hydrochloric acid Methanol Nitric acid Sodium dodecyl sulphate
Sigma-Aldrich (St. Louis, MO)	Ammonium persulfate (APS) Antifoam Y-30 Emulsion Bromophenol blue Chelex 100 sodium form; 50-100 mesh (dry) Coomassie Brilliant Blue R-250 Dipicolinic acid (DPA) Ethylenediaminetetraacetic acid (EDTA) Indium standard for ICP-MS 4-(2-Pyridylazo)resorcinol (PAR) Tetramethylethylenediamine (TEMED) TraceSELECT water Urea Zinc standard for ICP-MS

All metal salts (analytical reagent grade) were purchased from Sigma-Aldrich (St. Louis, MO) as sulfate or chloride salts. All other chemical reagents were obtained from the suppliers indicated in Table 3.1.

3.2 General methods

3.2.1 Solution and buffer preparation

Unless stated otherwise, all solutions were prepared in MilliQ ultrapure water (≥ 18.2 MΩ cm resistivity). In the case of buffers, pH adjustments were done using minimal volumes of 1 M sodium hydroxide or hydrochloric acid. Hepes buffer was used at 50 mM and pH 7.4 for all experiments. Trace metal certified pipette tips were used for the preparation of all solutions.

S-*p*NA (a 14-mer peptide of the sequence Ac-Gly-Tyr-β-Ala-Arg-Arg-Arg-Arg-Arg-Arg-Arg-Arg-Val-Leu-Arg-*p*NA) stock solutions were prepared by adding approximately 1 mg of *S*-*p*NA to 1 mL of Hepes buffer (50 mM, pH 7.4), and were stored at -20 °C. The concentration of the *S*-*p*NA stock solutions was determined spectrophotometrically at 342 nm using an extinction coefficient of $\varepsilon_{342nm} = 8270\ M^{-1}\ cm^{-1}$ (95).

Stock solutions (2 mM) of 4-(2-pyridylazo)resorcinol, PAR, were prepared by dissolving the compound in Hepes buffer (50 mM, pH 7.4) containing 5% (v/v) dimethyl sulfoxide (DMSO). Due to its light sensitivity, the solutions were stored at 4 °C in a 15 mL centrifuge tube wrapped in aluminum foil.

A ^{70}Zn stock solution was prepared by dissolving 10.29 mg of the ^{70}Zn metal (Cambridge Isotope Laboratories, Tewksbury, MA) in 88.41 μL of 5 M HNO_3 (3:1 molar ratio of HNO_3:Zn). This solution was diluted to 50 mM ^{70}Zn using TraceSELECT water and

kept at 4 °C as a working stock in a 15 mL centrifuge tube wrapped in aluminum foil. The isotopic distribution of the metal was $^{64}Zn < 0.02\%$, $^{66}Zn < 0.02\%$, $^{67}Zn = 0.16\%$, $^{68}Zn = 4.49\%$, and $^{70}Zn = 95.35\%$, as determined by the supplier. The molecular weight based on the isotopic enrichment was 69.83 g/mol.

Tetracycline stock solutions were prepared at 10 mg/mL in 70% (v/v) ethanol in water, and stored at -20 °C.

3.2.2 Solution treatment for trace metal analysis

For some studies, the concentrations of contaminating metal ions were minimized by treatment of buffers with Chelex 100 resin. Chelex 100 was added to the buffer solutions at 1.5 g per 100 mL. The solution was stirred for a minimum of 3 h at 25 °C using a shaker, after which time the resin was allowed to settle to the bottom of the flask for 24 h. The solution was transferred into a fresh clean tube using trace metal-certified pipette tips, and stored until further use.

3.2.3 Sterilization technique

All glassware used for cell cultivation, including Erlenmeyer flasks, the fermenter, and any pipette tips used for handling cells were autoclaved (at 121 °C and 15 psi for 30 min) using an AMSCO 3021 Gravity Sterilizer (Alfa Medical, Hempstead, NY).

3.3 Isolation of LF

In order to conduct the majority of this research pure samples of concentrated zinc lethal factor (ZnLF) were required. These samples were obtained by modifying a published

procedure that allows for the expression, purification, and concentration of LF from *Bacillus megaterium* containing the plasmid pWH1520 (84), which carries the gene for wild-type LF and a tetracycline resistance cassette. The cell line was provided by Dr. J. Mogridge (Dept. of Laboratory Medicine and Pathobiology, University of Toronto, Toronto, Canada).

3.3.1 Cell culture and protein expression

Agar plates were prepared with a solution containing 40 g LB Agar (Miller) powder (10 g tryptone, 5 g yeast extract, 10 g sodium chloride, 15 g agar) per L of water. Tetracycline was added to the agar at a final concentration of 10 μg/mL following sterilization. After the agar had settled and cooled, plates were stored at 4 °C until the addition of cells. A few microliters of a *Bacillus megaterium* stock (stored at -80 °C) were added to the plate using an aseptic streaking technique. These plates were sealed with Parafilm and placed bottom-up in an EchoTherm chilling incubator (Torrey Pines Scientific Inc., Carlsbad, CA) at 37 °C for 24 h.

A 150 mL starter culture solution was prepared using autoclaved LB Broth, Miller (10 g tryptone, 5 g yeast extract, 10 g sodium chloride per L of water). The starter culture was inoculated with a colony from an agar plate using a sterile loop (under aseptic conditions). Tetracycline was added to the broth at a final concentration of 10 μg/mL. Cells were grown in an Innova 4300 incubator shaker (New Brunswick Scientific, Edison, NJ) at 230 rpm and 37 °C until an OD_{600} of 1.6 – 1.7 was reached (typically after 16 h).

A volume of 2.7 L of Terrific Broth containing 36 g tryptone, 72 g yeast extract, and 12 mL glycerol was prepared in a BioFlo 110 fermenter (New Brunswick Scientific, Edison, NJ). A volume of 300 mL phosphate buffer was prepared containing 6.93 g potassium

dihydrogen orthophosphate and 37.62 g dipotassium hydrogen orthophosphate. Terrific Broth and phosphate buffer were autoclaved separately.

The 150 mL starter culture, as well as the phosphate buffer and tetracycline (10 μg/mL) were added to the fermenter. Growth was initiated at 37 °C and 800 rpm with moderate levels of aeration. After 30 min of initial growth, D-xylose was added to the fermenter to initiate LF expression. Sterile-filtered D-xylose was prepared by dissolving 15 g D-xylose in 75 mL of MilliQ water (20% w/v), and then transferring the mixture into clean, sterile tubes using a 30 mL syringe equipped with a 0.22 μm mixed cellulose ester filter (Fisher Scientific Canada, Whitby, ON). Antifoam (Y-30) was added throughout the growth period as needed. Every hour, following D-xylose addition, a 1 mL aliquot was taken from the fermenter and the OD_{600} was measured to monitor growth. After an OD_{600} between 1.8 – 1.9 was achieved (typically after 6 – 7 h), the culture medium was transferred to 1 L centrifuge bottles and spun at 7000 rpm for 25 min in an Avanti J-20 XPI centrifuge (Beckman Coulter, Brea, CA). The supernatant (~3 L) was then poured into a container with 3 L of 40% (w/v) polyethylene glycol 8000 (PEG-8000), covered with aluminum foil, and placed on a magnetic stirrer (moderate speed) at 4 °C for 16 h. The cell pellet was discarded.

3.3.2 Protein purification

Following exposure of the supernatant to PEG-8000, the mixture was centrifuged for 2 h at 7000 rpm to recover the protein pellet. The supernatant was suctioned off, and the protein pellet was transferred to a 50 mL centrifuge tube using a 10 mL syringe. The slurry was centrifuged at 8000 × *g* for 20 min using an IEC Multi RF refrigerated centrifuge

(Thermo Scientific, Waltham, MA). The PEG-8000 supernatant was subsequently discarded, and the tube containing the protein pellet was placed on ice until further purification.

The protein pellet was resolubilized in 20 mM Tris-HCl buffer (pH 8.0). Resolubilized protein was centrifuged for 20 min at 5400 × *g* to separate any residual cell debris. The supernatant, which contained the protein, was transferred into a new 50 mL centrifuge tube and centrifuged again at 5400 × *g* for 20 min. The pellets were discarded, and the protein-containing solution was kept on ice.

A Q-Sepharose chromatography column was prepared and equilibrated with 20 mM Tris-HCl buffer (pH 8.0) according to the manufacturer's recommended protocol. A Q-Sepharose bed volume of 10 mL was used. The flow rate was adjusted to ~1 mL/min at 20 °C. Resolubilized protein was added to the column, which was then washed with 10 mL of equilibration buffer followed by elution with equilibration buffer containing 150 mM, 350 mM, and finally 550 mM NaCl (20 mL of each). Fractions were collected every 10 mL in 15 mL centrifuge tubes. LF eluted predominately in the 350 mM NaCl-containing fractions. Hence, these fractions were pooled and concentrated using an Amicon Ultra-15 centrifugal filter with a 30 kDa molecular weight cut-off (Millipore, Bedford, MA) at 3350 × *g* for 12-14 min. The concentrated protein was then diluted with 50 mM Hepes (pH 7.4), and centrifuged again at 3350 × *g* for 12-14 min. This washing/rebuffering step was repeated once more, and the protein was concentrated to a final volume of ~1.0 mL. Protein was stored at -80 °C.

The purity of the protein was ascertained by sodium dodecyl sulfate gel electrophoresis (SDS-PAGE; see section 3.4). The concentration and zinc content of LF were determined as outlined in sections 3.5 and 3.6, respectively, and its enzymatic activity was assessed using a standard activity assay (see section 3.7).

3.4 SDS-PAGE

Sodium dodecyl sulfate polyacrylamide gel electrophoresis (SDS-PAGE) was performed to assess the purity of LF (90 kDa). The procedure was modified from that reported by Laemmli (96). A resolving gel was prepared with 4.5 mL acrylamide/bis-acrylamide mixture (30%), 3.75 mL Tris-HCl (1.5 M; pH 8.8), 150 µL SDS (10% [w/v]), and then filled to 15 mL with MilliQ water. A volume of 50 µL of 10% (w/v) ammonium persulfate (APS) and 10 µL of tetramethylethylenediamine (TEMED) were added before pouring the mixture into the electrophoresis apparatus. The stacking gel was prepared with 1.3 mL acrylamide/bis-acrylamide mixture (30%), 2.5 mL Tris-HCl (0.5 M; pH 6.8), 100 µL of 10% (w/v) SDS, diluted to 10 mL with MilliQ water. 50 µL of 10% APS and 10 µL of TEMED were added before pouring the mixture into the electrophoresis apparatus. The stacking gel was allowed to settle in a Mini-Protean tetra system (Bio-Rad Laboratories Inc., Hercules, CA) gel electrophoresis apparatus with a 10-well comb. Samples were prepared by adding 10 µL Laemmli buffer to 10 µL of each sample (fractions from Q-Sepharose elution). The samples were denatured by boiling for 5 min. Running buffer was added to the electrophoresis apparatus, the 10-well comb was removed, and 10 µL of each sample was loaded into the wells. Running buffer was prepared with 3.0 g Tris base, 14.4 g glycine, and 1.0 g SDS in 1 L of water (pH adjusted to 8.8). A protein ladder (Fermentas, Waltham, MA) with known molecular weights was also prepared for reference. The electrophoresis was performed at 75 V through the stacking gel and at 150 V through the resolving gel. The bands were visualized using Coomassie Brilliant Blue (0.2% (w/v) Coomassie Blue R-250) in a 45:45:10 methanol:water:acetic acid solution. Destaining was accomplished using a solution of 40% (v/v) methanol and 10% (v/v) acetic acid in water.

3.5 Determination of LF concentration

The concentration of LF (in 50 mM Hepes buffer; pH 7.4) was determined from an absorption spectrum recorded between 250 and 350 nm on a Cary 60 UV-Vis spectrophotometer (Agilent Technologies, Mississauga, ON), by solving the Beer-Lambert law using the recorded absorbance at 280 nm and the corresponding extinction coefficient of $\varepsilon = 74200\ M^{-1}\ cm^{-1}$ (83).

3.6 Colourimetric zinc assay

A zinc assay, which was modified from a published procedure (83), was performed in a 96 well plate, with a total volume of 200 μL per sample or standard to assess the zinc content of LF. Isolated LF (between 2 and 8 μM) was denatured with 4 M guanidine hydrochloride (Gdn-HCl) in 50 mM Hepes (pH 7.4), along with 50 μM 4-(2-pyridylazo)resorcinol (PAR), a chromophoric chelator (97), for 1 h at room temperature. Zinc standards (0, 1, 2, 4, 6, 8, 10 μM) were also prepared under the same conditions. The absorbance values at 500 nm for both LF samples and zinc standards were determined using a PowerWaveX microplate reader (BioTek Instruments, Inc., Winooski, VT) at 20 °C. A standard line was constructed using the A_{500} values for the zinc standards. The zinc content of the protein was estimated using the trendline and the A_{500} values of the LF-containing solution. Typically, the zinc concentration was found to be between 90-100% of the protein's concentration, indicating a zinc content of 0.9 – 1.0 Zn^{2+}/LF. In a few instances, significantly less than one (0.7 – 0.9) zinc ion per protein molecule was found. In such cases, $ZnSO_4$ was added to the protein preparation to achieve a 1:1 molar ratio of metal and enzyme.

3.7 LF activity assay

Enzymatic activity was determined by monitoring the changes in absorbance at 405 nm over time as LF cleaved the chromogenic substrate *S*-*p*NA, a commonly used LF substrate (83). Typically, 50 nM LF was exposed to 10 μM *S*-*p*NA in 50 mM Hepes buffer (pH 7.4) at 25 °C in a quartz cuvette with a final volume of 100 μL. Immediately following addition of *S*-*p*NA, the A_{405} values were monitored for 60 s in 0.1 s intervals using a Cary 60 UV-Vis spectrophotometer (Agilent Technologies, Mississauga, ON). Unless stated otherwise, all LF activity assays were performed under these conditions.

Activities were determined using the slope of the trendline through the initial linear portion (5 – 10 s) of the A_{405} vs. time plots.

3.8 Preparation of metal-substituted LF

3.8.1 Preparation of apoLF

ApoLF was required for the preparation of metal-substituted LF as well as for a few other experiments. Metal-free LF was prepared in Hepes buffer (50 mM, pH 7.4) according to a previously established protocol (83) as follows: native ZnLF (10 μM) was exposed to two strong metal chelators, dipicolinic acid (DPA) and ethylenediaminetetraacetic acid (EDTA) at concentrations of 1 mM and 10 mM, respectively. After 48 h incubation at 4 °C, the excess chelator was removed with an Amicon Ultra-15 centrifugal filter (30 kDa MWCO). The mixture was spun according to the recommended protocol (at 4500 × *g*) until the sample volume was below 1 mL. The filter was then filled using Chelex-treated Hepes buffer (50 mM, pH 7.4), and was spun again. This procedure was repeated until EDTA concentrations were less than 0.3 μM.

A PAR assay was performed to confirm the low level of zinc remaining in the solution, as well as to ensure the absence of chelators. To assess the zinc content, a standard PAR assay was performed (see section 3.6). To verify that the two chelators had successfully been removed from the sample, 5 μM zinc was added to the prepared apoLF sample according to a published protocol (83). The absorbance at 500 nm for this solution was compared to that of PAR-supplemented zinc standards with zinc concentrations ranging from 0 μM to 10 μM. Because EDTA will outcompete PAR for zinc, if less than 5 μM zinc was to be observed in the sample, then it could be concluded that EDTA was still present in the apoLF preparation. If less than 5 μM zinc was observed, the apoLF preparation underwent additional spins using an Amicon Ultra-15 centrifugal filter (30 kDa MWCO) and the PAR assay was repeated. The protein concentration was determined as described in section 3.5, followed by storage of the apoprotein at -80 °C.

3.8.2 Preparation of cobalt LF

Cobalt LF (CoLF) was prepared according to the so-called "direct exchange method" (84). ZnLF was diluted to a total volume of 2 mL in Chelex-treated Hepes buffer (50 mM, pH 7.4) to achieve a final concentration of 10 μM. The sample was passed through a Hepes-equilibrated Q-Sepharose chromatography column (5 mL bed volume). A volume of 50 mL of 5 mM $CoCl_2$ (in 50 mM Hepes, pH 7.4) was then applied to the column to allow for exchange with protein-bound zinc. Excess cobalt and released zinc were removed by washing the column with 50 mL Hepes buffer (50 mM, pH 7.4). Finally, the protein was eluted using 400 mM NaCl in 50 mM Hepes buffer (pH 7.4). The solution was concentrated

using an Amicon Ultra-15 centrifugal filter (30 kDa MWCO), and the sample was stored at -80 °C.

The success of the cobalt exchange was determined using an activity assay. The activity of CoLF was tested using the standard assay procedure, with CoLF at 50 nM and *S-p*NA at 10 μM in 50 mM Hepes (pH 7.4). If the activity of the CoLF preparation was between 210 - 230% relative to that of ZnLF prior to exchange, the exchange was considered successful (85). A second activity assay was conducted under the same conditions but an additional 10 μM $CoSO_4$ was added and given a 10 min incubation period. If no increase in activity was observed, it was concluded that ZnLF had fully exchanged to CoLF. To ensure the absence of an excess of cobalt and residual zinc in the protein solutions, the amount of cobalt and zinc was analyzed using PAR. Five standards were prepared in Hepes buffer (50 mM, pH 7.4) containing one of the following: 10 μM Co^{2+}, 10 μM Zn^{2+}, 5 μM Co^{2+}, 5 μM Zn^{2+}, and 5 μM Co^{2+} + 5 μM Zn^{2+}. A sample containing 7 μM CoLF was also prepared under the same conditions in Hepes buffer (50 mM, pH 7.4). Then, PAR (50 μM) and 4 M Gdn-HCl were added to each of the samples and standards. Following 1 h of incubation at room temperature, absorption spectra were recorded between 300 and 750 nm on a Cary 60 UV-Vis spectrophotometer, and analyzed using a previously published protocol for the simultaneous determination of zinc and cobalt in protein samples (98). If excess cobalt or residual zinc appeared to be contaminating the sample, CoLF was reapplied to the column and the washing procedure was repeated.

Cobalt LF was also prepared by reconstitution of the apoenzyme. ApoLF was diluted to 1 μM in Chelex-treated Hepes buffer (50 mM, pH 7.4). $CoSO_4$ (5 μM) was then added, and the solution was incubated for 30 min at 4 °C. CoLF was then stored at -80 °C.

3.8.3 Preparation of copper LF

Copper LF (CuLF) was prepared using apoLF. Direct exchange was found to be inefficient, and never yielded a pure copper protein, likely due to copper precipitation clogging the Q-Sepharose exchange column. ApoLF was diluted to 1 μM in a microcentrifuge tube using 50 mM Hepes buffer (pH 7.4). $CuSO_4$ (5 μM) was added and incubated for a minimum of 30 min at 4 °C, followed by storage of the sample at -80 °C.

The effectiveness of copper insertion was ascertained by an activity assay using 20 nM CuLF and 10 μM *S*-*p*NA in 50 mM Hepes (pH 7.4). Under these conditions, the activity of CuLF is expected to be approximately 160-200% relative to that of 50 nM ZnLF (85). If the activity fell in this range, it was concluded that copper was present in the active site of LF.

The copper content of the protein was also confirmed with a PAR assay. Both copper and zinc-bound PAR absorb at 500 nm (85), but previous tests had already determined zinc to be absent from the apoprotein solution. Copper assays were performed in a 96-well plate. Copper-substituted LF was denatured using 4 M Gdn-HCl in 50 mM Hepes buffer (pH 7.4) in the presence of 50 μM PAR for 1 h at room temperature. Copper-PAR standards (0, 1, 2, 4, 6, 8, 10 μM with respect to the metal ion) were also prepared under the same conditions. The absorbance at 500 nm was then measured. A trendline was constructed using the A_{500} values for the copper standards, which was then used to estimate the copper concentration in the protein sample. The occupancy of LF's active site was calculated based on the known protein concentration. The preparation of CuLF was considered successful if the enzymatic activity was in the expected range, and if more than 90% of LF's active site was occupied by copper.

3.9 Estimation of LF-metal dissociation rate constants

To determine whether it is feasible for metal exchange to occur via a dissociative mechanism, an experiment was designed using EDTA, a commonly used metal chelator. Previous studies have shown EDTA to be a non-invasive, S_N1-type chelator (57). This is an important characteristic for the chelator as tertiary complexes cannot be formed (i.e., EDTA will not affect the rate at which active site zinc will dissociate from LF).

3.9.1 Zinc LF

To estimate the LF-Zn dissociation rate constant, 50 nM ZnLF was incubated with 10 mM EDTA at 25 °C in 50 mM Hepes (pH 7.4) in a 15 mL centrifuge tube. At desired time points, aliquots were taken from the tube, and the activity of the enzyme was immediately measured with 10 μM *S*-*p*NA. Relative activities (RAs) were determined by dividing the activity at a given time point "*t*" by the activity measured for a separate EDTA-free mixture (LF only) at the same time (EDTA-free standard). The reaction was stopped when the relative activity was less than 5% (typically after 30 h). Three independent experiments were performed under the same conditions on different days. The dissociation rate constant (k_{off}) was estimated by fitting experimental results to equation 3 using GraFit 4.0 data analysis software (Erithacus Ltd, Staines, UK):

$$RA = e^{(-k_{off}\, t)} \qquad \text{(eq. 3)}$$

where RA is the relative activity at time t. In addition, the data was fit (by a linear regression analysis constrained to an exact zero-intercept) to the linearized version of equation 3 (see equation 4), with the slope of this plot representing the k_{off} value.

$$-\ln RA = k_{off}\, t \qquad \text{(eq. 4)}$$

3.9.2 Cobalt and copper LF

The k_{off} values for CuLF and CoLF were estimated using slightly different conditions since metal release was found to be more rapid. A concentration of 50 nM of either CuLF or CoLF was incubated with 10 mM EDTA in a 500 µL microcentrifuge tube. The incubation time started immediately after the addition of EDTA. At the desired time interval, the solution was transferred from the microcentrifuge tube into a 100 µL micro quartz cuvette where 10 µM *S*-*p*NA was added followed by an immediate monitoring of the protein activity at 405 nm. Relative activities were determined as before, i.e., by dividing the activity (at a time *t*) by the activity measured for CuLF or CoLF in the absence of EDTA. Three independent experiments for each metal were conducted.

The k_{off} values were estimated for CoLF and CuLF using equations 3 and 4 as described for ZnLF, again using a regression analysis –ln(RA) vs *t* constrained to an exact zero-intercept.

3.10 Metal exchange

Assays were designed to gain insight into the kinetics of metal exchange in LF. These assays monitored metal exchange using either enzymatic activities or inductively-coupled plasma mass spectrometry (ICP-MS) to determine active site metal content.

3.10.1 Zinc-to-cobalt exchange

The zinc-to-cobalt exchange was monitored using activity assays. If one considers the activity of ZnLF to be 100%, fully cobalt-substituted LF has an expected activity of approximately 220% (84,85). ZnLF (50 nM) was incubated with 1 mM $CoSO_4$ in 50 mM Hepes buffer (pH 7.4). At appropriate time intervals, aliquots of this solution were taken and 10 μM *S*-*p*NA was added immediately prior to determining the activity under standard conditions. The same conditions, with water in place of $CoSO_4$, were used as a reference (ZnLF activity). A minimum of three independent experiments for each time point were completed.

3.10.2 Cobalt-to-zinc exchange

The cobalt-to-zinc exchange was performed using CoLF prepared via the apoLF route (see section 3.8.2). CoLF was diluted to 50 nM in 50 mM Hepes buffer (pH 7.4) in a 1.5 mL microcentrifuge tube. This solution contained 250 nM $CoSO_4$ from the preparation of CoLF; then, 250 nM $ZnSO_4$ was added to the mixture, and incubated at 25 °C. After the desired incubation time an aliquot was taken from the mixture and the activity was measured using 10 μM *S*-*p*NA.

3.10.3 Zinc-to-copper exchange

The zinc-to-copper exchange was analyzed using a standard activity assay. Fully exchanged CuLF is expected to have an activity four times greater than that of ZnLF (85), which was used as a reference. ZnLF was diluted to 20 nM with 50 mM Hepes buffer (pH 7.4) in a quartz cuvette. The exchange was initiated by addition of $CuSO_4$ at a final

concentration of 10 μM. After the desired incubation time, 10 μM *S*-*p*NA was added and the activity was measured. The t=0 reading was taken by premixing *S*-*p*NA with $CuSO_4$, and adding it to LF in 50 mM Hepes (pH 7.4) immediately prior to recording the absorbance at 405 nm. A sample of 20 nM ZnLF in the absence of $CuSO_4$ was used as a reference.

The zinc-to-copper exchange in Hepes buffer (50 mM, pH 7.4) was also monitored by stopped-flow UV-Vis spectrophotometry on an OLIS RSM-1000 spectrophotometer (OLIS Inc., Bogart, GA) using a two-syringe setup. One syringe was filled with ZnLF in Hepes buffer. The second syringe contained $CuSO_4$ and *S*-*p*NA in buffer. Injection resulted in the mixing of these two solutions to achieve final concentration of 200 nM ZnLF, 10 μM $CuSO_4$, and 10 μM *S*-*p*NA. UV-Vis spectra were recorded for 60 s with a rate of 63 scans/s immediately following injection. Two reference samples were also measured. One contained 200 nM ZnLF with Chelex-treated water in place of the $CuSO_4$. This sample provided the baseline activity (i.e., ZnLF at t=0). The second reference sample contained fully exchanged CuLF (200 nM), prepared by loading one syringe with ZnLF and $CuSO_4$, followed by 10 min incubation. The second syringe contained only *S*-*p*NA in buffer. This reference provided an estimation of the maximum activity of fully exchanged CuLF under these conditions.

3.10.4 (Naturally abundant) Zinc-to-^{70}Zn exchange

To determine how the active site zinc ion in LF exchanges with extraneous zinc, isotopically enriched zinc (^{70}Zn) was used. Because the kinetic isotope effect for zinc is expected to be very small, activity measurements cannot be used to monitor the isotope

exchange. Hence, a new procedure to observe zinc exchange in LF using ICP-MS was developed.

3.10.4.1 Experimental conditions

To investigate the rate of isotope exchange, 7 μM ZnLF was exposed to 70 μM $^{70}Zn^{2+}$ (in the form of $^{70}Zn(NO_3)_2$) in 25 mM ammonium acetate buffer (pH 7.0) in a 1.5 mL microcentrifuge tube at room temperature. After the desired time of incubation, the exchange reaction was quenched by adding 80 μM EDTA. This solution was immediately vortexed and transferred to a 2 mL Zeba spin desalting column (Thermo Fisher Scientific, Burlington, ON) previously equilibrated with ammonium acetate (25 mM, pH 7.0) according to the manufacturer's instructions. The solution was passed through the desalting gel by centrifugation (1000 × *g* for 3 min). The eluate was recovered (typically 300 μL), and the protein concentration was determined using UV-Vis spectroscopy as outlined in section 3.5. All samples were stored at -20 °C until recovery for metal content determination by ICP-MS (see section 3.13). A control sample (t = 0 s) was prepared by pre-exposing 70 μM $^{70}Zn^{2+}$ to 80 μM EDTA in ammonium acetate (25 mM, pH 7.0). This solution was then added to 7 μM ZnLF, followed by immediate application of the solution to an ammonium acetate-equilibrated Zeba desalting column.

The isotope exchange was also performed at a lower concentration of $^{70}Zn^{2+}$ to determine if the rate of exchange is dependent on the concentration of free metal (as would be expected for an associative exchange mechanism). For this exchange, 7 μM ZnLF was incubated with 7 μM $^{70}Zn^{2+}$ for 10 s in 25 mM ammonium acetate (pH 7.0). Then, 80 μM EDTA was added to quench the exchange reaction, followed by processing through an

ammonium acetate-equilibrated Zeba column, as outlined above. The metal content of the protein-containing eluate was assessed using ICP-MS (see section 3.13).

3.10.4.2 ICP-MS data analysis and the ttr formalism

Following the determination of metal isotopes (^{64}Zn, ^{66}Zn, ^{67}Zn, ^{68}Zn, ^{70}Zn) by ICP-MS (see section 3.13) the data was analyzed using a tracer-to-tracee ratio (*ttr*) formalism (99-104) that allows for the determination of the number of metal ions exchanged in a system when the tracer (metal introduced into the system) and tracee (metal originally present in the system) have different isotopic distributions. In the case of the natural zinc-to-^{70}Zn exchange experiment, the tracer was the extraneous $^{70}Zn^{2+}$ enriched metal whereas the tracee was the natural isotopic zinc originally bound to the active site of LF (see Table 3.2). The $ttr^{(x,y)}$ value can be calculated for any system with known isotopic distributions for both tracer and tracee and the experimentally determined (by ICP-MS) isotope ratio ($r^{(x/y)}$) of the enriched isotope, *x*, and a reference isotope, *y*, using equation 5:

$$ttr^{(x,y)} = \frac{r^{(x/y)} - r^{(x)}_{tracee}}{r^{(x)}_{tracer} - r^{(x/y)}} \left(\sum_{i=1}^{z} r^{(i)}_{tracer} \Big/ \sum_{i=1}^{z} r^{(i)}_{tracee} \right) \qquad \text{(eq. 5)}$$

where $r^{(i)}$ is the isotope ratio of nuclide *i* and reference isotope *y*, $r^{(x)}$ denotes the quotient of abundances of isotopes *x* and *y* of either the tracer or tracee, and *z* denotes the number of stable isotopes (*z* = 5 for zinc).

Table 3.2: Isotope abundance of zinc and isotope ratios of tracee and enriched ^{70}Zn tracer.

	Abundance		**Isotope ratio**	
Isotopes	Tracee [a]	^{70}Zn tracer	Tracee	^{70}Zn tracer
64	0.4889	0.0002	1.0000	1.0
66	0.2781	0.0002	0.5688	1.0
67	0.0411	0.0016	0.0841	8.0
68	0.1857	0.0449	0.3798	224.5
70	0.0062	0.9535	0.0127	4767.5
SUM	**1.0000**	**1.0000**	**2.0454**	**5002.0**

[a] Values for the natural isotope abundance of zinc were taken from: *Handbook of Chemistry and Physics (51st Edition);Weast, R. C., Ed.; CRC Press, Cleveland, 1970-1971*.

In the case of this experiment, the $ttr^{(x,y)}$ value was obtained using the experimentally determined $r^{(70/64)}$ ratios, with ^{64}Zn serving as the reference isotope. Based on the values presented in Table 3.2, equation 5 can be rewritten in the following form:

$$ttr^{(70,64)} = \frac{r^{(70/64)} - 0.0127}{4767.5 - r^{(70/64)}} (5002/2.0454) \qquad \text{(eq. 6)}$$

In the case of the zinc-to-^{70}Zn exchange, the maximum $ttr^{(70,64)}$ value obtainable is 10, due to $^{70}Zn^{2+}$ (tracer) being present at a 10-fold excess over the tracee found in the active site of LF prior to exchange.

The $ttr^{(x,y)}$ value can be used to determine the number of ions exchanged in the system (*N* value) with the aid of the following equation:

$$N = n\left(\frac{ttr^{(x,y)}}{ttr^{(x,y)} + 1}\right) \qquad \text{(eq. 7)}$$

where n is the number of metal binding sites available ($n = 1$ in the case of LF). The maximum *N* value (N_{max}) obtainable can be calculated by replacing $ttr^{(x,y)}$ in equation 7 with the maximum $ttr^{(x,y)}$ value. This results in an N_{max} value of 10/11 (0.909) for the 7 μM ZnLF + 70 μM $^{70}Zn^{2+}$ exchange, and 0.5 for the 7 μM ZnLF + 7 μM $^{70}Zn^{2+}$ exchange. The kinetics

of the metal exchange in LF were assessed by recording the $^{70}Zn/^{64}Zn$ ratios as a function of the time of $^{70}Zn^{2+}$ exposure.

3.11 Metal inhibition studies

3.11.1 Cobalt inhibition

To assess the inhibition of LF by Co^{2+}, 50 nM ZnLF was incubated with $CoSO_4$ at concentrations between 100 nM and 100 mM in 50 mM Hepes buffer (pH 7.4) for 20 min. Following incubation, the mixture was transferred into a quartz cuvette, and 10 μM *S*-*p*NA was added to initiate a standard activity assay (total volume of 100 μL). Reference ZnLF activities were determined using H_2O in the place of $CoSO_4$.

In some instances, $CoSO_4$ was replaced by $CoCl_2$ or $MgSO_4$ to assess the contribution of ionic strength to the inhibition of LF by Co^{2+}.

3.11.2 Mode of inhibition by zinc

In order to determine the mode of inhibition that metals exert on LF, 50 nM ZnLF was incubated for 15 min with either 0 μM, 15 μM, or 30 μM of $ZnSO_4$, in 50 mM Hepes buffer (pH 7.4). For each inhibitor concentration, various concentrations of *S*-*p*NA (ranging from 3 μM to 10 μM *S*-*p*NA) were used. The substrate was added immediately prior to measuring enzymatic activity. Activity assays were performed in a quartz cuvette in a total volume of 100 μL.

The velocity data obtained was fit to various inhibition modalities (105) using GraFit 4.0 data analysis software (Erithacus Ltd., Staines, UK). The best fit of the data was obtained with a pure non-competitive model using equation 8:

$$V = V_{max} \frac{K_I}{K_I + [I]} \frac{[S]}{K_M + [S]} \quad \text{(eq. 8)}$$

where V is the reaction rate, $[S]$ is the concentration of the substrate and $[I]$ is the concentration of the inhibitor (i.e., Zn^{2+}). The inhibition constant (K_I), the Michaelis constant (K_M), and the maximum velocity (V_{max}) served as the fitting parameters. The k_{cat} value was calculated from the experimentally determined V_{max} and a $\Delta\varepsilon_{405}$ value of 9920 M^{-1} cm^{-1} (106).

3.12 Terbium studies

3.12.1 Influence of terbium on metal exchange

To investigate the influence of inhibitory metal on active site exchange, experiments were designed mimicking previous exchange conditions with inhibitory concentrations of Tb^{3+} (83). ZnLF (7 μM) was preincubated with 150 μM $TbCl_3$ for 3 min in ammonium acetate (25 mM, pH 7.0), followed by the addition of 70 μM $^{70}Zn^{2+}$ to initiate the active site zinc-to-^{70}Zn exchange. The exchange was allowed to proceed for 10 s, followed by quenching of the exchange reaction with 300 μM EDTA. This solution was quickly vortexed and transferred to a 2 mL Zeba spin desalting column previously equilibrated with ammonium acetate (25 mM, pH 7.0) according to the manufacturer's instructions. The sample was passed through the spin column by centrifugation at 1000 × *g* for 3 min. The eluate was recovered and the protein concentration was measured using UV-Vis spectroscopy (see section 3.5). A minimum of three independent experiments for each sample were completed. Samples were stored at -20 °C until preparation for ICP-MS analysis to determine metal content (see section 3.13).

3.12.2 Tyrosine-sensitized terbium luminescence spectroscopy

The spectroscopic properties of terbium-bound LF were investigated using an OLIS RSM-1000 spectrofluorometer equipped with a 150 W xenon arc lamp. A 450 nm cut-off filter was used to eliminate Rayleigh scattering. ApoLF (1 μM) was incubated with 100 μM $TbCl_3$ in 50 mM Hepes buffer (pH 7.4) for 10 min in a total volume of 1 mL. The sample was placed in a 1 mL fluorescence cell and LF's tyrosine residues were excited at 274 nm (93). The emission spectrum was recorded between 470 nm and 630 nm. The solution was then titrated with $CuSO_4$ (from 250 nM to 500 μM), with additional emission spectra taken after each titration step. Solutions were given a 2 min incubation period before each spectrum was measured. A second titration was conducted (under the same conditions) using 1 μM CuLF and extraneous Cu^{2+} concentrations ranging from 0 μM to 100 μM (CuLF was pre-exposed to 100 μM $TbCl_3$). The titration of terbium-exposed apoLF was repeated using the same experimental conditions with zinc in place of copper, and zinc concentrations ranging from 1 μM to 100 μM.

3.13 Determination of metal content by ICP-MS

All samples from the (naturally abundant) zinc-to-^{70}Zn exchange and the terbium studies were analyzed using an iCAP Q ICP-mass spectrometer (Thermo Fisher Scientific, Nepean, ON). Samples (volumes ranging from 250 to 450 μL) were recovered from the -20 °C freezer, and were allowed to thaw at room temperature. A volume of 200 μL of MilliQ water was added to each, followed by dilution to a final volume of 2 mL using Chelex-treated ammonium acetate (25 mM, pH 7.0). Standards were prepared to allow for approximation of metal concentrations in ammonium acetate (25 mM, pH 7.0). $^{70}Zn^{2+}$ and

terbium standards were prepared at final concentrations of 1 ppb, 10 ppb, and 30 ppb using the 50 mM $^{70}Zn^{2+}$ stock solution and a 100 mM $TbCl_3$ solution, respectively. Zinc (naturally abundant) standards were also prepared to have a concentration of 1 ppb, 10 ppb, 30 ppb, 50 ppb, and 100 ppb using an ICP-MS zinc standard solution (1000 ppm in 1% [w/v] HNO_3). All solutions (both samples and standards) were supplemented with 5 ppb indium (from an ICP-MS indium standard solution, 1000 ppm in 1% [w/v] HNO_3) and 1% (w/v) trace metal grade HNO_3.

ICP-MS measurements took place on the same day the samples were prepared. They were transported on ice to Cambrian College, Sudbury, Ontario, where the ICP-MS measurements were conducted. The isotopes measured were ^{64}Zn, ^{66}Zn, ^{67}Zn, ^{68}Zn, ^{70}Zn, ^{113}In, ^{115}In, and ^{159}Tb.

4. Results

The experiments conducted in this thesis were aimed at determining several mechanistic aspects of LF, including the mechanism of metal exchange, and the mode by which metals such as Zn^{2+}, Co^{2+}, and Cu^{2+} exert their inhibitory effect. Insight into the mechanism of metal exchange and inhibition might provide concrete evidence that these two processes occur using a common (second) metal binding site in LF.

4.1 Determination of dissociation rate constants

To assess whether metal exchange in LF can proceed via a dissociative (D-type) mechanism, the rate constants for ZnLF, CuLF, and CoLF were determined with the aid of EDTA, an S_N1-type chelator (57). The activity of the protein, relative to that of an EDTA-free mixture, can serve as a guide indicating the percentage of metal still being protein-bound at any given time. EDTA was used in these studies because it cannot form ternary complexes with the protein-bound metal (S_N2-type chelation). Therefore, EDTA does not bind the zinc ion until it has dissociated from LF, hence, allowing for an accurate approximation of the dissociation rate constant (57). As the metal dissociates from the active site of LF, it is immediately bound to the chelator. In the current experiment, EDTA was present in at least a 10^5-fold excess to completely shift the equilibrium (see below) towards the formation of the EDTA-Zn complex and apoLF, rather than allowing the metal to be reinserted into apoLF:

$$\text{LF-M} \underset{k_{on}}{\overset{k_{off}}{\rightleftharpoons}} \text{apoLF} + \text{M} \overset{+EDTA}{\rightleftharpoons} \text{apoLF} + \text{EDTA-M}$$

This is important because in the estimation of the dissociation rate constant (k_{off}), the dissociation of EDTA-Zn and concomitant uptake of the released metal by apoLF can be ignored.

By plotting the relative activity of LF against the time of incubation with EDTA, insight can be gained into the rate of metal dissociation. As shown in Fig. 4.1, the data could be fit reasonably well to equation 3 (with the repression constraint to exact zero-intercept).

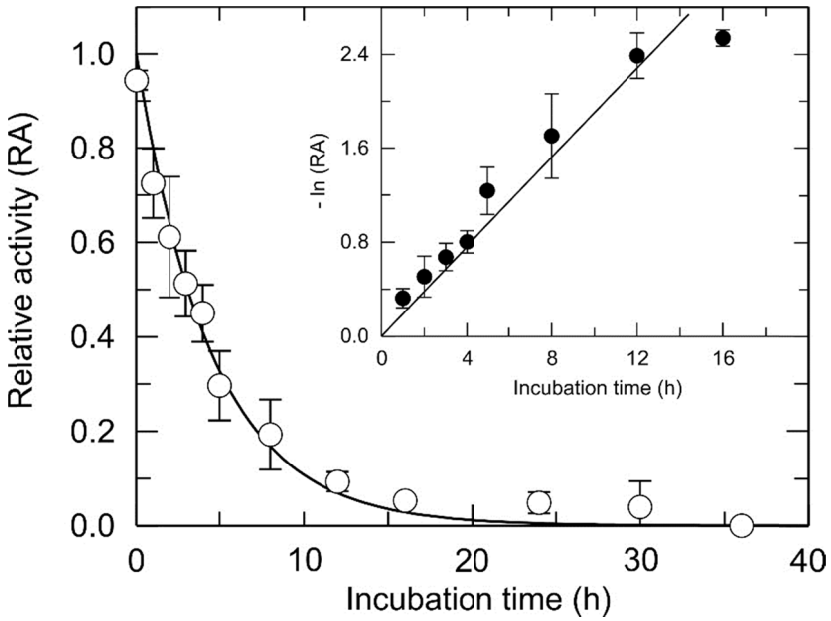

Figure 4.1: Effect of EDTA on the activity of ZnLF. ZnLF (50 nM) was incubated with 10 mM EDTA in Hepes buffer (50 mM, pH 7.4) for the desired amount of time prior to monitoring activity using *S*-*p*NA (10 μM). Relative activity is defined as the activity relative to that recorded for 50 nM ZnLF in the absence of EDTA. Values shown represent the mean ± 1 S.D. of three independent experiments. Inset: Replot of the data showing the linear relationship between –ln (RA) and incubation time.

The dissociation rate constant (k_{off}) was obtained from the fit of the data shown in Fig. 4.1, and was found to be $(6.19 \pm 0.29) \times 10^{-5}$ s^{-1}. Using the known dissociation constant (K_d; 1.2 pM (83)), the association rate constant (k_{on}) was determined as follows:

$$k_{on} = \frac{k_{off}}{K_d} = \frac{6.19 \times 10^{-5} s^{-1}}{1.2 \times 10^{-12} M} = (5.2 \pm 0.5) \times 10^{7} M^{-1} s^{-1}$$

The $t_{1/2}$ value (time required to demetallate half of the LF molecules) was calculated with the experimentally determined dissociation rate constant as follows:

$$t_{1/2} = \frac{\ln 2}{k_{off}} = \frac{\ln 2}{6.19 \times 10^{-5} s^{-1}} \sim (11200 \pm 520)\ s$$

In light of these results, it can be concluded that if metal exchange were to occur via a dissociative mechanism, the time of half exchange would be expected to be ~3 h.

The dissociation rate constants for CoLF (Fig. 4.2) and CuLF (Fig. 4.3) were determined in a fashion analogous to that for ZnLF. The dissociation rate constant for CoLF was k_{off} = (3.57 ± 0.14) ×10^{-3} s^{-1}, whereas that for CuLF was (2.94 ± 0.22) ×10^{-3} s^{-1}.

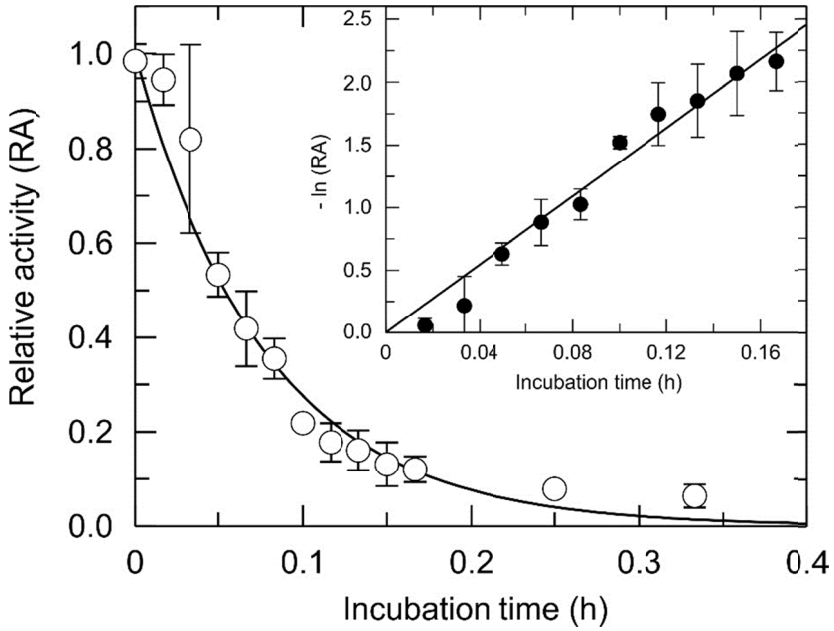

Figure 4.2: Effect of EDTA on the activity of CoLF. CoLF (50 nM) was incubated with 10 mM EDTA in Hepes buffer (50 mM, pH 7.4). Activity was measured using *S*-*p*NA (10 µM). Relative activity is defined as the activity relative to that recorded for 50 nM CoLF in the absence of EDTA. Values shown represent the mean ± 1 S.D. of three independent experiments. Inset: Replot of the data showing the linear relationship between –ln (RA) and incubation time.

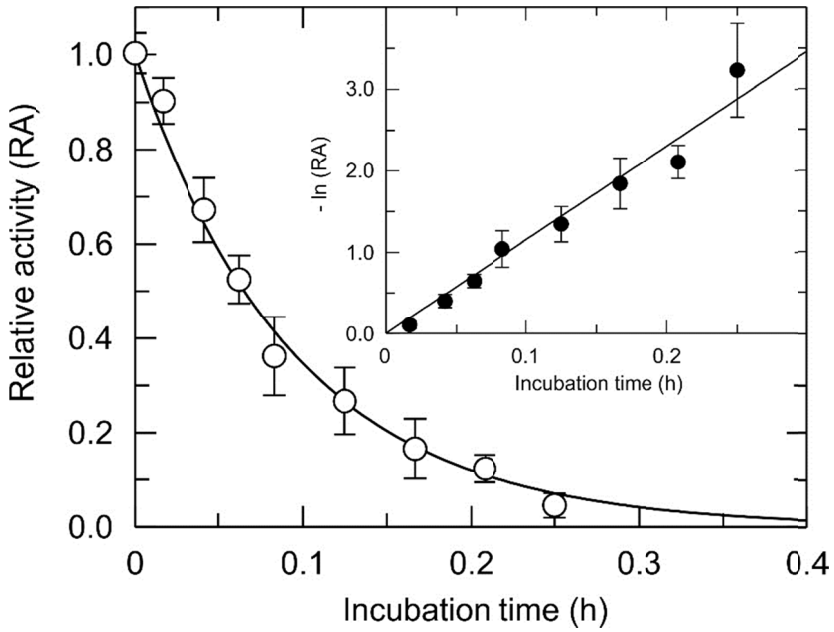

Figure 4.3: Effect of EDTA on the activity of CuLF. CuLF (50 nM) was incubated with 10 mM EDTA in Hepes buffer (50 mM, pH 7.4). Activity was measured using *S*-*p*NA (10 μM). Relative activity is defined as the activity relative to that recorded for 50 nM CuLF in the absence of EDTA. Values shown represent the mean ± 1 S.D. of three independent experiments. Inset: Replot of the data showing the linear relationship between –ln (RA) as a function of incubation time.

The two k_{off} values were then used to estimate the association rate constants (k_{on}), using the known dissociation constants (Table 4.1). In addition, the $t_{1/2}$ values were calculated using the experimentally determined k_{off} values (Table 4.1), revealing that metal exchange via a D-type mechanism would require only a few minutes in the case of CoLF and CuLF (as opposed to hours for ZnLF).

Table 4.1: Experimentally determined dissociation rate constants, association rate constants, and $t_{1/2}$ values.

LF species	Dissociation constant (K_d) / pM [a]	Dissociation rate constant (k_{off}) / s^{-1}	Association rate constant (k_{on}) / M^{-1} s^{-1}	$t_{1/2}$ value / s
ZnLF	1.2 ± 0.1	$(6.19 \pm 0.29)\times10^{-5}$	$(5.2 \pm 0.49)\times10^{7}$	11200 ± 520
CoLF	75 ± 4	$(3.57 \pm 0.14)\times10^{-3}$	$(4.8 \pm 0.32)\times10^{7}$	190 ± 8
CuLF	0.34 ± 0.02	$(2.94 \pm 0.22)\times10^{-3}$	$(8.6 \pm 0.82)\times10^{9}$	240 ± 18

[a] K_d values were obtained from (83-85).

4.2 Metal exchange

A series of assays was performed to assess whether the rates of metal exchange were in agreement with the determined $t_{1/2}$ values for a dissociative exchange.

4.2.1 Zinc-to-cobalt exchange

The zinc-to-cobalt exchange was monitored using the activity of the protein. The results of the exchange are shown in Fig. 4.4. As expected, the initial relative activity of LF was approximately 1 (the activity of ZnLF). As the exchange progressed, the relative activity reached a maximum at ~2.2, a value expected for fully substituted CoLF (84,85). The experimental time of half-exchange can be estimated by taking the time point at which the activity of the protein is halfway between the activities of ZnLF and fully exchanged CoLF. This point occurred (at a relative activity of ~1.6) between 1 and 3 min.

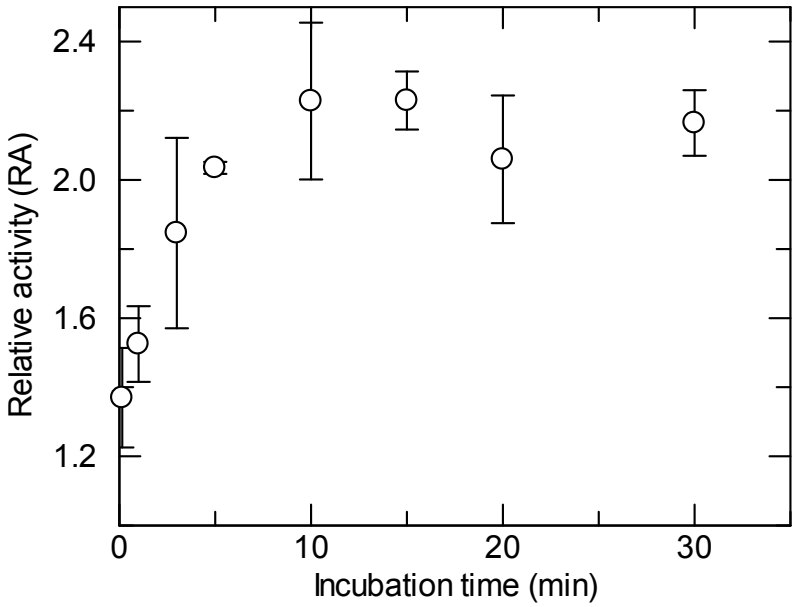

Figure 4.4: Time-dependence of zinc-to-cobalt exchange in LF. ZnLF (50 nM) was incubated for the time indicated in the figure with 1 mM Co^{2+} in Hepes buffer (50 mM, pH 7.4). Activity was measured following the addition of *S*-*p*NA (10 μM). Relative activity is defined as the activity relative to that recorded in the absence of Co^{2+}. Values shown represent the mean ± 1 S.D. of three independent experiments.

4.2.2 Cobalt-to-zinc exchange

The second exchange studied was a cobalt-to-zinc exchange, which was also monitored using activity assays. This exchange utilized very different exchange conditions, where equal amounts of cobalt and zinc were presented to CoLF. As shown in Fig. 4.5, the relative activity reached a minimum of RA ~$(2.2)^{-1}$ ~0.45, which is expected of fully (back-) exchanged ZnLF (84,85). A time of half-exchange can be estimated from the time at which the relative activity is halfway between the initial CoLF activity and the activity of fully exchanged ZnLF. This point was found to be at a relative activity between 0.70 and 0.75, occurring after approximately 8 min.

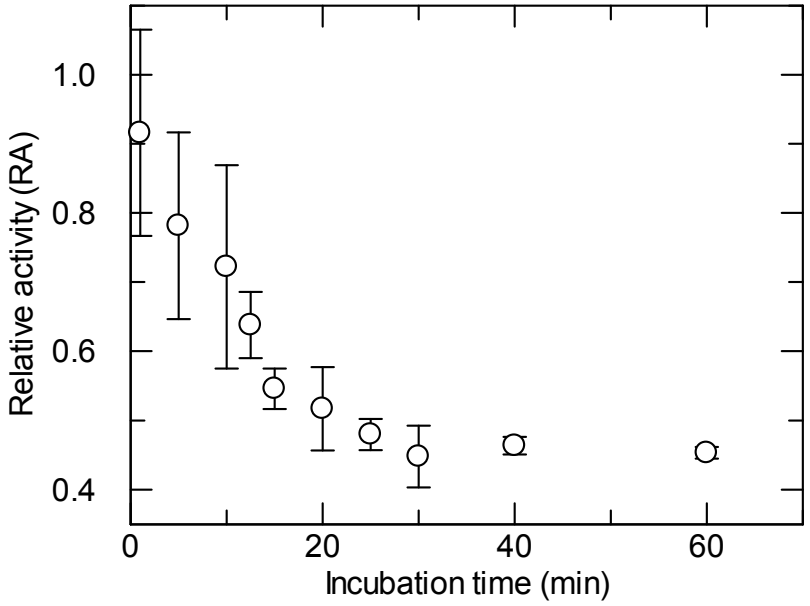

Figure 4.5: Time-dependence of cobalt-to-zinc exchange in LF. CoLF (50 nM enzyme, containing 250 nM Co^{2+}) was incubated for the time indicated in the figure with 250 nM Zn^{2+} in Hepes buffer (50 mM, pH 7.4). Activity was measured following the addition of *S-p*NA (10 μM). Relative activity is defined as the activity relative to that recorded in the absence of Zn^{2+}. Values shown represent the mean ± 1 S.D. of three independent experiments.

4.2.3 Zinc-to-copper exchange

The zinc-to-copper exchange was the final exchange process monitored using activity assays. As shown in Fig. 4.6, the maximum relative activity was achieved much more quickly than in other exchange reactions (after 20 s). As expected, this maximum occurred at a relative activity of RA ~4.5, which is that expected for a full zinc-to-copper exchange (85). The time of half-exchange was found to be in the vicinity of 10 s (i.e., at RA ~2.75, which is halfway between the activities of ZnLF and CuLF).

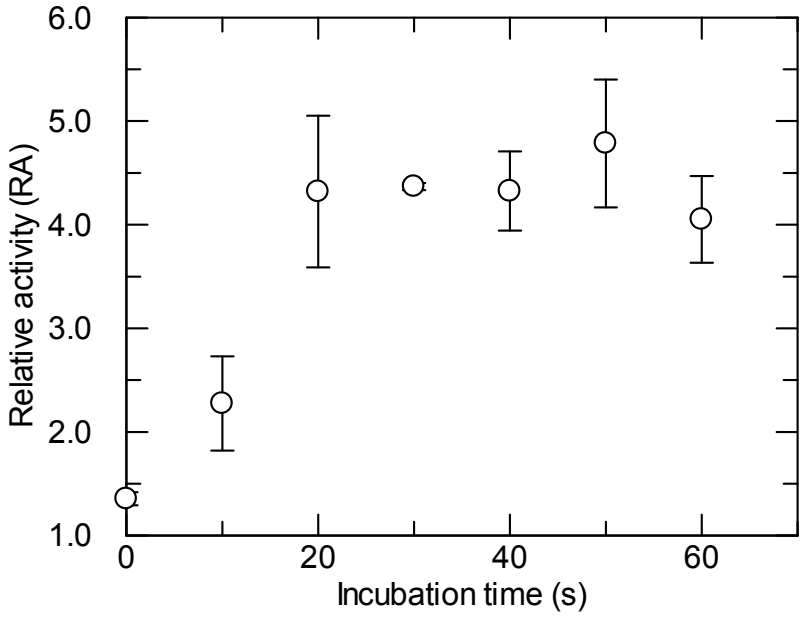

Figure 4.6: Time-dependence of zinc-to-copper exchange in LF. ZnLF (50 nM) was incubated for the time indicated in the figure with 10 μM Cu^{2+} in Hepes buffer (50 mM, pH 7.4). Activity was measured following the addition of *S*-*p*NA (10 μM). Relative activity is defined as the activity relative to that recorded in the absence of Cu^{2+}. Values shown represent the mean ± 1 S.D. of three independent experiments.

It is apparent that the zinc-to-copper exchange was more rapid than either of the previously studied exchanges. To gain additional insight into the rate of this exchange process, it was studied using stopped-flow spectrophotometry. This technique allows for the rapid mixing of ZnLF, Cu^{2+} (for exchange), and substrate (*S*-*p*NA) followed by immediate

measurement of absorbance (changes) in the millisecond time range. The results of zinc-to-copper exchange followed by stopped-flow spectrophotometry are shown in Fig. 4.7. A total of 3 samples were measured: the zinc-to-copper exchange sample and two controls containing either ZnLF or fully exchanged CuLF (200 nM ZnLF pre-exposed to 10 μM Cu^{2+} for 10 min). The two controls were used to demonstrate either the minimum (ZnLF) or maximum (CuLF) progress curves that could be expected during the zinc-to-copper exchange.

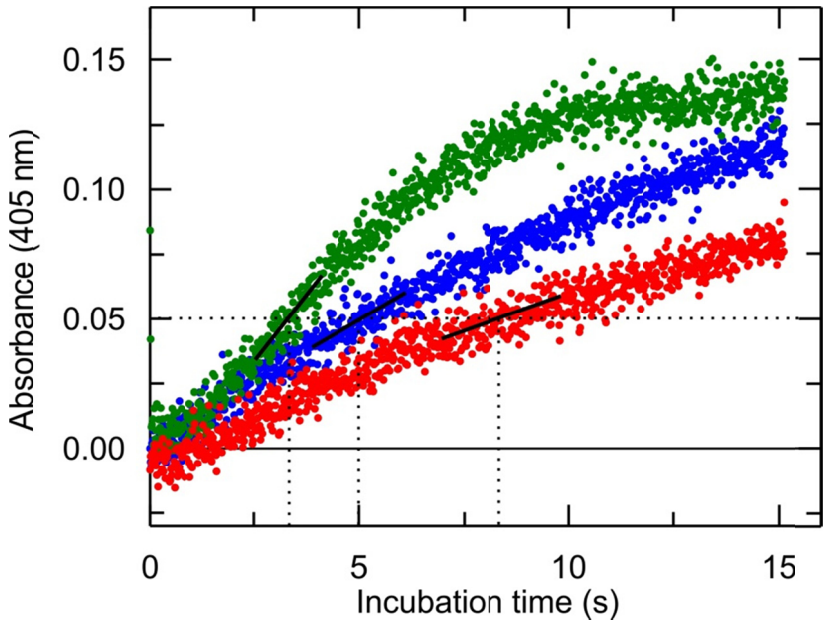

Figure 4.7: Progress curve of substrate hydrolysis during zinc-to-copper exchange. Using a two-syringe setup, ZnLF (200 nM) was rapidly introduced to a mixture of Cu^{2+} and substrate (both 10 μM final concentrations) in Hepes buffer (50 mM, pH 7.4) (blue). The progress of the reaction was monitored for 60 s (for the sake of clarity only progress for 15 s is shown). The controls contained 200 nM ZnLF (red) or CuLF (green) in the absence of extraneous metal. Black lines intersecting at Abs_{405} ~0.05 represent enzyme activities at indicated times (see text).

It is clear that the initial rate of substrate hydrolysis was immediately higher for the zinc-to-copper exchange sample (relative to the Cu^{2+}-free ZnLF control). The decline in activity over time observed in all three samples can be attributed to substrate (*S*-*p*NA) depletion. To

establish how these results compare to the previous exchange assays, the enzymatic activity was calculated at three different time points for the exchange sample (5 s, 10 s, 12 s) by determining the slope of the absorbance vs time plot (Fig. 4.7) at the specified time using a ± 1.5 s window (e.g., the enzymatic activity at 10 s was obtained by determining the slope of the trendline for all data points between 8.5 s and 11.5 s). The three determined activities were then compared to the activities of the CuLF and ZnLF controls at the same level of substrate depletion (ensuring that a decrease in activity due to substrate depletion is taken into account) to determine if the exchange sample was gaining activity over time. For example, the enzymatic activity for the zinc-to-copper exchange sample after 5 s was compared to that at 3.4 s for the CuLF control and at 8.4 s for the ZnLF control, where an equal degree of substrate depletion was observed (at an Abs_{405} value of ~0.05; see black lines in Fig. 4.7). The results of this comparison are shown in Table 4.2. The exchange progress was then estimated for each time point using equation 9:

$$Exchange\ progress\ (\%) = \frac{(Ex_{sam} - Zn_{ctrl})}{(Cu_{ctrl} - Zn_{ctrl})}\ 100\% \qquad \text{(eq. 9)}$$

where Ex_{sam} is the enzymatic activity of the exchange sample at a specified time, Zn_{ctrl} is the enzymatic activity of the ZnLF control at the same level of substrate depletion (as the exchange sample), and Cu_{ctrl} is the enzymatic activity of the CuLF control at the same level of substrate depletion (as the exchange sample). As shown in Table 4.2, at the 10 s time point, the exchange progress was 38%, a result that is comparable to the 37% exchange progress observed using standard activity assays, which was calculated with equation 9 using the data at 10 s in Fig. 4.6 $((2.3\text{-}1)(4.5\text{-}1)^{-1}100\%)$. It is clear that the exchange increases over time, and that the exchange sample attains an activity closer to that of CuLF as the exchange progresses (see Table 4.2).

Table 4.2: Enzymatic activities of samples from the zinc-to-copper exchange.

Exchange time (s)	**Enzymatic activity [$\Delta Abs_{405} \times 10^2\ s^{-1}$] [a]**			**Exchange progress (%) [b]**
	Exchange sample	CuLF control	ZnLF control	
5	0.85	1.81	0.54	25
10	0.75	1.40	0.35	38
12	0.61	0.93	0.21	56

[a] Enzymatic activity for the exchange sample was calculated using the slope of the trendline for data points at the time specified (± 1.5 s). The enzymatic activities for the controls were calculated at time points where the level of substrate depletion was identical to that observed for the exchange sample.

[b] The exchange progress was estimated using equation 9.

4.2.4 (Naturally abundant) Zinc-to-^{70}Zn exchange

The final exchange that was investigated was a (naturally abundant) zinc-to-^{70}Zn exchange. Since it is not possible to observe such exchange using activity assays (as there is no noticeable change in the activity of LF), the progress of the exchange reaction was monitored by ICP-MS. To ensure Zeba columns were suitable as a desalting medium, several preliminary experiments were performed with respect to sample preparation. To ensure that the active site metal remained bound to LF during Zeba processing, LF (7 μM) in ammonium acetate (25 mM, pH 7.0) was passed through the column, according to procedure outlined in section 3.10.4. The protein concentration in the filtrate was determined by UV-Vis spectroscopy, followed by a PAR assay to determine the zinc content (section 3.6), revealing that the metal content of LF was essentially unaffected by the Zeba filtration (data not shown). To confirm that extraneous metal was completely removed by the column, 150 μM $ZnSO_4$ was passed through the column and the filtrate was analyzed by a PAR assay, showing that the filtrate was devoid of Zn^{2+} (data not shown). Finally, to determine whether protein could non-specifically carry (extraneous) metal through the Zeba column, 10 μM bovine serum albumin (BSA), a protein which does not possess high-affinity zinc binding sites, was prepared in ammonium acetate (25 mM, pH 7.0), and was exposed to 70 μM

$ZnSO_4$ for 10 min. After incubation, the protein was passed through the Zeba column, and the zinc content was determined using a PAR assay, demonstrating that only a marginal amount of zinc (< 0.5 μM) was non-specifically carried through the column (data not shown). Based on these results, it was concluded that Zeba desalting columns were suitable to process LF samples incubated with $^{70}Zn^{2+}$ prior to their analysis by ICP-MS.

After incubation of ZnLF in the presence of a 10-fold excess of $^{70}Zn^{2+}$ for the desired time, the exchange process was halted by the addition of EDTA, and extraneous zinc was removed using a Zeba desalting column. The ratio of ^{70}Zn to ^{64}Zn in the LF samples was determined using ICP-MS. The experimentally determined isotope ratios were then used to calculate the $ttr^{(70,64)}$ and N (the amount of exchanged zinc) values, as described in the Materials and Methods section (see section 3.10.4). The results of the isotope exchange are shown in Fig. 4.8. These results indicate that the zinc-to^{70}Zn exchange was very rapid. The $t_{1/2}$ value is < 5 s, with the exchange reaching completion after 20 s. This exchange was the fastest of any of the exchange reactions studied in this work.

The zinc-to-^{70}Zn exchange experiment was repeated for one time point (t = 10 s) with a lower concentration of extraneous $^{70}Zn^{2+}$ provided (7 μM) to determine if the rate of exchange was dependent on the concentration of the free metal, which would be expected for an associative but not for a dissociative mechanism. As Table 4.3 shows, zinc exchange occurred more rapidly with the higher concentration of extraneous $^{70}Zn^{2+}$, suggesting that the exchange proceeds via an A-type mechanism.

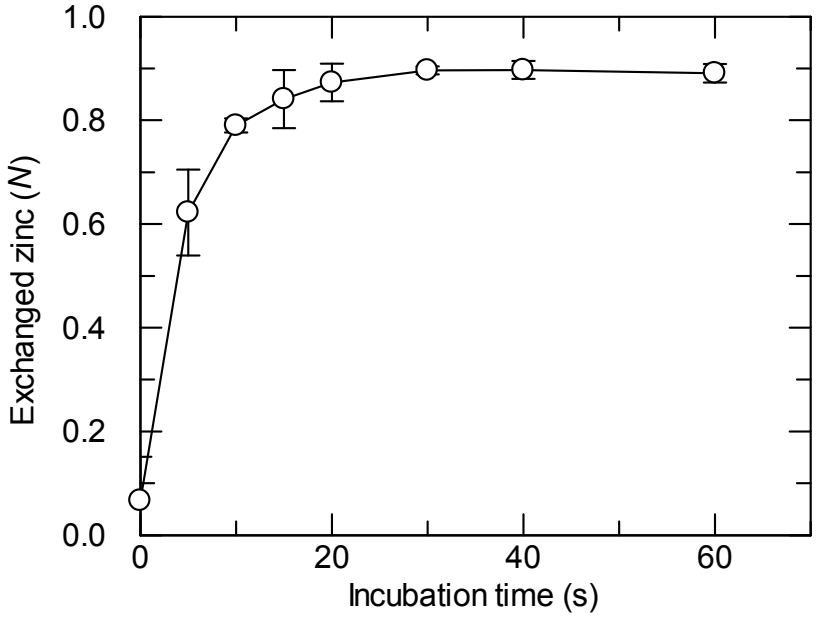

Figure 4.8: Time-dependence of (naturally abundant) zinc-to-^{70}Zn exchange. ZnLF (7 μM) was incubated with 70 μM $^{70}Zn^{2+}$ in ammonium acetate buffer (25 mM, pH 7.0) for the indicated time prior to terminating the exchange reaction by the addition of EDTA (80 μM), and removal of extraneous zinc by Zeba filtration. Isotope ratios (^{70}Zn/^{64}Zn) were measured using ICP-MS, and converted to *N* values (exchanged zinc) using equations 6 and 7. Values shown represent the mean ± 1 S.D. of three independent experiments.

Table 4.3: Experimentally determined *N* values for the (naturally abundant) zinc-to-^{70}Zn exchange for two different concentrations of extraneous $^{70}Zn^{2+}$.

Exchange conditions [a]	**Exchanged zinc (*N* value)** [b]	**Standard deviation**
7 μM $^{70}Zn^{2+}$	0.25	± 0.01
70 μM $^{70}Zn^{2+}$	0.79	± 0.01

[a] Both exchanges used 7 μM ZnLF in ammonium acetate buffer (25 mM, pH 7.0) with a 10 s exposure time.

[b] *N* values were determined from the measured ^{70}Zn/^{64}Zn ratios as described in the Materials and Methods section. Three independent experimented were performed.

4.2.5 Summary of exchange rates

Overall it is clear that the metal exchange process is quite rapid in LF. The time of half-exchange ranged from 8 min for the cobalt-to-zinc exchange to as quickly as less than 5 s for the zinc-to-^{70}Zn exchange (Table 4.4). Comparing these results to the half times of exchange (or $t_{1/2}$ values) predicted from the experimentally determined dissociation rate

constants (see Table 4.1) makes it apparent that the exchange cannot occur via a dissociative mechanism. If exchange was dependent on the dissociation of the metal from the active site prior to binding of a new (incoming) metal, the expected time of half-exchange would be much longer (approximately 3 h in the case of ZnLF). It is clear that an associative mechanism is operative during the exchange process. Hence, there must be a second metal binding site that is used to form a bimetallic intermediate. As previously mentioned, it is known that excess metal inhibits LF (83,85). Therefore, it is conceivable that the inhibitory metal binding site and the second metal binding site are one and the same.

Table 4.4: Experimentally determined time of half-exchange values ($t_{1/2}$) for various metal exchanges in LF.

Exchange	**Approximate time of half-exchange ($t_{1/2}$)**	**Conditions**
Zinc → Cobalt	1 - 3 min	*50 nM Zinc; 1 mM Cobalt*
Cobalt → Zinc [a]	8 min	*250 nM Cobalt; 250 nM Zinc*
Zinc → Copper	~ 10 s	*50 nM Zinc; 10 μM Copper*
Zinc → ^{70}Zn	< 5 s	*7 μM Zinc; 70 μM ^{70}Zinc*

[a] For the cobalt-to-zinc exchange, 50 nM apoLF was pre-exposed to 250 nM Co^{2+} prior to the addition of Zn^{2+}.

4.3 Metal inhibition

4.3.1 Inhibition by cobalt

The effect of cobalt on LF was investigated by exposing ZnLF to various concentrations of cobalt. The activity of LF was affected in two stages (see Fig. 4.9). Initially, cobalt increased the activity of LF due to the replacement of Zn^{2+} with Co^{2+} in the active site, which reached a maximum relative activity of RA ~2.2 (at 4 mM Co^{2+}). This was the same value observed for the zinc-to-cobalt exchange (see section 4.3.1). As the concentration of cobalt increased further, there was a dramatic reduction in LF activity as Co^{2+} became inhibitory in the low millimolar range. To ensure that the observed inhibition

was not a result of a decreased pH (due to the high metal concentration), the pH was measured for a sample containing 100 mM $CoSO_4$ (the highest concentration tested) in Hepes buffer (50 mM, pH 7.4). No significant drop in pH was detected ($\Delta pH \leq 0.15$). Since the concentration range for inhibition by Co^{2+} is approaching that where the ionic strength of the solution may affect LF activity (as previously observed for NaCl) (107), the contribution of ionic strength to the inhibition was investigated.

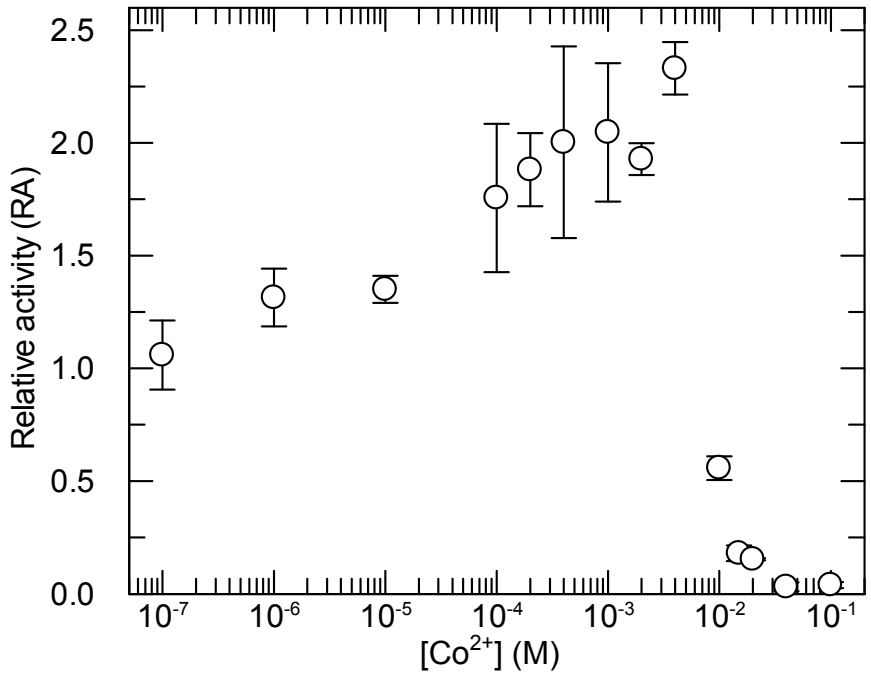

Figure 4.9: Effect of Co^{2+} on the activity of ZnLF. ZnLF (50 nM) was incubated with varying concentrations of Co^{2+} in Hepes buffer (50 mM, pH 7.4). Activity was measured using *S*-*p*NA (10 μM). Relative activity is defined as the activity relative to that recorded for 50 nM ZnLF in the absence of Co^{2+}. Values represent the mean ± 1 S.D. of three independent experiments.

4.3.2 Influence of ionic strength on inhibition of LF by cobalt

To determine whether the inhibition observed with Co^{2+} was due to the high ionic strength of the solution or due to cobalt binding to the inhibitory site, two experiments were conducted. The first one was aimed at assessing the difference in inhibition of two solutions

of the same ionic strength containing 20 mM $CoSO_4$ or 27 mM $CoCl_2$. It was anticipated that the $CoCl_2$ solution, which has a higher concentration of Co^{2+}, would act as a more potent inhibitor, and would thus indicate that Co^{2+} has an inhibitory effect on LF. Surprisingly, $CoSO_4$ was found to be more inhibitory than $CoCl_2$, revealing that the counter ion (SO_4^{2-} vs. Cl^-) affects LF activity (data not shown). Therefore, the inhibition of ZnLF by $CoSO_4$ and $MgSO_4$ was assessed. Because these two salts exert the same ionic strength (at the same concentration), and have the same counter anion (SO_4^{2-}), any differences in inhibition can be attributed to Co^{2+}.

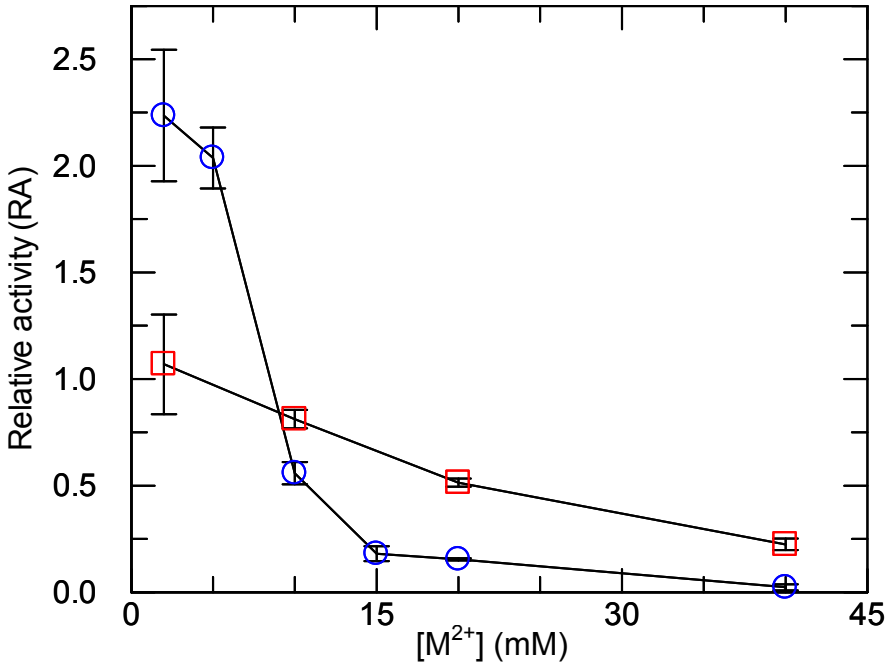

Figure 4.10: Effect of $CoSO_4$ (blue circles) and $MgSO_4$ (red squares) on ZnLF activity. ZnLF (50 nM) was incubated with varying concentrations of $CoSO_4$ or $MgSO_4$ in Hepes buffer (50 mM, pH 7.4). Activity was measured with *S*-*p*NA (10 µM). Relative activity is defined as the activity relative to that recorded for 50 nM ZnLF in the absence of $CoSO_4$ or $MgSO_4$. Values represent the mean ± 1 S.D. of three independent experiments.

As shown in Fig. 4.10, the profound drop in activity between 5 and 10 mM in the case of $CoSO_4$ (but not for $MgSO_4$) clearly demonstrates that Co^{2+} is more inhibitory than Mg^{2+},

suggesting that Co^{2+} does indeed have an inhibitory effect on LF. The half maximal inhibitory concentration (IC_{50}) for $CoSO_4$ was found to be between 5 mM and 10 mM, and hence nearly three orders of magnitude higher than the IC_{50} values observed for Zn^{2+} and Cu^{2+} (85).

4.3.3 Zinc inhibition

The enzymatic activity of ZnLF was determined for various concentrations of substrate (*S*-*p*NA) and inhibitor (Zn^{2+}) to obtain information regarding the mode of inhibition. The data was fit to several inhibition modalities (competitive, uncompetitive, mixed-type, non-competitive), with the best fit being obtained using a pure non-competitive model (see Fig. 4.11).

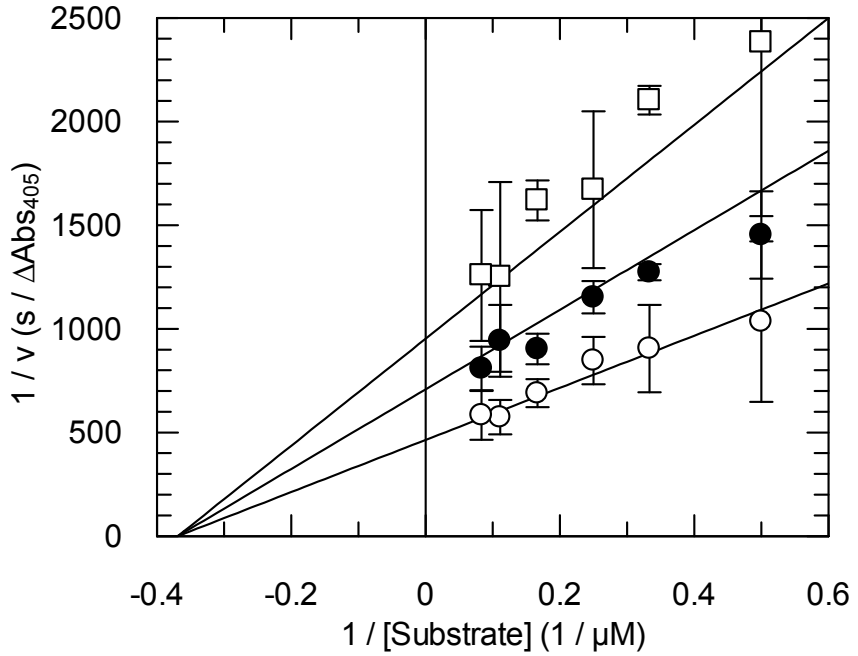

Figure 4.11: Lineweaver-Burk plot of ZnLF inhibition by Zn^{2+}. Three concentrations of the inhibitor, Zn^{2+}, were tested: 0 μM (white circles), 15 μM (black circles), and 30 μM (white squares). The data was fit to a non-competitive inhibition model using the non-linear least squares method as described in section 3.11.2. Values represent the mean ± 1 S.D. of three independent experiments.

This fitting resulted in the determination of various kinetic parameters for Zn^{2+} inhibition of LF, including $K_M = 2.71 \pm 0.37$ μM, $K_I = 28.5 \pm 2.3$ μM, and $k_{cat} = 4.3 \pm 0.2$ s^{-1}. The K_M and k_{cat} values are in agreement with those found in the literature ($K_M = 3.5$ μM, $k_{cat} = 3.7$ s^{-1}) (84).

A similar experiment was performed to determine the mechanism of inhibition of CuLF by Cu^{2+}. However, Cu^{2+} inhibition was found to be much more pronounced, and it was not possible to obtain reliable data as slight changes in the concentration of extraneous Cu^{2+} yielded very different activities leading to large standard deviations.

4.4 Terbium studies

As discussed before, terbium (III) is a lanthanide ion with a high affinity for calcium binding sites, and is often employed in studying calcium sites in proteins due to its spectroscopic properties and its ability to occupy these sites at much lower concentrations (87). Previous studies have determined that Tb^{3+} is capable of binding and inhibiting LF with an IC_{50} value of 23 μM (83), a concentration strikingly similar to the IC_{50} values from the literature for Zn^{2+} and Cu^{2+} (85). This observation raises the possibility that Tb^{3+} might occupy the same (inhibitory) site as Zn^{2+} and Cu^{2+}. Thus, investigations into terbium's role in metal exchange and inhibition in LF were initiated.

4.4.1 Metal exchange in the presence of terbium

If an associative mechanism were to be operative for metal exchange in LF involving the occupation of the inhibitory site, and if Tb^{3+} were to occupy this site, then the rate of exchange would be decreased in the presence of the lanthanide ion. Terbium is an ideal

candidate for such an experiment because it is expected to bind the inhibitory site in LF, but it should not be capable of binding to the active site due to its large size and preference for a coordination number higher than four (LF's active site zinc ion is four-coordinate) (87). This was confirmed with ICP-MS. Incubation of ZnLF (7 μM) with an excess of Tb^{3+} (150 μM) for 10 min did not significantly decrease the amount of Zn^{2+} following removal of extraneous metal with a Zeba desalting column (data not shown). To determine if the rate of the exchange process decreased in the presence of Tb^{3+}, previously applied (naturally abundant) zinc-to-^{70}Zn exchange conditions were used except for the addition of an inhibitory concentration of Tb^{3+} (150 μM). The processing of these samples, including the determination of the metal content, was repeated exactly as described for the zinc-to-^{70}Zn exchange (see section 3.10.4). The results of this exchange are listed in Table 4.5.

Table 4.5: Experimentally determined *N* values for the (naturally abundant) zinc-to-^{70}Zn exchange in the absence and presence of Tb^{3+} (150 μM).

Exchange conditions [a]	**Exchanged zinc (*N* value)** [b]	**Standard deviation**
LF	0.79	± 0.01
LF + Tb^{3+}	0.61	± 0.01

[a] Both exchanges used 7 μM ZnLF and 70 μM ^{70}Zn in ammonium acetate buffer (25 mM, pH 7.0) with a 10 s exposure time.
[b] Values represent the mean of two independent experiments.

The results indicate that Tb^{3+}-binding impedes active site metal exchange, suggesting that Tb^{3+} and $^{70}Zn^{2+}$ compete for a common binding site. The amount of exchanged zinc decreased by almost 20%. This suggests that occupying the inhibitory site is important for metal exchange.

Additional samples were prepared in ammonium acetate buffer (25 mM, pH 7.0) to determine how Tb^{3+} interacts with apoLF. One sample contained 7 μM apoLF, which was exposed to 10 μM $^{70}Zn^{2+}$ for 10 s, followed by quenching of the reaction with 300 μM

EDTA. The second sample was prepared by pre-incubating 7 μM apoLF with 150 μM $TbCl_3$ for 3 min. After incubation, 10 μM $^{70}Zn^{2+}$ was added, and the mixture was allowed to incubate for 10 s prior to quenching (with EDTA). Following the quenching of these samples, they were immediately processed through an ammonium acetate-equilibrated Zeba column. Determination of the metal content using ICP-MS revealed the apoLF sample that had been pre-exposed to Tb^{3+} to have 50% less protein bound-$^{70}Zn^{2+}$ than the apoLF sample that did not contain any Tb^{3+} (0.26 occupancy compared to 0.50 occupancy). This result suggests that for the apo-form of LF, Tb^{3+} may compete with $^{70}Zn^{2+}$ binding to the active site.

4.4.2 Tyrosine-sensitized terbium luminescence spectroscopy

Studies were designed to explore how terbium-binding is affected by the addition of other metals known to bind LF. Terbium is a metal that can be used to explore the relationship between the active site and the inhibitory site in LF. Excitation of tyrosine residues at 274 nm will cause FRET with nearby protein-bound Tb^{3+} (see sections 1.5). This energy transfer will cause terbium to luminesce, and the intensity of the luminescent signal is dependent on the distance between the tyrosine residues and the Tb^{3+} ion(s) (93). The effect of Cu^{2+}-binding on FRET between apoLF and Tb^{3+} was investigated.

As shown in Fig. 4.12, the addition of apoLF to Tb^{3+} (prior to addition of Cu^{2+}) resulted in a 75-fold enhancement of the luminescence signal at 543 nm. Furthermore, the results clearly indicate that increasing the concentration of Cu^{2+} in solution decreased the luminescence intensity of Tb^{3+}. This would suggest that Cu^{2+} and Tb^{3+} share a common binding site. Increasing the concentration of Cu^{2+} dislodges Tb^{3+} from LF and forces it back

into solution, resulting in a weakened luminescence signal. In order to demonstrate more clearly this feature, the data was replotted, only considering the peak intensity at 543 nm as a function of the Cu^{2+} concentration (Fig. 4.13).

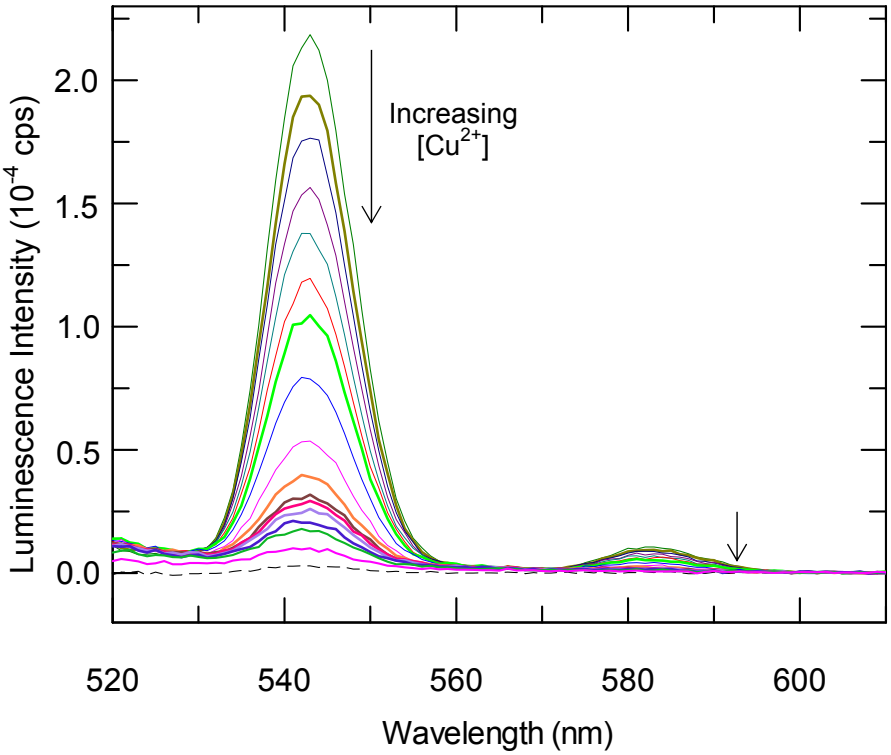

Figure 4.12: The effect of Cu^{2+} on tyrosine-sensitized terbium luminescence spectra of apoLF. ApoLF (1 μM) was incubated with 100 μM $TbCl_3$ in Hepes buffer (50 mM, pH 7.4) for 2 min followed by sequential addition of $CuSO_4$ (0, 0.25, 0.50, 0.75, 1.0, 1.5, 2.0, 3.0, 5.0, 6.0, 7.0, 10, 12, 15, 25, 50 μM). The spectrum of Tb^{3+} (100 μM) in the absence of apoLF is shown as a dashed black line. All spectra were recorded using an excitation wavelength of 274 nm.

The decrease in luminescence intensity upon the addition of Cu^{2+} appears to occur in two steps. Initially, a small increase in the Cu^{2+} concentration causes a dramatic decrease in the luminescence signal, with a 50% reduction in luminescence observed at only 2 μM Cu^{2+} (2-fold excess over apoLF). It is likely that the sharp decrease in luminescence intensity is a result of Cu^{2+} being inserted into the active site. The decrease in luminescence intensity becomes more gradual at Cu^{2+} concentrations of ≥6 μM. This result suggests that the active

site becomes fully occupied by Cu^{2+} at concentrations below 6 μM, and that the sharp decrease in the luminescence signal is due to the migration of Tb^{3+} into another (inhibitory) site. As the Cu^{2+} concentration continues to increase (up to 100 μM), the signal is eventually reduced to that of Tb^{3+} in solution, indicating that Cu^{2+} has fully occupied the inhibitory site, and Tb^{3+} is no longer protein-bound.

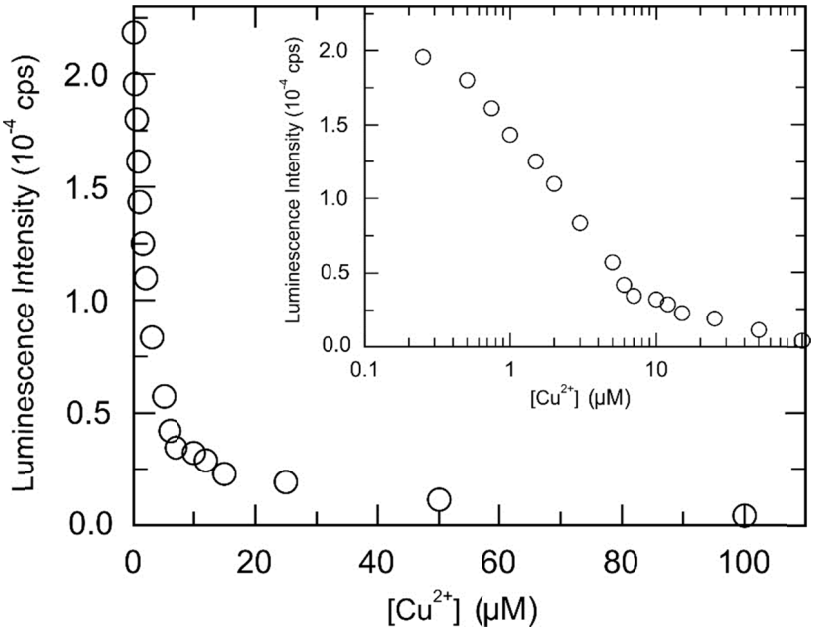

Figure 4.13: Dependence of the luminescence intensity at 543 nm as a function of the Cu^{2+} concentration. Spectra were recorded as indicated in the caption of Fig. 4.12. Inset: Replot of the data using a logarithmic scale for the x-axis.

To confirm that the initial drop in luminescence signal (between 0 μM and 5 μM) was a result of the insertion of Cu^{2+} into the active site, a similar experiment was conducted with CuLF in place of apoLF (to ensure there is no competition for active site ligands between Tb^{3+} and Cu^{2+}). These results are shown in Fig. 4.14.

The titration of CuLF with Cu^{2+} did not display the same dramatic 75-fold luminescence enhancement that was observed for apoLF (see Fig. 4.12). Indeed, the increase in luminescence intensity upon the addition of CuLF to Tb^{3+} was found to be only 10-fold.

This result appears to suggest that the large 75-fold enhancement observed in apoLF is due to the availability of vicinal active site residues for Tb^{3+} binding, likely involving a direct interaction with Tyr728 (see Discussion).

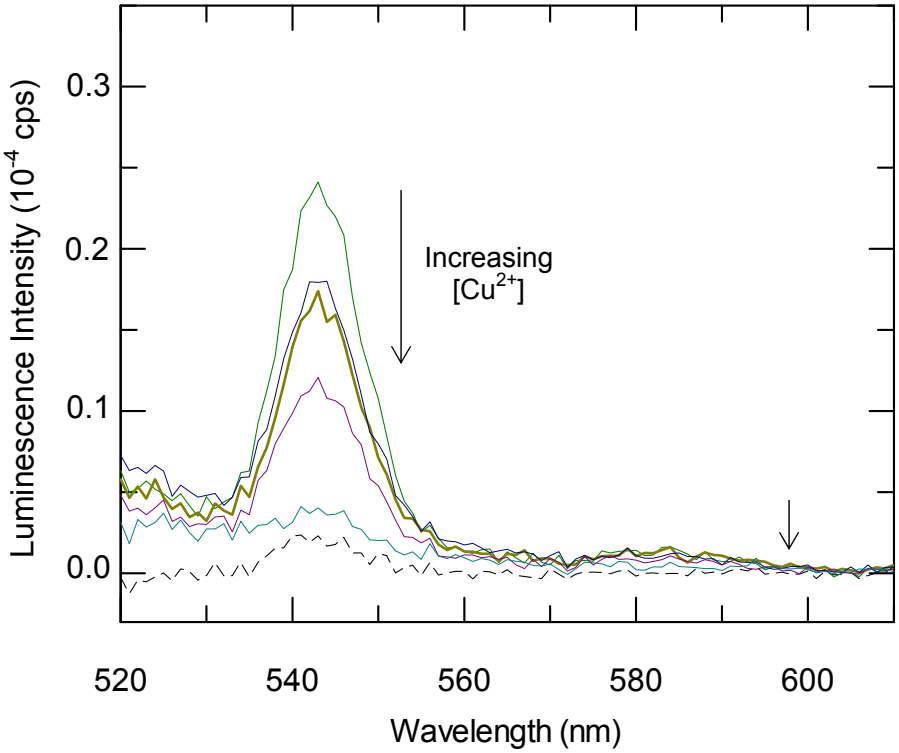

Figure 4.14: The effect of Cu^{2+} on tyrosine-sensitized terbium luminescence spectra of CuLF. CuLF (1 μM) was incubated with 100 μM $TbCl_3$ in Hepes buffer (50 mM, pH 7.4) for 2 min followed by sequential addition of $CuSO_4$ (0, 2, 10, 25, 100 μM). The spectrum of Tb^{3+} (100 μM) in the absence of LF is shown as a dashed black line. All spectra were recorded using an excitation wavelength of 274 nm.

5. Discussion

Due to the importance of metal substitution for investigations of the mechanism and inhibition of metalloproteins, an understanding of the process by which metal exchange can occur is crucial to allow for the optimization of such replacement processes. This research was aimed at gaining a deeper understanding of the metal exchange process in LF. LF is a representative member of the zinc-dependent endopeptidase family as it contains the HExxH thermolysin-like zinc binding consensus motif, which is common to many zinc proteases (108). Thus, insight gained from studies on LF's active site may be applicable to many related proteins. LF is also a protein of considerable interest due to its potential use as a component of biological weapons. The 2001 anthrax attacks in the United States resulted in 11 confirmed human infections with *Bacillus anthracis*, five of which resulted in death (109). This was the first time that anthrax spores had been used effectively as a weapon of bioterrorism. Since these attacks, a vast amount of research has gone into gaining an understanding of the pathogenesis and molecular function of the toxins responsible for this disease. This research aims to provide additional knowledge on the metal exchange process and the identity of the inhibitory metal binding site in LF.

5.1 Kinetics and mechanism of metal exchange

The first objective of this research was to gain insight into the mechanism of metal exchange in LF by determining whether this process occurs primarily by a dissociative (D-type, S_N1) or an associative (A- type, S_N2) mechanism. Initial investigations into the kinetics of active site metal displacement revealed that the removal of zinc (from ZnLF) using an S_N1-type chelator (i.e., EDTA) was a slow process, with a time required to demetallate half

of the LF molecules ($t_{1/2}$) of ~3 h. From this experiment, the dissociation rate constant was determined for ZnLF to be 6.19×10^{-5} s^{-1}. The dissociation rate constants for CoLF (3.57×10^{-3} s^{-1}) and CuLF (2.94×10^{-3} s^{-1}) were much higher than that observed for ZnLF. The higher value for CoLF can be explained by the larger dissociation constant (K_d) for Co^{2+}. Indeed, the ratio of the dissociation constants of CoLF and ZnLF (see Table 4.1) is 62.5, and hence is very similar to the ratio of the corresponding dissociation rate constants:

$$\frac{k_{off}(CoLF)}{k_{off}(ZnLF)} = \frac{3.57 \times 10^{-3} s^{-1}}{6.19 \times 10^{-5} s^{-1}} = 57.7$$

This suggests that the association rate constants are similar (5.2×10^{7} M^{-1} s^{-1} for ZnLF, 4.8×10^{7} M^{-1} s^{-1} for CoLF). The calculated association rate constant for ZnLF (5.2×10^{7} M^{-1} s^{-1}) is comparable to those reported for two peptides designed from the structural zinc site of alcohol dehydrogenase (7.0×10^{6} M^{-1} s^{-1}) and from a zinc finger consensus motif (2.3×10^{6} M^{-1} s^{-1}) (110). Although the association rate constant for ZnLF is higher than for either of these peptides, it is clearly below the approximate diffusion-controlled association rate limit (10^{9} M^{-1} $s^{-1} \leq k_{on} \leq 10^{10}$ M^{-1} s^{-1}) (52). CuLF has a dissociation rate constant similar to CoLF, although it has the lowest dissociation constant (340 fM) of the three species. This suggests a very high association rate constant (8.6×10^{9} M^{-1} s^{-1}). Indeed, the high lability of Cu^{2+} is a well-documented feature, resulting in unusually fast water exchange rates, which are a consequence of either a Jahn-Teller distortion elongating two bonds of the octahedral Cu^{2+} complex (3,111), or based on fluctuations between trigonal bipyramidal and square pyramidal geometries in a fivefold coordination state (112).

The dissociation of zinc from ZnLF would be the first and rate-limiting step in a dissociative exchange pathway (see Fig. 1.3). Because of this, any metal exchange via a dissociative mechanism with ZnLF would have a time of half-exchange of at least 3 h.

Considering the results from the metal exchange assays with ZnLF, it is clear that a dissociative mechanism can be ruled out. Indeed, the time of half-exchange for the three ZnLF exchanges monitored (ZnLF-to-CoLF, ZnLF-to-CuLF, and ZnLF-to-^{70}ZnLF) ranged from 10 s to 3 min, and was thus $10^3 - 10^4$ times faster than that anticipated based on a D-type metal exchange. Hence, it is apparent that metal exchange in LF proceeds via an associative mechanism. This view is consistent with a hypothesized associative mechanism of metal exchange between metalloproteins *in vivo* (113,114). For instance, proteins that mediate metal homeostasis, including metal sensor proteins such as InrS (nickel-responsive efflux derepressor) and ZiaR (zinc-responsive efflux derepressor), have low dissociation constants (InrS: $K_{Ni}^{2+} = 2.1\times10^{-14}$ M, ZiaR: $K_{Zn}^{2+} \sim 5\times10^{-13}$ M) for the metals they regulate (113,114). Because of these high affinities, the free concentrations of the metals they regulate are typically kept below 10^{-9} M, rendering them not freely available in the solution (114). Therefore, based on the high affinities of these proteins (and their slow dissociation rate constants), it is "not credible for metal partitioning to and from solution to reach equilibrium in a viable timeframe" (dissociative mechanism) (114). However, the rates of metal exchange observed in cells could be explained by an associative mechanism using the polydisperse buffer of the cytosol (113,114).

Of the four metal exchanges described in this work, the zinc-to-copper and zinc-to-^{70}Zn exchanges were the fastest, followed by the zinc-to-cobalt and finally the cobalt-to-zinc exchange. The order of the rates of exchange is identical to that observed for the water exchange rates of the metal-aqua complexes of 3d transitions metals (3). Cu^{2+} has a water exchange rate (at 25 °C) of 1×10^9 s^{-1}, followed by Zn^{2+} (2×10^7 s^{-1}), and Co^{2+} (3×10^6 s^{-1}). It is interesting to note that the cobalt-to-zinc exchange seems to be quite slow compared to the

other three exchanges, with a $t_{1/2}$ value of 8 min. However, the lower rate of this exchange can be attributed to the different exchange conditions that were applied. For this exchange, equal amounts of Co^{2+} and Zn^{2+} were incubated with CoLF, and the results suggest that the exchange was simply a consequence of the different affinities for the active site. In the other exchange reactions, the extraneously provided metal was present in excess (≥ 10-fold).

The two zinc-to-^{70}Zn exchanges (performed with equal quantities of ZnLF and $^{70}Zn^{2+}$, and with a 10-fold excess of $^{70}Zn^{2+}$) provided insight into the mechanism of exchange. Because it was hypothesized that exchange occurs via an associative mechanism using the inhibitory binding site, the degree of occupation of the inhibitory site should directly correlate with the rate of the exchange. For either of the concentrations of extraneous $^{70}Zn^{2+}$, the amount of enzyme that is bound by inhibitory zinc can be determined using equation 11 (derived from equation 10):

$$K_I = \frac{(E_{tot} - E_{Zn_I})(Zn_{tot} - E_{Zn_I})}{E_{Zn_I}} \qquad \text{(eq. 10)}$$

$$\left(E_{Zn_I}\right)^2 - (Zn_{tot} + E_{tot} + K_I)E_{Zn_I} + (Zn_{tot}E_{tot}) = 0 \qquad \text{(eq. 11)}$$

where Zn_{tot} is the total concentration of (extraneous) zinc, E_{tot} is the total enzyme concentration, K_I is the dissociation constant of the inhibitory zinc ion, and E_{Zn_I} is the concentration of enzyme to which the inhibitory zinc is bound. Using the experimentally determined K_I value (28.5 μM, see section 4.3.2), and the concentration for E_{tot} of 7 μM, E_{Zn_I} was determined by solving the quadratic equation (equation 11). The occupancy of the inhibitory site was then determined using equation 12:

$$Occupancy = \frac{E_{Zn_I}}{E_{tot}}\ 100\% \qquad \text{(eq. 12)}$$

In the case of the zinc-to-^{70}Zn exchange with 7 μM $^{70}Zn^{2+}$ (Zn_{tot}), the occupancy of the inhibitory site was 17%, whereas for the exchange with 70 μM $^{70}Zn^{2+}$, the occupancy was 70%. The ratio of these two values (70% / 17% = 4.1) closely reflects the ratio of the amount of exchange (*N* value) determined by ICP-MS (see Table 4.3) (0.79 / 0.25 = 3.2). This result would suggest that the level of occupation of the inhibitory site is a good indicator of the rate of exchange, supporting the hypothesis that exchange proceeds through occupation of the inhibitory site.

5.2 Metal inhibition

Studies with respect to the influence of Co^{2+} on LF activity revealed that inhibition occurs in the low millimolar range. Although the inhibition observed can partly be attributed to the high ionic strength, it is clear that Co^{2+} itself has an inhibitory effect on LF. The nearly 10^3-fold decreased affinity for Co^{2+} to the inhibitory site (IC_{50} ~10 mM, compared to 12 μM for Zn^{2+} and 15 μM for Cu^{2+}) is similar to the decreased affinity for Co^{2+} in the active site (84). This is consistent with the Irving-Williams series which predicts Co^{2+}-complexes to have much lower stability than the same complexes formed with Zn^{2+} and Cu^{2+} (7). Requiring such high levels of Co^{2+} for the inhibition would make this phenomenon biologically irrelevant, since the concentration of free Co^{2+} in cells is not expected to ever exceed 100 pM (1,114).

The mechanism of inhibition that Zn^{2+} exerts on ZnLF has been experimentally determined to be non-competitive. Interestingly, this observation is supported by results of the zinc-to-copper exchanges in LF after 10 s of exposure of the enzyme to Cu^{2+}, studied with both standard activity assays and under stopped-flow conditions. While the enzyme was

pre-exposed to Cu^{2+} (for 10 s) prior to the addition of *S*-*p*NA in the standard activity assay, ZnLF was exposed to Cu^{2+} and substrate simultaneously in the stopped-flow studies (i.e., there was no pre-incubation of LF with Cu^{2+}). Interestingly, the exchange progress after 10 s of the initiation of the (stopped-flow) reaction (38%) was virtually identical to that determined for the standard activity assay (37%) (see section 4.2.3). This result suggests that substrate binding does not impede the exchange process, and thus does not interfere with inhibitory site binding (as would be expected for non-competitive inhibition).

The fact of having Zn^{2+} acting as a non-competitive inhibitor is somewhat at odds with what has been observed for related zinc enzymes, including thermolysin and carboxypeptidase A. For both of these enzymes, the mechanism of inhibition has been determined to be competitive (60,65). As mentioned previously, in the case of these two enzymes, the competitive inhibition occurs because the inhibitory Zn^{2+} is bridged to the active site Zn^{2+} ion by the water molecule that is used in the hydrolytic cleavage of the substrate. This interaction between inhibitory and active site Zn^{2+} ions blocks the entry of the substrates to the active sites. Hence, substrate and inhibitory Zn^{2+} binding are mutually exclusive (competitive inhibition). Because the inhibitory site in LF is predicted to be located immediately adjacent to the active site, it would intuitively suggest that the mode of inhibition is competitive. However, this is clearly not the case. The non-competitive nature of the inhibition, hence suggests that the inhibitory Zn^{2+} is coordinated to amino acid residues not directly involved in substrate binding, and that there is no steric hindrance between the two.

LF is not the only zinc-dependent enzyme that is non-competitively inhibited by Zn^{2+}. A very similar situation has been observed for botulinum neurotoxin serotype A (BoNT A).

This zinc-dependent protease is the most potent of all botulinum neurotoxins, the causative agents of botulism, and one of the most toxic substances known to man (115). In BoNT A, Zn^{2+} is required at the catalytic site for hydrolytic cleavage of its substrate. An inhibition constant of 10.2 μM has been determined for Zn^{2+} (116), which is similar to the inhibition constant (28.5 μM) determined in this work for the inhibition of LF by Zn^{2+}. Interestingly, the inhibitory site in BoNT A is predicted to be located immediately adjacent to the active site (Fig. 5.1), similar to what is proposed for LF. However, the cysteine residue coordinating the inhibitory Zn^{2+} in BoNT A (116) is absent in LF. Nonetheless, these observations demonstrate that non-competitive inhibition can occur even if the inhibitory site is located directly adjacent to the active site, and that proximal Zn^{2+} binding would not necessarily impede substrate binding.

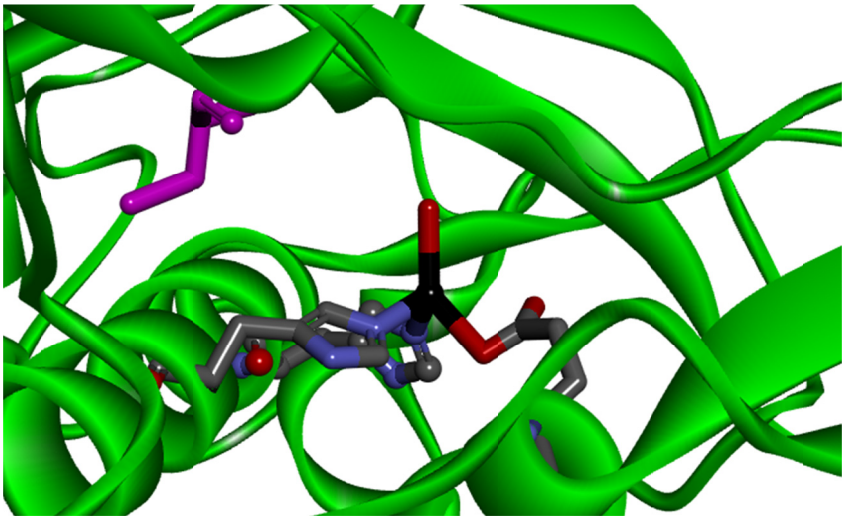

Figure 5.1: Structure of the BoNT A active site (PDB ID: 1XTG) (117). The protein is shown in green, the active site Zn^{2+} is in black, shown with its coordinating residues. The adjacent cysteine residue thought to coordinate the inhibitory Zn^{2+} is shown in magenta.

A second example where Zn^{2+} exerts an inhibitory effect in a mode different from competitive is in dipeptidyl peptidase III (DPP III). DPP III is a zinc metallopeptidase that is uncompetitively inhibited by excess zinc. The active site of this enzyme uses a HELLGH-E

motif to bind zinc, with a dissociation constant of 500 fM (44). Excess zinc inhibits DPP III with a K_I of 10 μM (44), which is very similar to the K_I value for Zn^{2+} and Cu^{2+} inhibiting LF.

Non-competitive inhibition has also been observed for metal ions with several other unrelated metalloproteins. For example, urease, a nickel-dependent amidohydrolase, uses two Ni^{2+} ions in its active site. This enzyme is non-competitively inhibited by Cu^{2+}, Ni^{2+}, Pb^{2+}, and Co^{2+} in the low micromolar range (K_I values ranging from 5 to 30 μM) (118). Another example where non-competitive inhibition is observed is CphA from *Aeromonas hydrophila*. This Zn^{2+}-dependent β-lactamase is non-competitively inhibited by excess Zn^{2+} in the low micromolar range (71). Phosphoglucomutase, an enzyme that catalyzes the interconversion of glucose 1-phosphate and glucose 6-phosphate, uses Mg^{2+} in its active site. This enzyme is non-competitively inhibited by Cu^{2+} by binding at an inhibitory site (119). In summary, although competitive Zn^{2+} inhibition is what has been observed for thermolysin and carboxypeptidase A, two proteins related to LF, there is precedence for metalloproteins to be non-competitively inhibited by metals, even when the two metal binding sites are located in close proximity.

5.3 Terbium studies

Several important properties of LF were elucidated from the terbium studies. The first was that Tb^{3+} apparently binds in the vicinity of the active site. This was demonstrated by the data from the tyrosine-sensitized terbium luminescence studies. If the Tb^{3+} binding site were to be independent of the Cu^{2+} binding site, addition of Cu^{2+} to Tb^{3+}-supplemented apoLF would have had no effect on the luminescence signal emitted by Tb^{3+}. However, the

effect of Cu^{2+} addition was quite profound, with a drastic decrease of the luminescence proceeding in two phases (see Fig. 4.12 and Fig. 4.13). The first phase, between 0.25 μM and 6 μM Cu^{2+}, likely originates from Cu^{2+} insertion into the active site. If the inhibitory site is located adjacent to the active site, Tb^{3+} would bind to apoLF in the vicinity of Tyr728, which would give rise to the high intensity of the luminescence when the lanthanide binds to the apoprotein. The first phase of the Cu^{2+} titration appears to decrease the luminescence signal to a level similar to that observed for CuLF in place of apoLF (see Fig. 4.14). The notion of Tb^{3+} interacting with a site vicinal to the active site is reinforced by additional data from ICP-MS measurements using apoLF (section 4.4), where the amount of $^{70}Zn^{2+}$ taken up by apoLF was determined to be decreased by 50% when LF was pre-exposed to Tb^{3+}. Occupation of the active site with Cu^{2+} caused a large decrease in Tb^{3+} luminescence. Prior to the addition of Cu^{2+}, there was a 75-fold enhancement of the luminescence signal at 543 nm with respect to the signal of extraneous Tb^{3+}. A similarly high luminescence enhancement factor has been observed in transferrin when Tb^{3+} is directly bound to tyrosinate (120). It is proposed that Tb^{3+} directly binds Tyr728 in its deprotonated form in apoLF, thus resulting in highly efficient energy transfer. At 10 μM Cu^{2+} (when the active site is fully occupied with Cu^{2+}), this enhancement was only 10-fold. Therefore, the sharp drop in luminescence appears to be the result of Cu^{2+} (by binding to the active site) forcing Tb^{3+} to migrate away from its original position, causing the cleavage of the Tb^{3+}-Tyr728 bond. The increase in distance between Tb^{3+} and Tyr728 would likely result in the protonation of tyrosinate, hence, leading to a decrease in the efficiency of FRET. To ensure that the pronounced reduction in luminescence was not due to a spectral overlap between Cu^{2+} absorption and Tb^{3+} luminescence (a feature observed in Tb^{3+}-containing cobalt

thermolysin (93)), a titration was conducted with Zn^{2+} in place of Cu^{2+}. At 10 μM Zn^{2+}, the luminescence enhancement factor was 8.5-fold (relative to extraneous Tb^{3+}; data not shown), a value comparable to that obtained for Cu^{2+} (10-fold enhancement). Since Zn^{2+} is spectroscopically silent, and hence a spectral overlap between Tb^{3+} luminescence and Zn^{2+} absorption is not possible, the nearly identical luminescence enhancement with Zn^{2+} and Cu^{2+} rules out that the Cu^{2+}-induced decrease in luminescence intensity is a result of FRET.

The second phase of the apoLF titration, between Cu^{2+} concentrations of 6 μM and 100 μM, showed a much more gradual decrease in luminescence (see Fig. 4.12 and Fig. 4.13). The strength of the signal approached that of extraneous Tb^{3+} at 100 μM Cu^{2+}. This second phase appears to originate from the binding of Cu^{2+} to the inhibitory site, thus displacing Tb^{3+} completely from LF. Indeed, at 100 μM Cu^{2+}, a near full occupation of the inhibitory site by Cu^{2+} is expected due to the relatively high affinity of Cu^{2+} for this site (IC_{50} = 15 μM) (85).

Another conclusion that can be drawn from the Tb^{3+} studies is that occupation of the inhibitory site appears to be a step required for the metal exchange process. This was demonstrated by the zinc-to-^{70}Zn exchange conducted in the absence and presence of Tb^{3+} at inhibitory concentrations (150 μM). Without Tb^{3+}, the number of exchanged zinc ions (*N* value) was 0.79 compared to 0.61 when Tb^{3+} was present. Because Tb^{3+} will not strongly compete with $^{70}Zn^{2+}$ for the active site, the difference in *N* values can be attributed to a competition between Tb^{3+} and $^{70}Zn^{2+}$ for the inhibitory site, hence slowing down the metal exchange process. Although the concentration of Tb^{3+} was over 2-fold higher than that of $^{70}Zn^{2+}$ ($[Tb^{3+}]$ = 150 μM; $[Zn^{2+}]$ = 70 μM), the fact that the latter ion binds more tightly to

the inhibitory site (as evidenced by its 2-fold lower IC_{50} value (83,85)) explains why the zinc-to-^{70}Zn exchange still proceeds at a relatively rapid rate ($N = 0.61$ after 10 s).

5.4 Proposed link between inhibition and exchange

In order to substantiate the link between metal inhibition and exchange, a closer look at the active sites of LF and thermolysin in its Zn^{2+}-inhibited form is warranted. As Fig. 5.2 shows, the active site Zn^{2+} is coordinated nearly identically in these two proteins (using the HExxH motif). In thermolysin, the inhibitory zinc is coordinated to a histidine residue (His231) and a tyrosine residue (Tyr157). In LF, the two most proximally located amino acids that do not coordinate the active site Zn^{2+} are Tyr728 and Glu687. It is proposed here that these residues might be critical in the coordination of the inhibitory Zn^{2+} in LF. The results of the tyrosine-sensitized terbium luminescence studies show that the inhibitory Zn^{2+} must be located near the active site, and being coordinated to these residues would fulfill that requirement. This location of the inhibitory binding site would also explain the strong luminescence emitted by Tb^{3+}.

Interestingly, the literature shows that mutation of Tyr728 to alanine results in an enzymatically inactive protein that has a decreased zinc content (from 2 Zn^{2+} per LF to approximately 1 Zn^{2+} per LF (121)). If this is correct, it is feasible that the removal of this tyrosine residue prevents the second (inhibitory) zinc from binding LF, leaving only the active site zinc in the protein (hence explaining the decrease from two Zn^{2+} per LF molecule to one). This would clearly suggest not only that the inhibitory site is directly adjacent to the active site, but also that Tyr728 is important in the coordination of the inhibitory metal.

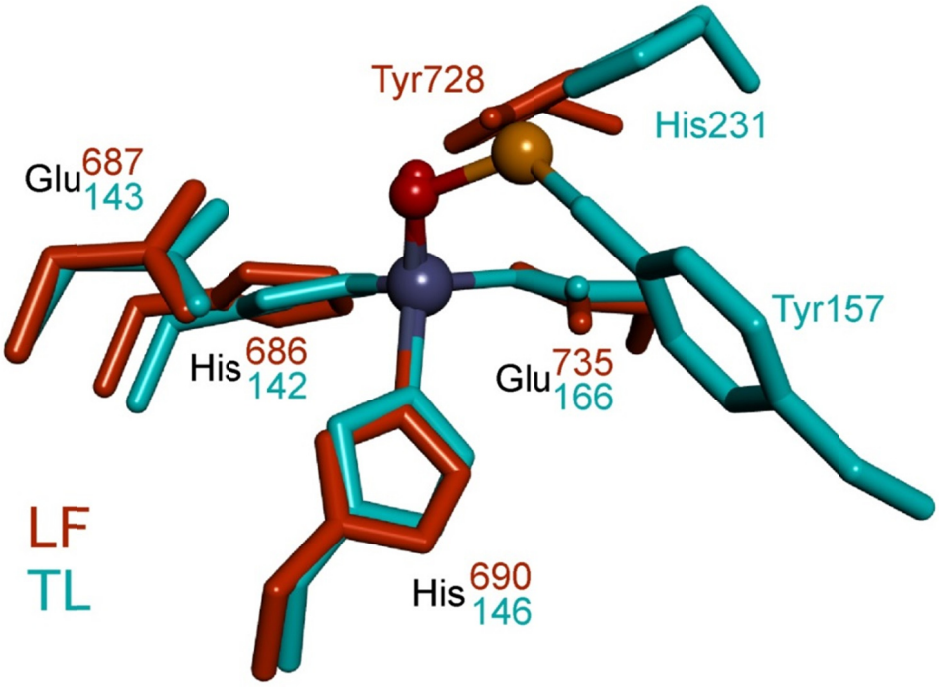

Figure 5.2: Superimposed active sites of LF and zinc-inhibited thermolysin (TL). The active site zinc ion is shown in dark blue, the inhibitory zinc ion (of TL) is shown in brown, water ligands are shown in red, along with the surrounding amino acids (60,80).

Regarding the labilization of the active site metal, it is likely that the binding of the inhibitory metal causes active site ligand sharing or swapping, resulting in a drastically reduced affinity for the Zn^{2+} in the active site. Furthermore, the presence of a second (inhibitory) Zn^{2+} ion located immediately adjacent to the active site Zn^{2+} would most likely decrease the metal affinity of the active site by electrostatic repulsion. Such repulsion could then allow for the (experimentally observed) high kinetic lability, with metal exchanges occurring with a $t_{1/2}$ value as low as 5 s. A plausible mechanism for such an exchange reaction is depicted in Fig. 5.3, where an extraneous metal first occupies the inhibitory site.

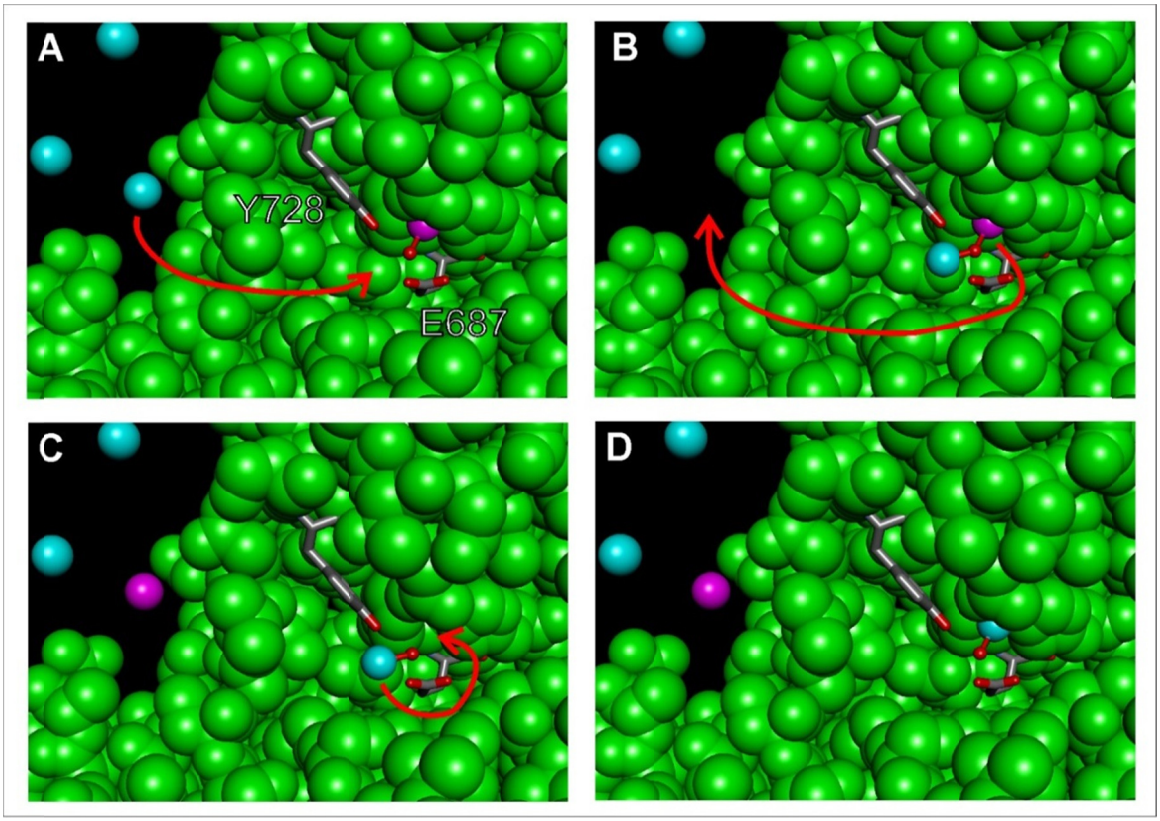

Figure 5.3: Proposed mechanism of metal exchange in LF. The substrate binding pocket of LF (PDB ID: 1J7N (80)) is shown in green, originally bound metal in magenta, and extraneous (exchanging) metal in cyan. The two residues (Tyr728 and Glu687) potentially involved in coordinating the inhibitory metal are depicted as stick models. In the proposed mechanism, the diffusion of the extraneous metal ion into the inhibitory metal binding site (A) leads to the formation of a water-bridged bimetallic species (B), in which the affinity for the active site ion is substantially decreased. Following dissociation of the active site ion (C), the process of metal exchange is completed by migration of the inhibitory (and previously extraneous) metal ion into the active site (D).

Once the active site metal has been labilized (through ligand sharing/swapping or electrostatic repulsion), and removed from the active site, a new metal can either enter the active site through the inhibitory site (depicted by the arrow in Fig. 5.3) or a metal can be taken up directly from solution with concomitant release of the metal ion from the inhibitory site.

In summary, the results discussed here have given insight into the metal exchange process in LF. A mechanism for metal exchange has been proposed utilizing the inhibitory

metal binding site to solve the apparent paradox of LF exhibiting rapid exchange kinetics despite the high metal affinities.

6. Conclusions and Future Work

The studies presented in this thesis provide insight into the high kinetic lability of the active site metal ion of LF despite its low dissociation constant. In addition, a proposal for the mechanism of metal inhibition and exchange were put forward. From the results presented, the following can be concluded: (i) the dissociation rate constants for various metallated forms of LF are too small for a dissociative exchange mechanism, and therefore an associative route is most likely utilized during the metal exchange process, (ii) the exchange process is rapid (with $t_{1/2}$ values ranging from 5 s to 8 min) and dependent on the concentration of extraneous metal, (iii) the level of occupation of the inhibitory site appears to correlate with the rate of metal exchange, (iv) Zn^{2+} exerts its inhibitory effect in a pure non-competitive fashion, and (v) Tb^{3+} competes with Zn^{2+} and Cu^{2+} with respect to the occupation of the inhibitory binding site. Combined, these results have led to the conclusion that rapid metal exchange in LF proceeds through a vicinal inhibitory metal-binding site.

Future studies should address the exact nature of the coordination environment of the inhibitory metal. Although Tyr728 is suggested as the primary candidate to be involved in inhibitory metal coordination, there is currently limited evidence to support this claim. X-ray crystallography with Zn^{2+}-soaked crystals of LF, and mutational studies replacing amino acid residues that could potentially form an inhibitory metal binding site are possible methods to gain further insight. Furthermore, tyrosine-sensitized terbium luminescence spectroscopy could be used to probe the interactions of Tb^{3+} and other metallated forms of LF (other than CuLF examined in this thesis) to determine if similar effects on lanthanide luminescence are observed. Finally, because the metal exchange mechanism described here for LF might also be operative in a large number of zinc-dependent proteases, similar work should be

performed with proteins such as thermolysin or carboxypeptidase A, which have properties similar to those of LF (e.g., rapid metal exchange kinetics, high active site metal affinity, an inhibitory metal binding site located adjacent to the active site).

In conclusion, this work has provided a framework designed to explain how metal exchange and inhibition occur in LF. This work may have implications in improving protocols to prepare metal-substituted metalloproteins (for spectroscopic studies), as well as to provide insight into how cellular metal pools remain dynamic at low metal concentrations *in vivo*.

References

1. Fraústo da Silva, J. J. R., and Williams, R. J. P. (2001) *The Biological Chemistry of the Elements: The Inorganic Chemistry of Life*, 2nd ed., Oxford University Press, Oxford

2. Bertini, I., Gray, H. B., Stiefel, E. I., and Valentine, J. S. (2006) *Biological Inorganic Chemistry: Structure and Reactivity*, University Science Books, Sausalito

3. Lippard, S. J., and Berg, J. M. (1994) *Principles of Bioinorganic Chemistry*, University Science Books, Mill Valley

4. Kaim, W., and Schwederski, B. (1991) *Bioinorganic Chemistry: Inorganic Elements in the Chemistry of Life*, Wiley, Chichester

5. Kieffer, F. (1991) *Metals and Their Compounds in the Environment - Occurrence, Analysis and Biological Relevance*, VCH, Weinheim

6. Lipscomb, W. N., and Sträter, N. (1996) Recent advances in zinc enzymology. *Chem. Rev.* **96**, 2375-2434

7. Irving, H., and Williams, R. J. P. (1953) The stability of transition-metal complexes. *J. Chem. Soc.*, 3192-3210

8. Wolfe, S. A., Nekludova, L., and Pabo, C. O. (2000) DNA recognition by cys2his2 zinc finger proteins. *Annu. Rev. Biophys. Biomol. Struct.* **29**, 183-212

9. Layat, E., Probst, A. V., and Tourmente, S. (2013) Structure, function and regulation of transcription factor IIIA: from *Xenopus* to *Arabidopsis*. *Biochim. Biophys. Acta* **1829**, 274-282

10. Foster, M. P., Wuttke, D. S., Radhakrishnan, I., Case, D. A., Gottesfeld, J. M., and Wright, P. E. (1997) Domain packing and dynamics in the DNA complex of the N-terminal zinc fingers of TFIIIA. *Nat. Struct. Biol.* **4**, 605-608

11. Benini, S., Rypniewski, W. R., Wilson, K. S., Miletti, S., Ciurli, S., and Mangani, S. (1999) A new proposal for urease mechanism based on the crystal structures of the native and inhibited enzyme from *Bacillus pasteurii*: why urea hydrolysis costs two nickels. *Structure* **7**, 205-216

12. Carter, E. L., Flugga, N., Boer, J. L., Mulrooney, S. B., and Hausinger, R. P. (2009) Interplay of metal ions and urease. *Metallomics* **1**, 207-221

13. Auld, D. S. (1988) Methods for metal substitution. *Methods Enzymol.* **158**, 71-79

14. Murakami, M., and Hirano, T. (2008) Intracellular zinc homeostasis and zinc signaling. *Cancer Sci.* **99**, 1515-1522

15. Yamasaki, S., Sakata-Sogawa, K., Hasegawa, A., Suzuki, T., Kabu, K., Sato, E., Kurosaki, T., Yamashita, S., Tokunaga, M., Nishida, K., and Hirano, T. (2007) Zinc is a novel intracellular second messenger. *J. Cell Biol.* **177**, 637-645

16. Yamasaki, S., Hasegawa, A., Hojyo, S., Ohashi, W., Fukada, T., Nishida, K., and Hirano, T. (2012) A novel role of the L-type calcium channel α1D subunit as a gatekeeper for intracellular zinc signaling: zinc wave. *PLOS One* **7**, e39654

17. Valdez, C. E., Smith, Q. A., Nechay, M. R., and Alexandrova, A. N. (2014) Mysteries of metals in metalloenzymes. *Acc. Chem. Res.* **47**, 3110-3117

18. Holm, R. H., Kennepohl, P., and Solomon, E. I. (1996) Structural and functional aspects of metal sites in biology. *Chem. Rev.* **96**, 2239-2314

19. Sigfridsson, K. (1998) Plastocyanin, an electron-transfer protein. *Photosynth. Res.* **57**, 1-28

20. Solomon, E. I., and Hadt, R. G. (2011) Recent advances in understanding blue copper proteins. *Coord. Chem. Rev.* **255**, 774–789

21. Perutz, M. F. (1976) Structure and mechanism of haemoglobin. *Br. Med. Bull.* **32**, 195-208

22. Paoli, M., Liddington, R., Tame, J., Wilkinson, A., and Dodson, G. (1996) Crystal structure of T state haemoglobin with oxygen bound at all four haems. *J. Mol. Biol.* **256**, 775-792

23. Magnus, K. A., Ton-That, H., and Carpenter, J. E. (1994) Recent structural work on the oxygen transport protein hemocyanin. *Chem. Rev.* **94**, 727–735

24. Park, S. Y., Yokoyama, T., Shibayama, N., Shiro, Y., and Tame, J. R. (2006) 1.25 Å resolution crystal structures of human haemoglobin in the oxy, deoxy and carbonmonoxy forms. *J. Mol. Biol.* **360**, 690-701

25. Plum, L. M., Rink, L., and Haase, H. (2010) The essential toxin: impact of zinc on human health. *Int. J. Environ. Res. Public Health* **7**, 1342-1365

26. Andreini, C., Bertini, I., and Cavallaro, G. (2011) Minimal functional sites allow a classification of zinc sites in proteins. *PLOS One* **6**, e26325

27. Kägi, J. H., and Vallee, B. L. (1960) The role of zinc in alcohol dehydrogenase. V. The effect of metal-binding agents on the structure of the yeast alcohol dehydrogenase molecule. *J. Biol. Chem.* **235**, 3188-3192

28. Scrutton, M. C., Wu, C. W., and Goldthwait, D. A. (1971) The presence and possible role of zinc in RNA polymerase obtained from *Escherichia coli*. *Proc. Natl. Acad. Sci. USA* **68**, 2497-2501

29. Vallee, B. L., Rupley, J. A., Coombs, T. L., and Neurath, H. (1959) The role of zinc in carboxypeptidase. *J. Biol. Chem.* **235**, 64-69

30. Himo, F., and Siegbahn, P. E. (2001) Catalytic mechanism of glyoxalase I: a theoretical study. *J. Am. Chem. Soc.* **123**, 10280-10289

31. Gao, H., Yu, Y., and Leary, J. A. (2005) Mechanism and kinetics of metalloenzyme phosphomannose isomerase: measurement of dissociation constants and effect of zinc binding using ESI-FTICR mass spectrometry. *Anal. Chem.* **77**, 5596-5603

32. Scrutton, M. C., Young, M. R., and Utter, M. F. (1970) Pyruvate carboxylase from baker's yeast. The presence of bound zinc. *J. Biol. Chem.* **245**, 6220-6227

33. McCall, K. A., Huang, C., and Fierke, C. A. (2000) Function and mechanism of zinc metalloenzymes. *J. Nutr.* **130**, 1437S-1446S

34. Prasad, A. S. (2012) Discovery of human zinc deficiency: 50 years later. *J. Trace Elem. Med. Biol.* **26**, 66-69

35. Trumbo, P., Yates, A. A., Schlicker, S., and Poos, M. (2001) Dietary reference intakes: vitamin A, vitamin K, arsenic, boron, chromium, copper, iodine, iron, manganese, molybdenum, nickel, silicon, vanadium, and zinc. *J. Am. Diet. Assoc.* **101**, 294-301

36. Maret, W. (2013) Inhibitory zinc sites in enzymes. *Biometals* **26**, 197-204

37. Krężel, A., and Maret, W. (2006) Zinc-buffering capacity of a eukaryotic cell at physiological pZn. *J. Biol. Inorg. Chem.* **11**, 1049-1062

38. Supuran, C. T., Scozzafava, A., and Casini, A. (2003) Carbonic anhydrase inhibitors. *Med. Res. Rev.* **23**, 146-189

39. Huang, C. C., Lesburg, C. A., Kiefer, L. L., Fierke, C. A., and Christianson, D. W. (1996) Reversal of the hydrogen bond to zinc ligand histidine-119 dramatically diminishes catalysis and enhances metal equilibration kinetics in carbonic anhydrase II. *Biochemistry* **35**, 3439-3446

40. Maret, W. (2004) Zinc and sulfur: a critical biological partnership. *Biochemistry* **43**, 3301-3309

41. Coleman, J. E., and Vallee, B. L. (1961) Metallocarboxypeptidases: stability constants and enzymatic characteristics. *J. Biol. Chem.* **236**, 2244-2249

42. Day, E. S., Wen, D., Garber, E. A., Hong, J., Avedissian, L. S., Rayhorn, P., Shen, W., Zeng, C., Bailey, V. R., Reilly, J. O., Roden, J. A., Moore, C. B., Williams, K. P., Galdes, A., Whitty, A., and Baker, D. P. (1999) Zinc-dependent structural stability of human sonic hedgehog. *Biochemistry* **38**, 14868-14880

43. Sellin, S., and Mannervik, B. (1984) Metal dissociation constants for glyoxalase I reconstituted with Zn2+, Co2+, Mn2+, and Mg2+. *J. Biol. Chem.* **259**, 11426-11429

44. Hirose, J., Iwamoto, H., Nagao, I., Enmyo, K., Sugao, H., Kanemitu, N., Ikeda, K., Takeda, M., Inoue, M., Ikeda, T., Matsuura, F., Fukasawa, K. M., and Fukasawa, K. (2001) Characterization of the metal-substituted dipeptidyl peptidase III (rat liver). *Biochemistry* **40**, 11860-11865

45. Kiefer, L. L., Krebs, J. F., Paterno, S. A., and Fierke, C. A. (1993) Engineering a cysteine ligand into the zinc binding site of human carbonic anhydrase II. *Biochemistry* **32**, 9896-9900

46. Liang, W., Ouyang, S., Shaw, N., Joachimiak, A., Zhang, R., and Liu, Z. J. (2011) Conversion of D-ribulose 5-phosphate to D-xylulose 5-phosphate: new insights from structural and biochemical studies on human RPE. *FASEB J.* **25**, 497-504

47. Sobota, J. M., and Imlay, J. A. (2011) Iron enzyme ribulose-5-phosphate 3-epimerase in *Escherichia coli* is rapidly damaged by hydrogen peroxide but can be protected by manganese. *Proc. Natl. Acad. Sci. USA* **108**, 5402-5407

48. Anjem, A., Varghese, S., and Imlay, J. A. (2009) Manganese import is a key element of the OxyR response to hydrogen peroxide in *Escherichia coli*. *Mol. Microbiol.* **72**, 844-858

49. Martin, J. E., and Imlay, J. A. (2011) The alternative aerobic ribonucleotide reductase of *Escherichia coli*, NrdEF, is a manganese-dependent enzyme that enables cell replication during periods of iron starvation. *Mol. Microbiol.* **80**, 319-334

50. Dowling, D. P., Gattis, S. G., Fierke, C. A., and Christianson, D. W. (2010) Structures of metal-substituted human histone deacetylase 8 provide mechanistic inferences on biological function. *Biochemistry* **49**, 5048-5056

51. Helm, L., and Merbach, A. E. (2005) Inorganic and bioinorganic solvent exchange mechanisms. *Chem. Rev.* **105**, 1923-1959

52. Alberty, R. A., and Hammes, G. G. (1958) Application of the thoery of diffusion-controlled reactions to enzyme kinetics. *J. Phys. Chem.* **62**, 154–159

53. Pinter, T. B., and Stillman, M. J. (2015) Kinetics of Zinc and Cadmium Exchanges between Metallothionein and Carbonic Anhydrase. *Biochemistry* **54**, 6284-6293

54. Kägi, J. H., and Schäffer, A. (1988) Biochemistry of Metallothionein. *Biochemistry* **27**, 8509-8515

55. Maret, W., Larsen, K. S., and Vallee, B. L. (1997) Coordination dynamics of biological zinc "clusters" in metallothioneins and in the DNA-binding domain of the transcription factor Gal4. *Proc. Natl. Acad. Sci. USA* **94**, 2233-2237

56. Li, T. Y., Kraker, A. J., Shaw, C. F., III, and Petering, D. H. (1980) Ligand substitution reactions of metallothioneins with EDTA and apo-carbonic anhydrase. *Proc. Natl. Acad. Sci. USA* **77**, 6334-6338

57. Auld, D. S. (1988) Use of chelating agents to inhibit enzymes. *Methods Enzymol.* **158**, 110-114

58. Feder, J., Garrett, L. R., and Kochavi, D. (1971) Studies on the inhibition of neutral proteases by 1,10-phenanthroline. *Biochim. Biophys. Acta* **235**, 370-377

59. Holmquist, B., and Vallee, B. L. (1974) Metal substitutions and inhibition of thermolysin: spectra of the cobalt enzyme. *J. Biol. Chem.* **249**, 4601-4607

60. Holland, D. R., Hausrath, A. C., Juers, D., and Matthews, B. W. (1995) Structural analysis of zinc substitutions in the active site of thermolysin. *Protein Sci.* **4**, 1955-1965

61. Whittington, D. A., Rusche, K. M., Shin, H., Fierke, C. A., and Christianson, D. W. (2003) Crystal structure of LpxC, a zinc-dependent deacetylase essential for endotoxin biosynthesis. *Proc. Natl. Acad. Sci. USA* **100**, 8146-8150

62. Gomez-Ortiz, M., Gomis-Rüth, F. X., Huber, R., and Avilés, F. X. (1997) Inhibition of carboxypeptidase A by excess zinc: analysis of the structural determinants by X-ray crystallography. *FEBS Lett.* **400**, 336-340

63. Christianson, D. W. (1989) Carboxypeptidase A. *Acc. Chem. Res.* **22**, 62-69

64. Bukrinsky, J. T., Bjerrum, M. J., and Kadziola, A. (1998) Native carboxypeptidase A in a new crystal environment reveals a different conformation of the important tyrosine 248. *Biochemistry* **37**, 16555-16564

65. Larsen, K. S., and Auld, D. S. (1991) Characterization of an inhibitory metal binding site in carboxypeptidase A. *Biochemistry* **30**, 2613-2618

66. Gattis, S. G., Hernick, M., and Fierke, C. A. (2010) Active site metal ion in UDP-3-*O*-((R)-3-hydroxymyristoyl)-*N*-acetylglucosamine deacetylase (LpxC) switches between Fe(II) and Zn(II) depending on cellular conditions. *J. Biol. Chem.* **285**, 33788-33796

67. Segatore, B., Massidda, O., Satta, G., Setacci, D., and Amicosante, G. (1993) High specificity of cphA-encoded metallo-β-lactamase from *Aeromonas hydrophila* AE036 for carbapenems and its contribution to β-lactam resistance. *Antimicrob. Agents Chemother.* **37**, 1324-1328

68. Walsh, T. R., Toleman, M. A., Poirel, L., and Nordmann, P. (2005) Metallo-β-lactamases: the quiet before the storm? *Clin. Microbiol. Rev.* **18**, 306-325

69. Bebrone, C., Delbruck, H., Kupper, M. B., Schlomer, P., Willmann, C., Frère, J. M., Fischer, R., Galleni, M., and Hoffmann, K. M. (2009) The structure of the dizinc subclass B2 metallo-β-lactamase CphA reveals that the second inhibitory zinc ion binds in the histidine site. *Antimicrob. Agents Chemother.* **53**, 4464-4471

70. Garau, G., Bebrone, C., Anne, C., Galleni, M., Frère, J. M., and Dideberg, O. (2005) A metallo-β-lactamase enzyme in action: crystal structures of the monozinc carbapenemase CphA and its complex with biapenem. *J. Mol. Biol.* **345**, 785-795

71. Hernandez Valladares, M., Felici, A., Weber, G., Adolph, H. W., Zeppezauer, M., Rossolini, G. M., Amicosante, G., Frère, J. M., and Galleni, M. (1997) Zn(II) dependence of the *Aeromonas hydrophila* AE036 metallo-β-lactamase activity and stability. *Biochemistry* **36**, 11534-11541

72. Adekoya, O. A., and Sylte, I. (2009) The thermolysin family (M4) of enzymes: therapeutic and biotechnological potential. *Chem. Biol. Drug Des.* **73**, 7-16

73. Mock, M., and Fouet, A. (2001) Anthrax. *Annu. Rev. Microbiol.* **55**, 647-671

74. Collier, R. J., and Young, J. A. (2003) Anthrax toxin. *Annu. Rev. Cell Dev. Biol.* **19**, 45-70

75. Bradley, K. A., and Young, J. A. (2003) Anthrax toxin receptor proteins. *Biochem. Pharmacol.* **65**, 309-314

76. Liu, S., Moayeri, M., and Leppla, S. H. (2014) Anthrax lethal and edema toxins in anthrax pathogenesis. *Trends Microbiol.* **22**, 317-325

77. Tonello, F., and Montecucco, C. (2009) The anthrax lethal factor and its MAPK kinase-specific metalloprotease activity. *Mol. Aspects Med.* **30**, 431-438

78. Moayeri, M., Sastalla, I., and Leppla, S. H. (2012) Anthrax and the inflammasome. *Microbes Infect.* **14**, 392-400

79. Martinon, F., Mayor, A., and Tschopp, J. (2009) The inflammasomes: guardians of the body. *Annu. Rev. Immunol.* **27**, 229-265

80. Pannifer, A. D., Wong, T. Y., Schwarzenbacher, R., Renatus, M., Petosa, C., Bienkowska, J., Lacy, D. B., Collier, R. J., Park, S., Leppla, S. H., Hanna, P., and Liddington, R. C. (2001) Crystal structure of the anthrax lethal factor. *Nature* **414**, 229-233

81. Ascenzi, P., Visca, P., Ippolito, G., Spallarossa, A., Bolognesi, M., and Montecucco, C. (2002) Anthrax toxin: a tripartite lethal combination. *FEBS Lett.* **531**, 384-388

82. Turk, B. E., Wong, T. Y., Schwarzenbacher, R., Jarrell, E. T., Leppla, S. H., Collier, R. J., Liddington, R. C., and Cantley, L. C. (2004) The structural basis for substrate and inhibitor selectivity of the anthrax lethal factor. *Nat. Struct. Mol. Biol.* **11**, 60-66

83. Säbel, C. E., St-Denis, S., Neureuther, J. M., Carbone, R., and Siemann, S. (2010) Alkaline earth metals are not required for the restoration of the apoform of anthrax lethal factor to its holoenzyme state. *Biochem. Biophys. Res. Commun.* **403**, 209-213

84. Säbel, C. E., Carbone, R., Dabous, J. R., Lo, S. Y., and Siemann, S. (2011) Preparation and characterization of cobalt-substituted anthrax lethal factor. *Biochem. Biophys. Res. Commun.* **416**, 106-110

85. Lo, S. Y., Säbel, C. E., Webb, M. I., Walsby, C. J., and Siemann, S. (2014) High metal substitution tolerance of anthrax lethal factor and characterization of its active copper-substituted analogue. *J. Inorg. Biochem.* **140**, 12-22

86. Cerdá-Costa, N., and Gomis-Rüth, F. X. (2014) Architecture and function of metallopeptidase catalytic domains. *Protein Sci.* **23**, 123-144

87. Horrocks, W. D., Jr., and Sudnick, D. R. (1981) Lanthanide Ion Luminescence Probes of the Structure of Biological Macromolecules. *Acc. Chem. Res.* **14**, 384-392

88. Richardson, F. S. (1982) Terbium(III) and europium(III) ions as luminescent probes and stains for biomolecular systems. *Chem. Rev.* **82**, 541-552

89. Eigen, M. (1963) Fast elementary steps in chemical reaction mechanisms. *Pure Appl. Chem.* **6**, 97-116

90. Bruno, J., Horrocks, W. D., Jr., and Zauhar, R. J. (1992) Europium(III) luminescence and tyrosine to terbium(III) energy-transfer studies of invertebrate (octopus) calmodulin. *Biochemistry* **31**, 7016-7026

91. Miller, T. L., Bennet, L. W., and Spatz, D. S. (1986) Terbium luminescence from complexes of angiotensin II, small peptides, and amino acids. *Ohio J. Sci.* **86**, 140-143

92. Rhee, M. J., Sudnick, D. R., Arkle, V. K., and Horrocks, W. D., Jr. (1981) Lanthanide ion luminescence probes. Characterization of metal ion binding sites and intermetal energy transfer distance measurements in calcium-binding proteins. 1. Parvalbumin. *Biochemistry* **20**, 3328-3334

93. Horrocks, W. D., Jr., Holmquist, B., and Vallee, B. L. (1975) Energy transfer between terbium (III) and cobalt (II) in thermolysin: a new class of metal-metal distance probes. *Proc. Natl. Acad. Sci. USA* **72**, 4764-4768

94. Matthews, B. W., Weaver, L. H., and Kester, W. R. (1974) The conformation of thermolysin. *J. Biol. Chem.* **249**, 8030-8044

95. Tonello, F., Ascenzi, P., and Montecucco, C. (2003) The metalloproteolytic activity of the anthrax lethal factor is substrate-inhibited. *J. Biol. Chem.* **278**, 40075-40078

96. Laemmli, U. K. (1970) Cleavage of structural proteins during the assembly of the head of bacteriophage T4. *Nature* **227**, 680-685

97. Siemann, S., Brewer, D., Clarke, A. J., Dmitrienko, G. I., Lajoie, G., and Viswanatha, T. (2002) IMP-1 metallo-β-lactamase: effect of chelators and assessment of metal requirement by electrospray mass spectrometry. *Biochim. Biophys. Acta* **1571**, 190-200

98. Säbel, C. E., Shepherd, J. L., and Siemann, S. (2009) A direct spectrophotometric method for the simultaneous determination of zinc and cobalt in metalloproteins using 4-(2-pyridylazo)resorcinol. *Anal. Biochem.* **391**, 74-76

99. Toffolo, G., Shames, D. M., Stevanato, A., and Cobelli, C. (2001) Tracer-to-tracee Ratio for Compartmental Modelling of Stable-isotope Tracer Data. in *Advances in Isotope Methods for the Analysis of Trace Elements in Man* (Lowe, N., and Jackson, M. eds.), CRC Press, Boca Raton. pp 43-57

100. Woodhouse, L. R., and Abrams, S. A. (2001) Advances in Stable-isotope Methodology. in *Advances in Isotope Methods for the Analysis of Trace Elements in Man* (Lowe, N., and Jackson, M. eds.), CRC Press, Boca Raton. pp 1-22

101. Cobelli, C., Toffolo, G., Bier, D. M., and Nosadini, R. (1987) Models to interpret kinetic data in stable isotope tracer studies. *Am. J. Physiol.* **253**, E551-E564

102. Cobelli, C., Toffolo, G., and Foster, D. M. (1992) Tracer-to-tracee ratio for analysis of stable isotope tracer data: link with radioactive kinetic formalism. *Am. J. Physiol.* **262**, E968-E975

103. Buckley, W. T. (1988) The use of stable isotopes in studies of mineral metabolism. *Proc. Nutr. Soc.* **47**, 407-416

104. Siemann, S., Badiei, H. R., Karanassios, V., Viswanatha, T., and Dmitrienko, G. I. (2006) ^{68}Zn isotope exchange experiments reveal an unusual kinetic lability of the metal ions in the di-zinc form of IMP-1 metallo-β-lactamase. *Chem. Commun.*, 532-534

105. Silverman, R. B. (2000) *The Organic Chemistry of Enzyme-Catalyzed Reactions*, Academic Press, San Diego

106. Tonello, F., Seveso, M., Marin, O., Mock, M., and Montecucco, C. (2002) Screening inhibitors of anthrax lethal factor. *Nature* **418**, 386

107. Lo, S. Y., Säbel, C. E., Mapletoft, J. P., and Siemann, S. (2015) Influence of chemical denaturants on the activity, fold and metal status of anthrax lethal factor. *Biochem. Biophys. Rep.* **1**, 68-77

108. Hooper, N. M. (1994) Families of zinc metalloproteases. *FEBS Lett.* **354**, 1-6

109. Mourez, M., Lacy, D. B., Cunningham, K., Legmann, R., Sellman, B. R., Mogridge, J., and Collier, R. J. (2002) 2001: a year of major advances in anthrax toxin research. *Trends Microbiol.* **10**, 287-293

110. Heinz, U., Kiefer, M., Tholey, A., and Adolph, H. W. (2005) On the competition for available zinc. *J. Biol. Chem.* **280**, 3197-3207

111. Richens, D. T. (2005) Ligand substitution reactions at inorganic centers. *Chem. Rev.* **105**, 1961-2002

112. Pasquarello, A., Petri, I., Salmon, P. S., Parisel, O., Car, R., Tóth, E., Powell, D. H., Fischer, H. E., Helm, L., and Merbach, A. (2001) First solvation shell of the Cu(II) aqua ion: evidence for fivefold coordination. *Science* **291**, 856-859

113. Foster, A. W., Patterson, C. J., Pernil, R., Hess, C. R., and Robinson, N. J. (2012) Cytosolic Ni(II) sensor in cyanobacterium: nickel detection follows nickel affinity across four families of metal sensors. *J. Biol. Chem.* **287**, 12142-12151

114. Foster, A. W., Osman, D., and Robinson, N. J. (2014) Metal preferences and metallation. *J. Biol. Chem.* **289**, 28095-28103

115. Rossetto, O., and Montecucco, C. (2008) Presynaptic Neurotoxins with Enzymatic Activities. in *Pharmacology of Neurotransmitter Release* (Südhof, T. C., and Starke, K. eds.), Springer, New York City. pp 129-170

116. Minghao Feng, M. S. (2012) Metal ion-mediated inactivation and small molecule inhibition of the metalloprotease in botulinum neurotoxin A. in *Department of Chemistry*, Georgetown University, Washington, DC

117. Breidenbach, M. A., and Brunger, A. T. (2004) Substrate recognition strategy for botulinum neurotoxin serotype A. *Nature* **432**, 925-929

118. Prakash, O., and Vishwakarma, D. K. (2001) Inhibition of urease from seeds of water-melon (*Citrullus vulgaris*) by heavy metal ions. *J. Plant Biochem. Biot.* **10**, 147-149

119. Milstein, C. (1961) Inhibition of phosphoglucomutase by trace metals. *Biochem. J.* **79**, 591-596

120. White, G. F., Litvinenko, K. L., Meech, S. R., Andrews, D. L., and Thomson, A. J. (2004) Multiphoton-excited luminescence of a lanthanide ion in a protein complex: Tb(3+) bound to transferrin. *Photochem. Photobiol. Sci.* **3**, 47-55

121. Tonello, F., Naletto, L., Romanello, V., Dal Molin, F., and Montecucco, C. (2004) Tyrosine-728 and glutamic acid-735 are essential for the metalloproteolytic activity of the lethal factor of *Bacillus anthracis*. *Biochem. Biophys. Res. Commun.* **313**, 496-502